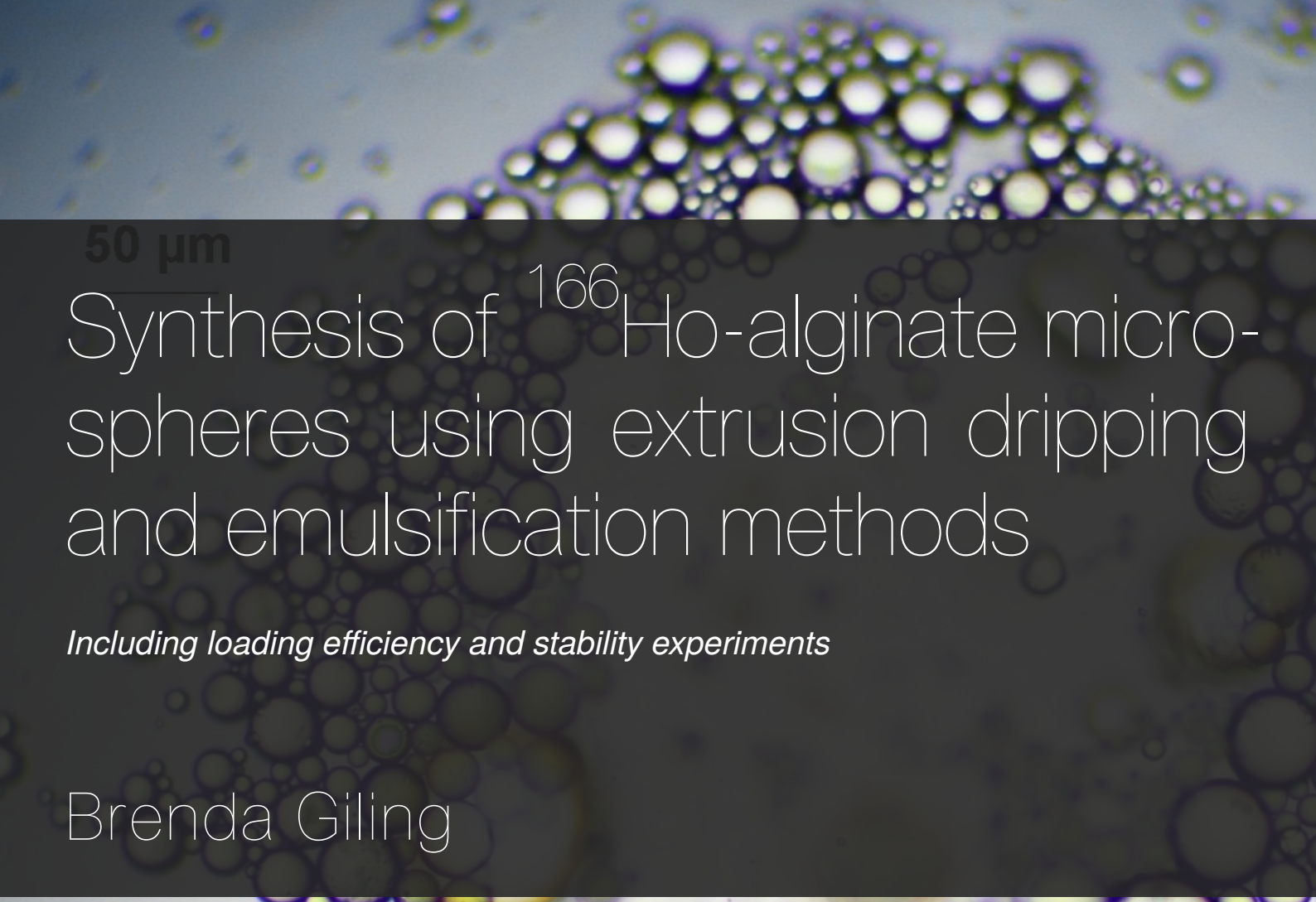


# Synthesis of $^{166}$Ho-alginate microspheres using extrusion dripping and emulsification methods

*Including loading efficiency and stability experiments*

Brenda Giling

Delft University of Technology

TU Delft

# Synthesis of $^{166}$Ho-alginate microspheres using extrusion dripping and emulsification methods

*Including loading efficiency and stability experiments*

by

Brenda Giling

To obtain the degree of Master of Science
at the Delft University of Technology,
to be defended publicly on Friday the 22nd of May 2026 at 10:00.


| | |
|---|---|
| Student number: | 5179203 |
| Thesis supervisor: | Prof. dr. ir. A.G. Denkova |
| Thesis committee: | Assoc. Prof. dr. ir. R. de Kruijff |
| | Dr. T.M. McCoy |
| Daily supervisors: | Ö. Chalashkan & E.J. van den Heuvel |
| Project duration: | November 2025 - May 2026 |
| Institute: | Delft University of Technology |
| Faculty: | Applied Sciences |
| Department: | Reactor Institute Delft |
| Research group: | Applied Radiation Isotopes |


Cover: Optical microscope picture of holmium-alginate microspheres

TU Delft

# Preface

*I would like to dedicate this thesis to my grandmother, whose apple pie was always warm when we crossed the doorstep, and whose enthusiastic waving stayed in our rear-view mirror until we turned the corner.*

First of all, I want to thank my supervisor Antonia for this challenging project. I was given three thesis subject options, and I remember choosing this one because somewhere in the meeting I heard 'well, we don't know that much about it really'. It gave me an opportunity to make this project my own, and gave me a way to implement my endless curiosity. I also want to thank Özlem and Eline for their support with experiments, ideas, my own thoughts and all other tiny research questions. It helped me build my confidence in the lab and to never be afraid to double-check. Thank you to all three for our many meetings when I had prepared another thirty slides, and for all the feedback that followed. You were always ready to help me improve.

For support, random discussions, new thoughts, and lunch in the sun, I want to thank my room-buddy Anna and all my other amigos in the ARI group. Your ideas and laughs made it so much easier to push through when the alginate microspheres did not do what I wanted them to do.

Last but certainly not least, I am immensely grateful for all my friends and family who saw how hard I worked throughout these seven years as a student. You encouraged me to keep going and supported me in every step. *Daar zijn we dan!*

B.M.R. (Brenda) Giling
Delft, May 2026

# Abstract

$^{166}$Ho-alginate microspheres could present a new type of device for the radioembolisation of liver cancer, where targeted radiation therapy is combined with embolisation of tumour blood vessels. Whereas current devices in radioembolisation are permanent, alginate offers a biodegradable device with a cheap and simple production process. The isotope holmium-166 (Ho-166) has been of interest in radiotherapy due to its favourable half-life and decay through $\beta$-emission. Furthermore, its paramagnetic properties allows visualisation using Magnetic Resonance Imaging (MRI) and its $\gamma$-emission allows for imaging using Single Photon Emission Computed Tomography (SPECT). This research investigates the synthesis, loading efficiency and stability of $^{166}$Ho-alginate microspheres. For synthesis of alginate microspheres, this research uses the extrusion dripping method and emulsification method. Here, process parameters are investigated to crosslink alginate with $Ca^{2+}$ and to obtain alginate particles having diameter of around 30 µm. In the extrusion dripping method, increasing pH showed crosslinking of alginate into viscous gel formations or alginate particles having a wrinkled surface. A pH of 4 offered the best conditions to produce spherical alginate particles with smoother surface morphology and smallest particle size. Particle size below 100 µm was not obtained in the extrusion dripping method, but the emulsification method in this research succeeded in particle formation with sizes between 10 to 60 µm. The Ca-alginate microspheres from the emulsification method were further used in an ion-exchange process to replace the $Ca^{2+}$ in the alginate structure with $Ho^{3+}$. Using Ho-166, an average loading efficiency of (86.5 $\pm$ 1.4)% was found. The obtained $^{166}$Ho-alginate microspheres were tested on their radiochemical stability in demiwater and 0.9% NaCl solution. Here, the microspheres in demiwater showed excellent stability, whereas their retention percentage in 0.9% NaCl decreased to ~60% after five minutes. Nevertheless, the retention percentage in 0.9% NaCl further remained stable for up to 24 hours. Further research could include stabilizing the alginate microspheres post-emulsification, as removal of surfactant during washing steps resulted in an increase of particle size. Secondly, investigation on process parameters within the emulsification method could bring the particle size between 20 to 60 µm with a smaller size distribution. Destined for radioembolisation, the $^{166}$Ho-alginate microspheres need improved loading efficiency and improved stability in physiological media such as 0.9% NaCl. Literature on Ho-alginate microspheres is very limited as of now, and this research takes a step towards $^{166}$Ho-alginate microspheres as radioembolic device for transarterial radioembolisation.

# Contents

# List of Figures

# List of Tables

# Nomenclature

## Abbreviations

| Abbreviation | Definition |
|---|---|
| BED | Backscattered Electron Detector |
| Ca | Calcium |
| CE | Conformité Européenne |
| Cl | Chlorine |
| Dy | Dysprosium |
| EDS | Energy Dispersive X-ray Spectroscopy |
| Er | Erbium |
| EtOH | Ethanol |
| HCC | Hepatocellular carcinoma |
| HEPES | 4-(2-hydroxyethyl)-1-piperazineethanesulfonic acid |
| Ho | Holmium |
| MRI | Magnetic Resonance Imaging |
| Na | Sodium |
| PET | Positron Emission Tomography |
| PLLA | Poly-L-lactic acid |
| RCF | Relative Centrifugal Force |
| rpm | Rounds per minute |
| SED | Secondary Electron Detector |
| SEM | Scanning Electron Microscopy |
| SIRT | Selective Internal Radiation Therapy |
| SPECT | Single Photon Emission Computed Tomography |
| TARE | Transarterial radioembolisation |
| TRIS | Trizma® base, 2-amino-2-(hydroxymethyl)-1,3-propaandiol |
| Y | Yttrium |
| w/v | weight by volume |

## Symbols

| Symbol | Definition | Unit |
|---|---|---|
| $cpm$ | Counts per minute | $min^{-1}$ |
| $t_{1/2}$ | Half-life | time |

# 1 Introduction

Of all predicted new cases for liver and intrahepatic bile duct cancer in 2026, only 27% is estimated to survive the diagnosis [1]. The total of these predicted cases accounts for almost 5% of the total estimated cancer deaths for 2026. With a 5-year relative survival rate of only 22%, liver cancer is placed as the fifth and seventh leading cases of deaths for males and females, respectively, in the US. As third leading cause of cancer mortality worldwide, hepatocellular carcinoma (HCC) specifically accounts for 75–85% of all primary liver cancer cases. However, treatment of HCC remains difficult. The cure rate of HCC is only ~25%, and its 5-year survival rate is set at ~15% [2, 3]. Underlying liver diseases and late diagnosis prevent effective curative treatments such as surgery or ablative techniques. These treatments are therefore only proposed to 20-30% of patients, and even in such cases there is a high percentage of reoccurrences [4].

Within nuclear medicine, Selective Internal Radiation Therapy (SIRT) is a treatment method of intra-arterial radiation therapy for patients with primary or secondary liver malignancies. SIRT can be combined with embolisation into transarterial radioembolisation (TARE), which has been explored since the 1950's. Here, radioisotopes embedded in microspheres are delivered through the blood supply of the liver and lodge in blood vessels of tumour sites. This blocks the blood flow and provides a radiation dose only to the site of interest, reducing radiation dose to healthy tissue. Several radionuclides have been investigated for their application in TARE, such as yttrium-90 and holmium-166. The radionuclides can be embedded in different microsphere material, such as glass, resin or polymer, to create a radioembolic device. The choice of radionuclide and microsphere carrier material is dependent on, but not limited to, the microspheres' chemical stability and radio-imaging potential. Currently, three types of microspheres have been approved for the European market. The $^{90}$Y-glass microspheres TheraSphere® (BTG International Ltd., London, United Kingdom), the $^{90}$Y-resin microspheres SIR-Spheres® (SIRTEX Medical Limited, North Sidney, New South Wales, Australia), and the $^{166}$Ho-poly-L-lactic acid (PLLA) microspheres QuiremSpheres® (Quirem Medical B.V., Deventer, The Netherlands) [5].

Since the start of this century, interest in Ho-166 for nuclear medicine has been growing, such as holmium-macroaggregates in rheumatoid arthritis disease treatment or holmium-microspheres for liver malignancies [6, 7]. Ho-166 is a promising radionuclide for radiodiagnostics and radiotherapy due to favourable decay characteristics and imaging opportunities [8]. Firstly, the half-life of Ho-166 is 26.79 hours, which is about two and a half times shorter than Y-90 [9]. This is a sufficient time between production and administration of the radionuclide to the patient, but short enough to limit the hospitalization of a patient. Within five days, the Ho-166 holds only 5% of its original radiation when Y-90 holds 30% of its original radiation. Compared to Y-90, patients with a Ho-166 treatment plan spend less time in isolation and can be discharged from the hospital sooner.
Secondly, both radionuclides decay through $\beta$-emission applicable to radiotherapy, where Y-90 has a maximum $\beta$-energy emission of 2.1 MeV and Ho-166 has a maximum $\beta$-energy emission

of 1.85 MeV. However, Ho-166 has additional imaging possibilities. Ho-166 is suitable for Magnetic Resonance Imaging (MRI) due to its paramagnetic properties, as well as suitable for Single Photon Emission Computed Tomography (SPECT) due to its $\gamma$-radiation emission. These characteristics make $^{166}$Ho-microspheres attractive for quantitative, *in-vivo* assessment and imaging compared to $^{90}$Y-labelled microspheres [10–13]. This visualization during injection of microspheres could promise an efficient, safer way of radioembolisation. The $^{166}$Ho-microspheres can also be used as scout doses in combination with $^{90}$Y-labelled microspheres treatment to predict the bio-distribution and set up accurate treatment planning [14].

The production of radioembolic devices is currently done using two different methods. For TheraSpheres and QuiremSpheres, the stable isotope is first embedded within the microsphere material, followed by activation of the isotope through neutron irradiation of the entire microsphere. The PPLA microspheres, however, disintegrated during long irradiations to activate the holmium. SIR-Spheres uses the process of ion-exchange, where fabricated microspheres exchange their ions within the resin structure for radioactive yttrium-ions.
The current glass and resin radioembolic microsphere materials are not degraded in the body, making their embolisation in liver tissue permanent with lasting changes in blood vessels and tissue. The PPLA microspheres were reported to be biodegradable, but this type of device is now discontinued [15–17]. In search of an alternative carrier material, the polysaccharide alginate is proposed for the ion-exchange production process.

The aim of this research was first of all to investigate alginate particle formation. In literature, there are several methods reported for the production of alginate microspheres. These include extrusion techniques, such as the jet cutter method or pressurized spray nozzle method, emulsification techniques, or microfluidic system techniques [18]. This research includes two methods for the production of alginate microspheres. Firstly, the extrusion dripping method is used to observe the effect of pH in formation of alginate particles. Secondly, the emulsification method is used to produce alginate microspheres with a goal particle diameter of 30 µm and a small size distribution.
Furthermore, this research investigates the loading efficiency of alginate microspheres with Ho-166 through the ion-exchange method. This research also examines the radiochemical stability of these Ho-alginate microspheres.

The background for understanding the concepts in this research is provided in Chapter 2. Chapter 3 describes the production methods of alginate microspheres, the ion-exchange towards holmium-alginate microspheres and its loading efficiency, and the stability experiments of holmium-alginate microspheres. The experimental results are provided and discussed in Chapter 4. The conclusion is given in Chapter 5, followed by recommendations for further research in Chapter 6.

# 2

# Theoretical background

This chapter covers the theoretical background necessary in understanding the concepts in this research. First, transarterial radioembolisation (TARE) and its radioembolic devices are explained in Section 2.1. Then, information on isotope Ho-166 is provided in Section 2.2. The structure of alginate and the formation of alginate microspheres is explained in Section 2.3. Then, background on the synthesis methods in this research is presented in Section 2.4. Lastly, the analytical instruments used in this research are explained in Section 2.5.

## 2.1. Transarterial radioembolisation

The liver contains a dual blood supply, consisting of the portal vein and the hepatic artery. Healthy liver tissue receives 75% of its blood flow through the portal vein and 25% of its blood flow through the hepatic artery. Primary and secondary liver tumour tissue, on the other hand, receive 90% of their blood supply through the hepatic artery [19]. This makes the hepatic artery the main target for TARE, where microspheres are injected with a size ranging from 20 to 60 µm. These particles lodge in the arterioles of a tumour (<100 µm), without crossing the sinusoid network (8-10 µm) towards healthy tissue [20–22]. Clinical trials showed effective radiation dosage with acceptable toxicity profiles, concluding TARE a treatment option with higher radiation doses to liver tumour than external beam radiation [5, 23, 24].

Three main types of microspheres for TARE have been developed, namely TheraSphere, SIR-Spheres and QuiremSpheres [5]. TheraSphere and SIR-Spheres were acknowledged as Active Implantable Medical Devices with a Conformité Européenne (CE) mark in the early 2000's, and have received pre-market approval from the Food and Drug Administration (FDA) in 2021 and 2002, respectively. The QuiremSpheres received their CE mark in 2015 and have only been available on the European market [25]. The radioembolic devices differ in activation method, choice of isotope and choice of microsphere carrier material. A summary of the characteristics of TheraSphere, SIR-Spheres and Quiremspheres is listed in Table 2.1. All three radioembolic devices are biocompatible, but the embolisation is permanent for TheraSphere and SIR-Spheres while QuiremSpheres can be degraded in the body [15, 16]. In 2025, the QuiremSpheres were announced to be discontinued by their company Terumo. It was stated that "the operational complexity makes the Holmium Platform SIRT product range commercially unviable for Terumo both now and in the future" (Terumo, 2025) [17].

**Table 2.1:** Characteristics of radioembolic devices TheraSphere, SIR-Spheres and QuiremSpheres [5].

| **Device name** | **TheraSphere** | **SIR-Spheres** | **QuiremSpheres** |
|---|---|---|---|
| Isotope | Y-90 | Y-90 | Ho-166 |
| Material | Glass | Resin | Poly-L-lactic acid |
| Mean diameter | 20-30 µm | 20-60 µm | 15-60 µm |
| Activation of microspheres | Neutron bombardment of Y-89 after microsphere fabrication | Ion-exchange process to incorporate Y-90 in the microspheres | Neutron bombardment of Ho-165 after microsphere fabrication |
| Activity per microsphere | 2500-4000 Bq | 75 Bq | 240-375 Bq |
| Characteristics | Biocompatible, permanent lodging | | Biocompatible, biodegradable |

## 2.2. Radioisotope Ho-166

Ho-166 is produced in a nuclear reactor using two different methods. Either through neutron activation by (n, $\gamma$) radiation of Ho-165, or through double neutron irradiation of dysprosium-164 [26, 27]. Due to the 100% natural abundance of Ho-165, the first pathway results in isotope of a high purity, but a large amount of inactive Ho-165 atoms. The second pathway requires extensive separation methods, but results in no-carrier-added Ho-166 with a high specific activity, especially favourable when high doses are required in radiotherapy [28]. Figure 2.1 shows the two production pathways and decay pathways of Ho-166, including cross sections, half-lives, and radiation types with corresponding energies [9, 29].

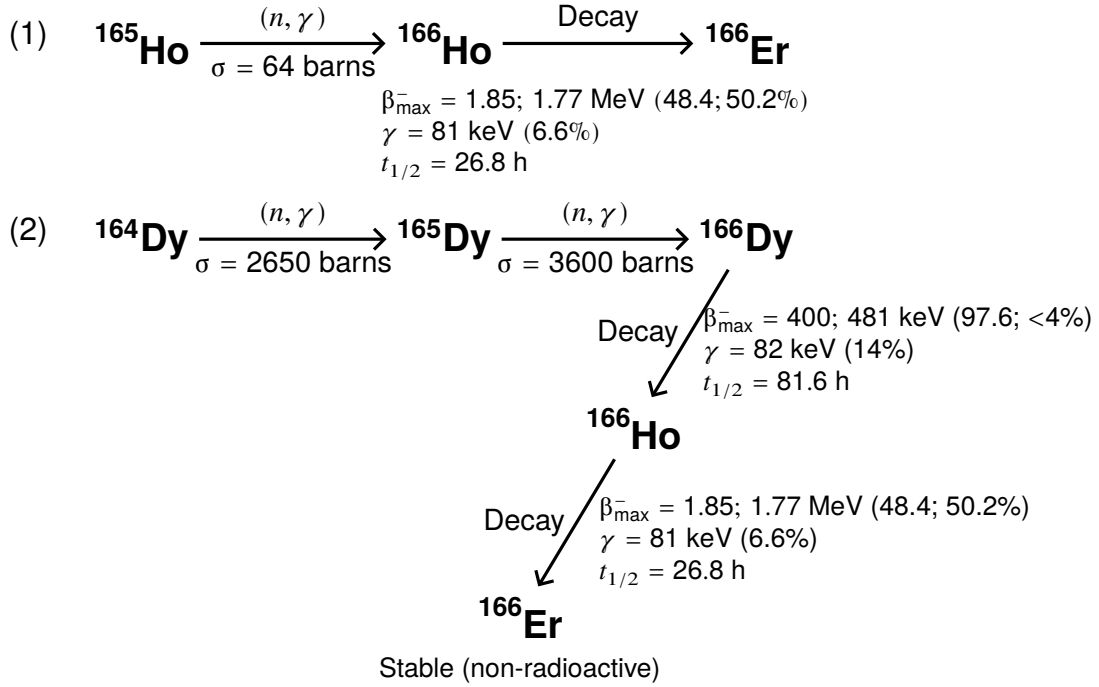


**Figure 2.1:** Diagram of the production pathways and decay of Ho-166 through neutron irradiation of (1) Ho-165 and (2) Dy-164. Only the major transitions are given [9, 29].

Ho-166 decays into the stable erbium-166 for 100% by emission of $\beta^-$ to either a ground state or an excited level of Er-166, with a maximum $\beta$-energy of 1.85 MeV. The schematic overview of the two major transitions is given in Figure 2.2 [29]. The $\beta^-$ emission with an average penetration depth of 1.2-2.5 mm and a maximum penetration depth of 8 mm in soft tissue makes the nuclide ideal for delivering local high doses in radiotherapy. The transition from excited state to ground state ejects $\gamma$-radiation of 81 keV, and these $\gamma$-rays can be detected *in-vivo* using Single Photon Emission Computed Tomography (SPECT) [30]. Furthermore, holmium can be detected using magnetic resonance imaging (MRI) due to its paramagnetic properties. In nuclear reactor production, the higher neutron-caption cross-section of holmium compared to yttrium (64 barns versus 1.28 barns, respectively) reduces the neutron-activation time to produce therapeutic radioactivity levels [31, 32].

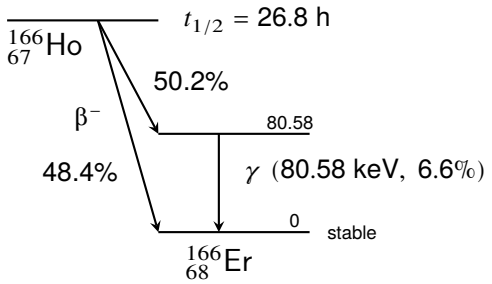


**Figure 2.2:** Decay scheme of Ho-166 to Er-166 through the major transitions [29].

Holmium microspheres have been investigated before in their stable form as MRI contrast agent or as radiolabelled form for therapeutic or diagnostic purposes [7]. Examples of the latter include but are not limited to $^{166}$Ho-DOTMP for bone metastases [33], or $^{166}$Ho-labelled chitosan [34] and previously mentioned $^{166}$Ho-PPLA microspheres for liver tumour [35, 36]. The published literature on synthesis and characterisation of holmium microspheres using alginate, especially towards radioembolisation, is very limited as of now.

## 2.3. Alginate

Alginate has been of interest for a wide range of applications, as its structure can be modified to obtain different functional properties [37]. Within the field of medicine, alginate has been used in wound-healing, tissue engineering and in drug delivery systems, where drugs are encapsulated and protected by alginate microspheres [38, 39]. In drug delivery, alginate microspheres have been widely investigated as a stable, polymer-type carrier device to control the release of drugs and provide the ability to deliver the drug to a specific target site [40–43]. These drug delivery alginate systems are biodegradable, and they are metabolized and eliminated from the body after the drug has been delivered [44]. Comparing alginate to poly-L-lactic acid for radioembolic devices, both polymers are biodegradable, biocompatible, and can be obtained from renewable bio-based sources. However, alginate can be found all over the world, and its production process is simple and cheap [45–48]. The concept of existing biodegradable alginate-systems in drug delivery, combined with the simple and cheap production process of alginate, propose a new purpose of alginate microspheres for non-permanent radioembolisation.

The structure of alginate is composed of copolymers of two uronic acid units, namely $\alpha$-L-guluronic acid and $\beta$-D-mannuronic acid, which are 1-4 linked in a linear chain. The $\alpha$-L-guluronic acid residues and $\beta$-D-mannuronic acid residues are arranged in polymeric regions, creating G-blocks and M-blocks, respectively, of polymer along the linear chain. The M/G ratio differs depending on the source of alginate, and can be determined by liquid-state nuclear magnetic reference analysis [49–51]. The chemical structure of and conformation of alginate with

its polymeric regions is presented in Figure 2.3.

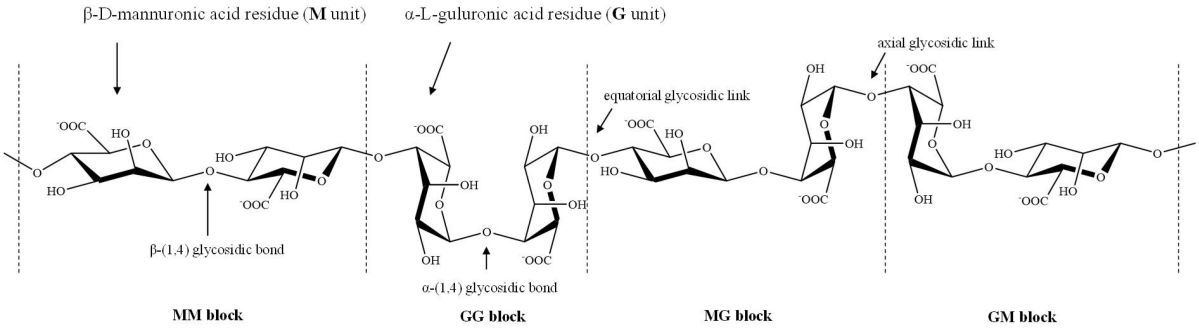


**Figure 2.3:** Chemical structure and conformation of alginate polymer. M unit: $\beta$-D-mannuronic acid residues; G unit: $\alpha$-L-guluronic acid residues; MM block: homopolymeric blocks of M units; GG block: homopolymeric blocks of G units; and MG or GM block: heteropolymeric blocks of M and G or G and M unit. Taken from [52].

The polymeric blocks can be crosslinked with divalent or trivalent cations in a process called gelation. When G-blocks are crosslinked, the alginate chains are structured in a so-called 'egg-box model'. Divalent charged calcium has been studied as a favourable ion in creating alginate gel, with its ability to crosslink the G-blocks with high affinity. The strength of the alginate gel also increases with increasing calcium concentration [53–56]. The schematic of this crosslinking is provided in Figure 2.4, taken from [53].

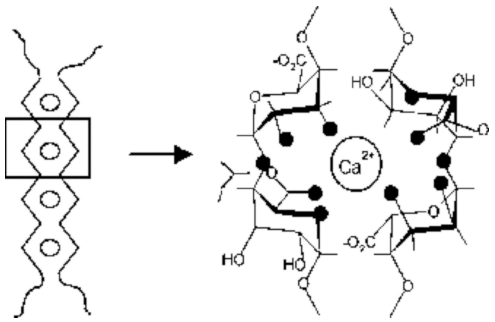


**Figure 2.4:** Schematic drawing of calcium crosslinking the alginate's G-blocks, creating the so-called 'egg-box model' structure. Taken from [53].

Several lanthanide ions have been investigated on their alginate crosslinking by DeRamos et al. [57]. This study showed a less positive preference of trivalent lanthanide ions for G-blocks than divalent ions like calcium. This difference was explained due to an increased participation of M-blocks in lanthanide ion binding. The study attributed the difference to additional water molecules in the inner sphere of the lanthanide ions. This way, the lanthanide ions pack less easily into the G and M-blocks compared to calcium. It was also concluded that the extent of metal-alginate binding increases with increasing atomic number, and thus with increasing charge density. This charge density was concluded to be a larger contributing factor to the extent of metal-alginate binding than the size of the trivalent ion. The highest atomic number in the study of DeRamos et al. was that of the lanthanide terbium (Tb, atom number 65). Following the conclusion on increasing metal-alginate binding for higher atomic numbers, it is expected that holmium (atom number 67) should exhibit an even higher affinity for alginate than the lanthanides studied by DeRamos et al.

The crosslinking of holmium with alginate has been studied once before by Zielhuis et al., who hardened alginate droplets with holmium or calcium in a crosslinking bath followed by characterisation of the microspheres [12]. It was mentioned that the binding capacity of alginate for

$Ho^{3+}$ is equal to that of $Ca^{2+}$, indicating that these cations have the same binding affinity for alginate. Zielhuis et al. also investigated the radiolabelling properties of alginate microspheres. Here, ion-exchange was done by adding Ho-166 to previously synthesized calcium-alginate microspheres. This ion-exchange method was adapted in this research to obtain $^{166}$Ho-alginate microspheres for loading efficiency and stability experiments.

## 2.4. Synthesis of alginate microspheres

Synthesis of alginate microspheres was done through two methods in this research. First, the extrusion dripping method is explained in Section 2.4.1, followed by the emulsification method in Section 2.4.2. In this research, it was desired to form Ca-alginate microspheres to eventually exchange the calcium for holmium in radiolabelling experiments. This is why both methods use a type of calcium source for crosslinking.

### 2.4.1. Extrusion dripping method - external gelation

The extrusion dripping method is a form of external gelation of alginate, and a schematic overview is given in Figure 2.5. A syringe loaded with sodium alginate (Na-alginate) solution is mounted to a vertical syringe pump, and alginate droplets from the syringe are dropped into a bath of crosslinking ions. In this research, a bath of $CaCl_2$ was used. The $Ca^{2+}$ is captured on the surface of the alginate droplets, hence the name external gelation, and diffuses from the surface into the sphere. This creates a hard outer shell of the alginate beads and a decreasing concentration gradient from the surface to the centre of the beads. The size of the alginate droplets is determined by the choice of needle width, alginate concentration and collection distance from the tip of the needle to the surface of the crosslinking bath [44]. Although it is not expected that this method leads to small particle size [58], the influence of pH on the particle size has been studied to determine the viability of smaller calcium-alginate microspheres.

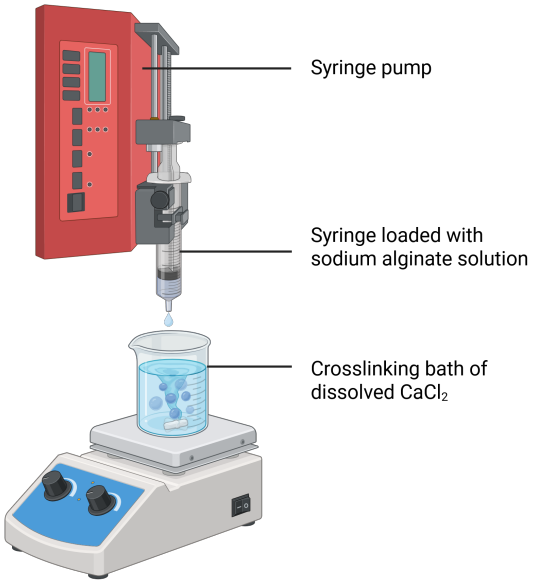


**Figure 2.5:** Schematic overview of the extrusion dripping method in this research, a form of external gelation in the production of alginate microspheres. Made with BioRender [59].

### 2.4.2. Emulsification method - internal gelation

The emulsification method is a form of internal gelation of alginate, and a schematic overview of the emulsification in this research is given in Figure 2.6. In this technique, an insoluble source of calcium, such as calcium carbonate ($CaCO_3$), is dispersed in a Na-alginate solution to create the water phase. The oil phase is prepared by adding the surfactant, Span 80, to paraffin oil. Under stirring, both phases are combined to form a water-in-oil emulsion, where the surfactant stabilizes Na-alginate droplets within the oil. Acetic acid is dropwise added to the emulsion, which releases $Ca^{2+}$ from the $CaCO_3$ inside the water phase droplets. The $Ca^{2+}$ ions then crosslink the alginate from within the droplets, hence the name internal gelation. As the ions are captured internally, there is no concentration gradient like the droplets created in external gelation. The particle size using emulsification can reach below 100 µm [60], which is promising in creating alginate microspheres for liver embolisation. The experiments in this research included adjusting the concentration of $CaCO_3$ and the acetic acid amount.

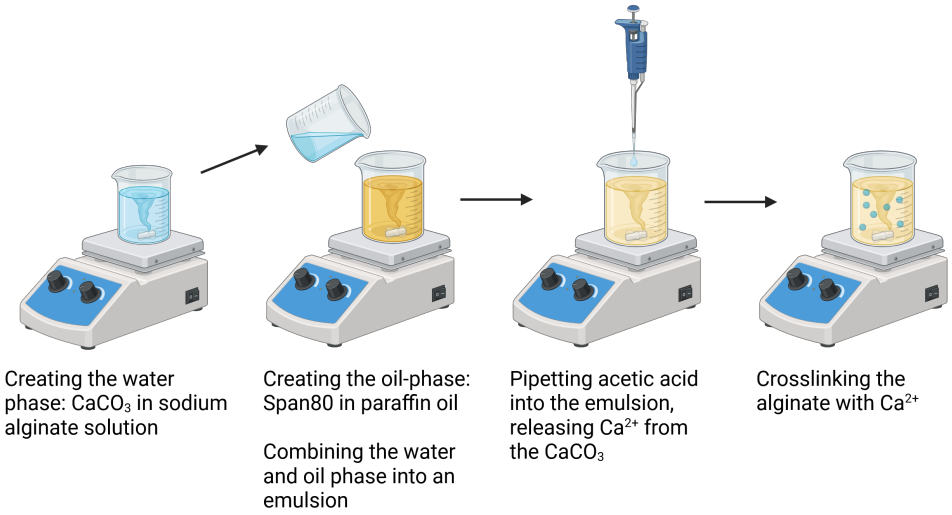


**Figure 2.6:** Schematic overview of the emulsification method in this research, a form of internal gelation in the production of alginate microspheres. Made with BioRender [59].

## 2.5. Analytical instruments

This section provides background theory on the analytical instruments used in this research. This includes the optical microscope, the scanning electron microscope, the Wallac automated gamma counter and the particle sizer.

### 2.5.1. Optical microscope

The optical microscope is used to visualize the alginate microspheres on a micrometer scale, where a brightfield light microscope images the microspheres against a bright background. Several objective lenses can be attached, and this research used 4x, 10x and 40x zoom lenses. By changing the light input (brightness) and aperture on the microscope, a good contrast is created to characterize the microspheres. The optical microscope is paired to a digital camera system to capture and display pictures on a computer. Within the provided computer program, scale bars are added and microsphere diameter can be calculated.

### 2.5.2. Scanning Electron Microscopy

Scanning Electron Microscopy (SEM) is an imaging technique to create high resolution images of a sample, and is used for the analysis of surface morphology [61]. A schematic overview of SEM is presented in Figure 2.7. The sample is attached to carbon tape on an aluminium stub, and placed in the chamber of the SEM. Under vacuum environment, electrons are accelerated with acceleration voltages up to 30 keV and aimed onto the sample. The interaction of the electron beam with the sample generates a.o. secondary electrons and characteristic x-rays, which can be detected using a Secondary Electron Detector (SED) or using Energy Dispersive X-ray Spectroscopy (EDS), respectively.

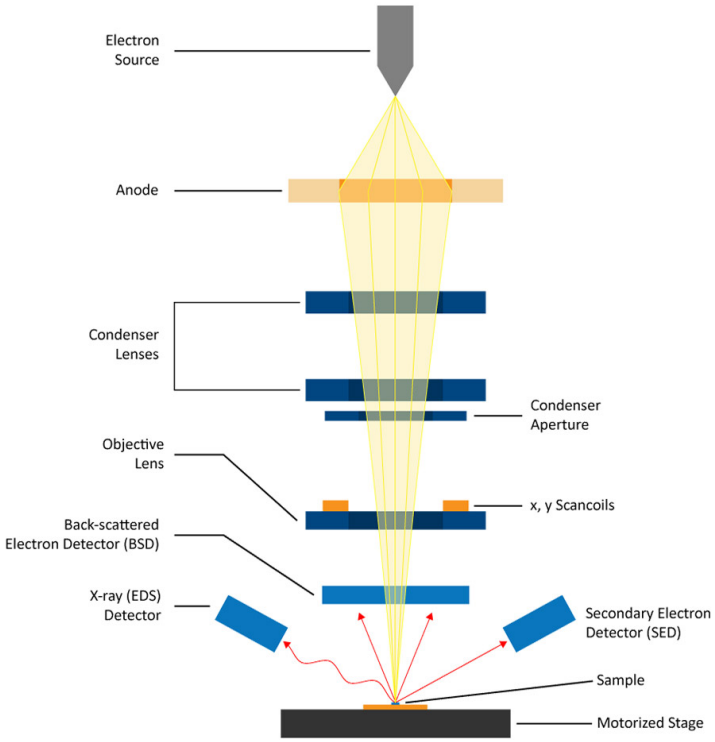


**Figure 2.7:** Schematic overview of Scanning Electron Microscopy (SEM), taken from [62].

The secondary electrons are generated by inelastic collisions at a depth of 0-10 nm from the sample [63]. In this research, the SED is used to obtain a 3D type of image of the sample's surface. SEM can be coupled with EDS to obtain an elemental composition of the sample. X-rays are emitted by the atoms in the sample when an excited electron in the electron shell relaxes to the ground state. The energy of these X-rays are characteristic to a specific element, and the EDS provides a quantitive and qualitative summary of the imaged sample. In EDS, the acceleration voltage for an element depends on the electron shell. Calcium has a minimum accelerating voltage of >5 keV for its only K-shell, whereas the holmium M-shell needs >5 keV, and the holmium L-shell needs >10 keV acceleration voltage to excite the electrons and generate characteristic X-rays. The option of elemental mapping using EDS provides a colour-coded, 2D image showing the spacial distribution of elements in the sample.

### 2.5.3. Wallac gamma counter

In this research, the counts per minute (cpm) of Ho-166 in a sample is determined by the Wallac automated gamma counter using the scintillation technique. In this instrument, a thallium-activated sodium iodide crystal (NaI(Ti) crystal) is used as scintillation medium. When a Ho-166 sample is placed in the detection chamber, its emitted $\gamma$-photons are absorbed by the NaI-crystal, which excites electrons to a higher energy state. Relaxation of these electrons back to the ground state emits a photon in the form of visible light. A photomultiplier tube then converts these light photons into electrical pulses, where the voltage of the pulse is related to the energy of the originally absorbed $\gamma$-photon [64]. The individual pulses are counted to create a $\gamma$-spectrum of the sample. Ho-166 has a characteristic $\gamma$-photon energy peak of 81 keV, and the gamma spectrum can be integrated in this region of interest to obtain the count-rate of Ho-166 [29]. The efficiency of the detector depends on sample geometry and $\gamma$-ray energy, providing only the counts per minute of the sample. The gamma counter should therefore not be used as a measurement of activity, but it is suitable for the calculations on loading efficiency and stability in this research. Sample geometry should be kept the same to be able to compare results between samples. The measurements can be corrected on background radiation by measuring an empty vial in each measurement series.

### 2.5.4. Particle sizer

Referred to in this research as the particle sizer, a Coulter Counter is used to determine the particle size of alginate microspheres. The instrument is based on the Coulter principle and is able to provide data on particle number, volume, mass, and surface area size. For each measurement, the particles are suspended in a conductive liquid (isotone) with two submerged electrodes located on either side of a small, electrified aperture. The Coulter principle is based on the change of electrical resistance when a particle passes through the aperture, which generates an electrical pulse. It is important that the particles are diluted enough in the conductive liquid, so that one particle at a time passes through the aperture. The number of electrical pulses is related to the number of particles, while the amplitude of the electrical pulse corresponds to a particle's volume [65]. The size of the aperture can go from 10 µm to 2 mm, and should be selected depending on the expected particle size. These apertures can measure particles within a size range of 0.2 µm to 1.6 mm, and their application ranges from micrometer-scale bacterial studies to millimetre-scale blood clots [66]. Coulter counters have been reported at high efficiency, with a variance of less than 2% [67]. The generated pulses are collected within the provided computer program, which generates the particle size distribution of the alginate microsphere solution. Before each measurement, the blank isotone solution is measured to correct for background.

# 3

# Materials and methods

This chapter begins with an overview of chemicals and devices used in this research in Section 3.1. Then, the experimental procedures for alginate microsphere synthesis using the extrusion dripping method as well as the emulsification method are outlined in Section 3.2. The calcium-holmium crosslinking and loading efficiency experiments are described in Section 3.3, followed by the stability experiments in Section 3.4. Lastly, specifications on the characterisation and analysis methods can be found in Section 3.5. Experiments were done at ambient temperature and atmospheric pressure, unless stated otherwise.

## 3.1. Materials

Table 3.1 provides the overview of chemicals used in the experimental procedures, stating the product name, chemical formula, CAS number and supplier per reagent. Similarly, Table 3.2 lists the devices used, including their product name and manufacturer.

**Table 3.1:** Specification of chemicals in this research.

| **Product name** | **Chemical Formula** | **CAS number** | **Supplier** |
|---|---|---|---|
| Acetic acid >99.5% | $CH_3COOH$ | 64-19-7 | Sigma-Aldrich |
| Beckman Coulter isotone solution | ISOTON-II | - | Beckman Coulter, Inc |
| Calcium carbonate, 99%, extra pure | $CaCO_3$ | 471-34-1 | Thermo Scientific |
| Calcium chloride dihydrate | $CaCl_2 \cdot 2\,H_2O$ | 10035-04-8 | Merck |
| Citric acid | $C_6H_8O_7$ | 77-92-9 | Sigma-Aldrich |
| Ethanol | $C_2H_6O$ | 64-17-5 | Central warehouse L&M |
| HEPES Pufferan >99.5% | $C_8H_{18}N_2O_4S$ | 7365-45-9 | Carl Roth |
| Holmium(III) chloride hexahydrate | $HoCl_3 \cdot 6\,H_2O$ | 14914-84-2 | STREM Chemicals INC |
| Holmium(III) nitrate pentahydrate, 99.9% | $Ho(NO_3)_3 \cdot 5\,H_2O$ | 14483-18-2 | Merck-Sigma |
| Sodium chloride Baker Analyzed | NaCl | 7647-14-5 | J.T. Baker (Avantor) |
| Paraffin oil CZ 600 | $C_nH_{2n+2}$ | 8012-95-1 | CMC |
| Alginic acid sodium salt, very low viscosity | $C_{28}H_{54}O_1$ | 9005-38-3 | Thermo Scientific |
| Sodium hydroxide | NaOH | 1310-7302 | Honeywell |
| Span(R) 80 | $C_{24}H_{44}O_6$ | 1338-43-8 | Sigma-Aldrich |
| Trizma(R) base (TRIS) | $C_4H_{11}NO_3$ | 77-86-1 | Merck |

**Table 3.2:** Specification of devices in this research.

| **Device** | **Product name** | **Manufacturer** |
|---|---|---|
| Centrifuge | VWR Mega Star 600R Cat.No. 521-3501 | VWR International bvba |
| Microscope glass slides | Objektträger geschliffen | Knittel Glass |
| Needles | 30 G x 1/2” (0.3 x 13mm) | BD Microlance 3 |
| Optical Microscope | Model ECLIPSE Ci-L, imaging software NIS-Elements D version 6.10.01 | Nikon Corporation |
| Particle sizer | Multisizer 3 Coulter Counter, Aperture tube diameter 100 µm | Beckman Coulter, Inc |
| Pasteur pipettes | 3 mL IN PE | Unknown |
| Pasteur pipettes | VWR Disposable transfer pipettes (23 mL, 1.5 mL) | Avantor |
| pH meter | FiveEasy F20 | Mettler-Toledo GmbH |
| pH meter probe | LE438 | Mettler-Toledo GmbH |
| Pipette | 2-10 mL | Unknown |
| Pipette tips | 10 mL | Gilson |
| Pipette tips | 5 mL | Sarstedt AG & Co. KG |
| Pipette tips | 200 uL | Greiner Bio-One GmbH |
| Pipettes | 2-20 uL, 20-200 uL, 0.5-5 mL | JoanLab Equipment Co. LTD |
| Plastic tubes | Tube 50 mL, 115x28 mm, PP | Sarstedt AG & Co. KG |
| Precision balance | New Classic MF | Mettler-Toledo GmbH |
| Rotating mixer | RMO-80PRO | Joan Lan Equipment Co. LTD |
| Scale | Mettler PE 2600 Delta Range | Mettler Instrumenten B.V. |
| Scanning Electron Microscope | JSM-IT100 | JEOL Ltd. |
| Scintillation vials | Scintillation Vials, 20 mL, Borosilicate Glass, with Screw Caps | VWR International bvba |
| Sonicator | Ultrasonic cleaner Model 200 46 KHz | Branson |
| Stirrer | HS5Pro | JoanLab Equipment Co. LTD |
| Syringe | BD 5mL Syringe Luer-Lok Tip | Becton, Dickinson & Co. |
| Syringe pump | Aladdin Single Syringe Pump | World Precision Instruments |
| Vortex mixer | Super Mixer II | Lab-line Instruments, Inc. |
| Wallac Automated NaI detector | 2480 Automatic Gamma Counter, Wizard$^2$ 3 | PerkinElmer |

## 3.2. Alginate microspheres synthesis

This section describes two synthesis methods for alginate microspheres, namely extrusion dripping and emulsification. For the alginate solutions, sodium alginate (Na-alginate) was weighed and dissolved in demiwater or pH buffer solution. These solutions were stirred at 55°C for 30 minutes to ensure a homogenous Na-alginate solution.

### 3.2.1. Extrusion dripping method - external gelation

For the alginate solutions, sodium acetate, HEPES and TRIS were dissolved in demiwater to obtain 100 mM buffer solutions and Na-alginate was added to form 2% w/v solutions. NaOH was used to adjust the HEPES-alginate solution to pH 7. Acetic acid was used to adjust the TRIS-alginate solution to pH 9. The sodium acetate-alginate solution was already at pH 4 and therefore did not need pH adjustment.
For the crosslinking solutions, sodium acetate, HEPES and TRIS were dissolved in demiwater to obtain 100 mM buffer solutions and $CaCl_2$ was added to a molarity of 100 mM. NaOH was used to adjust the sodium acetate-$CaCl_2$ and HEPES-$CaCl_2$ solutions to pH 4 and pH 7, respectively. NaOH and acetic acid were used to adjust the TRIS-$CaCl_2$ solution to pH 9.
For the reference solutions without buffer, 2% w/v Na-alginate in demiwater and 100 mM $CaCl_2$ in demiwater were prepared. The reference alginate solution had a pH of 6.85, and the reference $CaCl_2$ solution had a pH of 7.40.

The crosslinking bath was prepared by taking 50 mL 100 mM crosslinking solution in a petridisk. A 5 mL syringe with an internal diameter of 1.2 cm was loaded with 2 mL alginate solution. This created a ratio of Ca:alginate at 14:1 w/w. A 30G x 1/2” (0.3 x 13 mm) needle was used. While stirring at 300 rpm, the extrusion pump was set to a flow rate of 4.0 mL/min or 3.0 mL/min into the crosslinking bath at a collection distance of 6 cm. The first and the last droplets from the needle were collected to ensure homogeneous alginate solution flow. Crosslinking time was 30 minutes in these experiments. This method was repeated for all three buffer solutions and the reference solution without buffer. The crosslinking bath was collected and washed with demiwater. The high-speed centrifuge was set to 400 rpm (26 RCF) for 1 minute with soft de-acceleration, collecting the Ca-alginate particles at the bottom. The supernatant was removed and the washing step repeated. Demiwater was added to the resulting Ca-alginate and the sample was vortexed to suspend the Ca-alginate particles in the solution.

### 3.2.2. Emulsification method - internal gelation

A 100 mL paraffin oil bath was prepared with 1 mL Span 80, stirring at 1500 rpm. In a separate beaker, $CaCO_3$ was added to 25 mL 2% w/v Na-alginate to a molarity of 26 mM or 52 mM. This solution was sonicated and stirred until visually homogeneous. Giving the $CaCO_3$ no time to settle, the alginate-$CaCO_3$ solution was immediately added to the paraffin oil-Span 80 bath to form an emulsion while stirring at 1500 rpm. 100 µL or 200 µL acetic acid from the stock was dripped into the emulsion using a micropipette. The emulsion was left to crosslink for 2.5 hours at 1500 rpm. The resulting emulsion was divided into five plastic tubes. Washing of the sample was done twice with demiwater as follows: the tube was filled with demiwater until the 45 mL line, vortexed, centrifuged for 2 minutes at 1500 RCF with soft de-acceleration, and the supernatant was pipetted off. New caps were used for the tubes after every wash. After the second wash, demiwater was added, the samples vortexed, and all samples were collected and redistributed over new tubes to ensure homogeneous particle distribution. In the 26 mM $CaCO_3$ with 100 µL acetic acid emulsification, 60% EtOH was additionally used as washing solution instead of demiwater.

## 3.3. Calcium-holmium crosslinking and loading efficiency

### 3.3.1. Stable holmium crosslinking

Two stock solutions of $HoCl_3$ were made: (1) 26 mM $HoCl_3$ and (2) 2.6 mM $HoCl_3$. The pH of these solutions were 5.03 and 4.93, respectively.

#### Adding holmium directly into the crosslinking bath

The water-in-oil emulsion was prepared as previously explained in Section 3.2.2. After the acetic acid was added, 5 mL solution of a 2.6 mM $HoCl_3$ stock solution was pipetted into the bath, giving a molar ratio of Ca:Ho at 50:1. The emulsion was left to crosslink for 2.5 hours at 1500 rpm. The resulting emulsion was divided into tubes. The tubes were centrifuged for 2 minutes at 1500 RCF with soft de-acceleration and the supernatant was pipetted off. The tubes were washed twice with demiwater. The vortex mixer was used to break up alginate gel between washing and centrifuging. After the second wash, demiwater was added, the samples vortexed, and all samples were collected and redistributed over new tubes to ensure homogeneous particle distribution. Drying sample for SEM analysis was done by removing the supernatant first, and using a tissue to absorb the remaining liquid.

#### Calcium-holmium exchange using synthesized Ca-alginate microspheres

For the exchange of calcium with holmium, readily synthesized Ca-alginate microspheres were used from the previous emulsification experiments. An exchange bath was prepared as follows: 10 mL of $HoCl_3$ at 26 mM, 2.6 mM, 260 µM or 26 µM was added to a beaker. The latter two $HoCl_3$ concentrations were obtained by diluting the 2.6 mM stock solution. 1 mL of Ca-alginate microsphere solution was pipetted into the beaker, stirring at 300 rpm. The 26 mM and 2.6 mM solutions were left to exchange for 1 hour. The 260 µM and 26 µM solutions were left to exchange for 30 minutes. Each bath was distributed over two tubes, of which one was left unwashed and the other was washed twice with demiwater. Washing of the sample was done twice with demiwater as follows: the tube was filled with demiwater until the 45 mL line, vortexed, centrifuged for 2 minutes at 1500 RCF with soft de-acceleration, and the supernatant was pipetted off. After the second wash, demiwater was added and the sample was vortexed to suspend the particles in solution. Particle analysis was done using the optical microscope. Drying sample for SEM analysis was done by removing the supernatant first, and using a tissue to absorb the remaining liquid.

### 3.3.2. Radioactive holmium exchange and loading efficiency

Ho-166 was obtained by neutron irradiation of 0.97 mg $Ho(NO_3)_3$ with a thermal neutron flux of $4.57 \times 10^{12}$ $cm^{-2}/s$ in the BP3 facility at the Reactor Institute Delft, with a maximum activity of 4.5 MBq. The irradiated sample was added to 20 mL of demiwater to create the Ho-166 stock solution. When the stock solution was used, the solution was first pipetted up and down at least three times to obtain a homogeneous distribution. To measure the stock in an automated NaI detector, hereafter referred to as the Wallac gamma counter, 0.1 mL stock solution was added to 0.9 mL demiwater in a scintillation vial.

An exchange bath at 26 µM $^{166}Ho(NO_3)_3$ was prepared in a 40 mL beaker by combining 7.5 mL of demiwater with 2.5 mL of Ho-166 stock solution. Then, 2 mL of the Ca-alginate microspheres solution from the emulsion experiments was added. Under stirring at 300 rpm, the microspheres were left to exchange for 30 minutes. The solution was added to a 50 mL tube and the beaker was rinsed with demiwater until the solution in the tube was at a total of 45 mL. The tube was centrifuged at 1500 RCF for 2 minutes with soft de-acceleration. Then, 1 mL of supernatant at the top was separated into a scintillation vial. This kept the geometry the same as the stock solution scintillation vial. The remaining supernatant was removed until 5 mL solution at the

bottom of the tube remained. This 5 mL solution was kept for further stability experiments as described in Section 3.4. The scintillation vials each containing 1 mL of supernatant solution were measured in the Wallac gamma counter together with the Ho-166 stock solution scintillation vial. An empty scintillation vial was measured to use as background correction of all samples. The theoretical loading efficiency, also called encapsulation efficiency EE (%), is then calculated by:

$$\text{EE (\%)} = (1 - \frac{cpm_{supernatant}}{cpm_{stock}}) \times 100\% \tag{3.1}$$

Where:

- $cpm_{supernatant}$ is the counts per minute of Ho-166 from the exchange bath supernatant
- $cpm_{stock}$ is the counts per minute of Ho-166 from the stock solution

After all Ho-166 had decayed, the loading efficiency samples were analysed using the optical microscope.

## 3.4. Stability experiments using radioactive holmium

The 50 mL plastic tubes containing 5 mL Ca-Ho-alginate microsphere solution from the previous loading efficiency experiments were used in the stability experiments. For three tubes, one was filled with 30 mL demiwater, and the other two were filled with 30 mL 0.9% NaCl in demiwater. The pH of the 0.9% NaCl stock solution was 5.45. The tubes were placed in the rotating mixer shaker at 20 rpm. Sample of the supernatant was taken after 5 minutes, 30 minutes, 1 hour, 3 hours and 24 hours. This was done by centrifuging the tubes for 2 minutes at 1500 RCF with soft de-acceleration and taking 1 mL from the top of the supernatant into a scintillation vial. The supernatant samples were measured together with the Ho-166 stock solution scintillation vial in the Wallac gamma counter. An empty scintillation vial was measured to use as background correction of all samples. The stability was determined through the theoretical retention percentage, calculated by:

$$\text{Theoretical retention (\%)} = (1 - \frac{cpm_{supernatant}}{cpm_{stock}}) \times 100\% \tag{3.2}$$

Where:

- Theoretical retention is the percentage of Ho-166 remaining in the alginate microspheres after a given time
- $cpm_{supernatant}$ is the counts per minute of Ho-166 from the sample supernatant after a given time
- $cpm_{stock}$ is the counts per minute of Ho-166 from the stock solution

After 24 hours, the 0.9% NaCl samples were centrifuged and the 0.9% NaCl supernatant was pipetted off. The samples were then washed twice with demiwater as follows: the tube was filled with demiwater until the 45 mL line, vortexed, centrifuged for 2 minutes at 1500 RCF with soft de-acceleration, and the supernatant was pipetted off. After all Ho-166 had decayed, the particles were suspended in demiwater and analysed using the optical microscope.

## 3.5. Characterisation and analysis

### 3.5.1. Optical microscope analysis

The optical microscope was used in the extrusion dripping method, emulsification method, as well as in the exchange experiments and stability experiments. A pasteur pipette was used to take sample from the tube onto a microscope glass. The sample image was sharpened using 4x, 10x or 40x zoom to observe particle morphology. Light and contrast were manually adjusted on the optical microscope as desired. The built-in camera was used to take pictures. Pictures were edited post-production in contrast, brightness and exposure for clearer pictures.
The optical microscope pictures were used to determine whether crosslinking the alginate with calcium or holmium had been successful in producing 30-50 µm microspheres. When individual particles were found, the built-in sizing tool was used to obtain the size of particles. Once Ca-alginate particles were found in the emulsification experiments, the loading efficiency and stability experiments were performed.

### 3.5.2. SEM analysis and EDS mapping

Alginate microspheres were analysed for their particle morphology and surface morphology in the scanning electron microscope (SEM). Crosslinked alginate was too wet to immediately use for SEM analysis. Therefore, sample was scooped onto double sided carbon tape and left to air-dry for at least 24 hours before being placed in the SEM. Pictures were made using the secondary electron detector (SED), with an acceleration voltage of 5.0 to 15.0 keV in low vacuum.

Elemental analysis was performed to assess the presence and distribution of calcium and/or holmium throughout the alginate sample. This was done quantitatively and qualitatively. The outcome of the EDS in stable holmium exchange experiments was important to determine whether loading had been successful, before moving on to radioactive holmium exchange experiments. Optimal settings in detecting holmium were an acceleration voltage of 15 keV.

### 3.5.3. Wallac gamma counter measurements

To determine the loading efficiency of a sample, the supernatant samples were measured alongside a sample of the Ho-166 stock solution in the Wallac gamma counter. Similarly, to determine the stability of $^{166}$Ho-alginate microspheres, the counts of Ho-166 in the supernatant was measured using the Wallac gamma counter. All samples had a volume of 1 mL to obtain results at the same geometry. The protocol region of interest was set for Ho-166 without interference of Ho-166m using a low boundary of 60 keV and a high boundary of 90 keV for $\gamma$-rays. Samples were measured for 5 minutes each when the stock was not older than 3 days. Samples were measured for 10 minutes each when the stock was older than 3 days to assure enough counts.

### 3.5.4. Particle sizer analysis

The particle sizer was used to measure the size of Ca-alginate microspheres from the emulsification experiments. An aperture tube with a diameter of 100 µm was installed, suitable for particle sizes between 2.0 to 80 µm. The microsphere-solution was pipetted in a beaker containing isotone, supplied with the particle sizer, until the measured concentration was stable around 5%. Measuring time was 90 seconds. Analysis of the results was done in the Multisizer 3 3.53 supplied program. The results were background corrected by measuring the isotone solution before microsphere-solution was added.

# 4

# Results and discussion

This chapter presents and discusses the findings of the experiments in this research. The extrusion dripping method is discussed in Section 4.1, followed by the emulsification method in Section 4.2. The calcium-holmium exchange experiments, using stable holmium as well as radioactive holmium, are discussed in Section 4.3. Lastly, the outcome of the stability experiments is presented in Section 4.4.

## 4.1. Extrusion dripping method

The extrusion dripping method was the first synthesis method to be carried out during the experimental phase of this research. In the beginning, the buffers and concentrations of Na-alginate and $CaCl_2$ needed to be determined to obtain alginate particles. These choices are described in Section 4.1.1 and 4.1.2, respectively. Moving into the experimental phase, the extrusion pump settings were explored. Firstly, the highest achievable flowrate on the pump was used, namely 4 mL/min. However, 3 mL/min was deemed optimal for further experiments, as explained in Section 4.1.3. The results of alginate synthesis at different pH are discussed in Section 4.1.4.

### 4.1.1. Buffer selection

#### Choice of pH range

As a part of the general blood circulation, the hepatic artery carries blood at a pH range of 7.34 to 7.44 [68]. Alginate microspheres produced at pH 7 would require less steps before they can be used *in-vivo*, and therefore pH 7 was chosen for one set of experiments.

It was hypothesized that pH would affect the spacing of alginate molecules due to charging of functional groups, therefore leading to crosslinking into smaller microspheres or lowered aggregation chances compared to neutral pH. For the choice of pH, literature was consulted.

A lower pH would cause protonation of carboxylic groups, which would decrease repulsion forces and cause shrinkage of crosslinked particles [69]. However, study by Rosiak et al. reported that alginates are prone to degradation at low and high pH. Alginate can even undergo hydrolysis in acidic environment, as reported by Smidsrød et al. [37, 70]. When the pH is lowered below the pKa of uronic acid, an acid hydrogel is formed through the intermolecular network of hydrogen bonds. A study by Francis et al. measured the pKa of mannuronic acid and guluronic acid residues of alginate to be 3.38 and 3.65, respectively [71]. In the extrusion dripping method, the $H^+$ could then prevent crosslinking with $Ca^{2+}$. It was therefore decided that the lower bound in the extrusion dripping experiments should be set at pH 4. This prevents alginate degradation through complete protonation of the carboxylic groups but still provides an acidic environment to compare to microspheres crosslinked at higher pH.
It must be said however that post-experimental phase, new literature was found on the degradation of alginate. Here, Haug et al. reported on the significant degradation of alginate below pH 5

[72]. If this research was to be repeated, it is advised to set the lower bound pH at 5 instead of 4.

A higher pH would cause deprotonation of carboxylic groups, therefore increasing the repulsion of alginate. This was hypothesized to assist in avoiding aggregation, therefore creating individual microspheres when crosslinked. It was reported in literature that this repulsion would, however, cause the expansion of alginate microspheres due to swelling, which would not aid in creating the smallest particles possible [73]. On the rate of degradation of alginate at different pH, it was reported by Haug et al. that the degradation increased rapidly above pH 10 due to the elimination reaction of the carbonyl group [72]. Rosiak et al. also reported on the solubility of alginate, which decreases significantly when deprotonation of carboxyl groups occurs. With this in mind, the upper bound was set at pH 9.

**Choice of buffer**

The Buffer Reference Center by Sigma-Aldrich was consulted for the options of pH buffers in this research [74]. This provided useful pH ranges of biological buffer. HEPES was advised at pH 6.8 to 8.2, and TRIS was mentioned for pH range of 7.0 to 9.0. Both these chemicals were readily available at the research department and therefore chosen for pH 7 and pH 9, respectively. For pH 4, citric acid was first considered as buffer with its pH range of 3.0 to 6.2. However, there were concerns of precipitation when citric acid was used in combination with calcium. It is reported in literature that the reaction of citric acid with $Ca^{2+}$, mainly concerning the mineral calcite, gives insoluble precipitation of calcium citrate [75]. This resulted in the proposal of a pH 4 buffer made from the mixture of sodium acetate with acetic acid. This sodium acetate buffer has a pH range of 3.7 to 5.6. Within the crosslinking bath, sodium would already be present from the alginate, and calcium acetate is a highly soluble salt, leading to no precipitation problems.

### 4.1.2. The effect of alginate and $CaCl_2$ concentrations on particle formation

Previous unpublished research within the same research group looked at alginate concentrations at 1%, 2% and 3% w/v with $CaCl_2$ concentrations between 5 to 100 mM [76]. This previous research concluded an ideal alginate concentration of 2% w/v, which provided smaller particles than 3% w/v and more stable particles than 1% w/v. In terms of $CaCl_2$ concentration, the research concluded that although this had no influence on the particle size, increasing crosslinking concentration resulted in increasingly spherical particles with increasingly smoother particle surface. A study by Lee et. al reported that the minimum alginate concentration required to enable the formation of spherical bead was 15 g/L, or 1.5% w/v [77]. A study by Chuang et al. used three $CaCl_2$ crosslinker concentrations (1%, 5% and 10% w/v) at pH 1, 4, 7 and 10 for the crosslinking of three alginate solutions (0.8%, 1.6% and 2% w/v) [78]. This study concluded that the sphericity of particles decreased when the crosslinker concentration and the alginate concentration decreased. This result was especially noticeable at low pH. A study by Ramdhan et al. investigated the gel strength of cuboid alginate gels using 2% alginate solutions, with $CaCl_2$ crosslinking solutions between 0.05 M and 0.20 M at pH 4 to 11 [79]. This study concluded that a higher $CaCl_2$ concentration led to increased gel strength.

At the start of the experimental phase of this research, different crosslinking concentrations and alginate concentrations were tested by hand-needling the alginate solution into a crosslinking bath. These supportive experiments are provided in Appendix D. A 3% w/v alginate solution into a 8 mM $CaCl_2$ crosslinking bath proved to crosslink into gel substance rather than into individual particles. A 2% w/v alginate solution into a 4 mM $CaCl_2$ crosslinking bath did not crosslink into particles. A 2% w/v alginate solution into a 8 mM $CaCl_2$ crosslinking bath showed alginate particles under the optical microscope. Combining these supportive hand-needling experiments with literature, it was therefore decided to use an alginate concentration at 2% w/v. Building onto the unpublished research in the research group, a $CaCl_2$ concentration of 100 mM

was chosen, which gave a Ca:alginate ratio of 14:1 (w/w) in this research.

### 4.1.3. The effect of syringe pump flowrate on particle formation

Initial extrusion dripping experiments were set up using a flowrate of 4 mL/min for all three pH solutions. These settings were the highest achievable on this particular syringe pump in terms of speed and diameter of the syringe. Previous research at the department showed that a higher flow rate obtained smaller alginate particle size, therefore it was speculated that this maximum flow rate combined with a small needle diameter would result in the smallest achievable particle diameters. In literature, any type of extrusion method where pressure is applied to create a stream of alginate droplets into a crosslinking bath, a higher pressure or smaller nozzle/needle diameter usually resulted in smaller beads [80, 81]. In this research, the experiments at three different pH were analysed using the optical microscope, which showed the solutions mostly resulted in gel formation and only few separate alginate particles were found in pH 7 and pH 9 solutions. An example of the gel formation at pH 4 and the particles at pH 7 and 9 are shown in Figure 4.1.

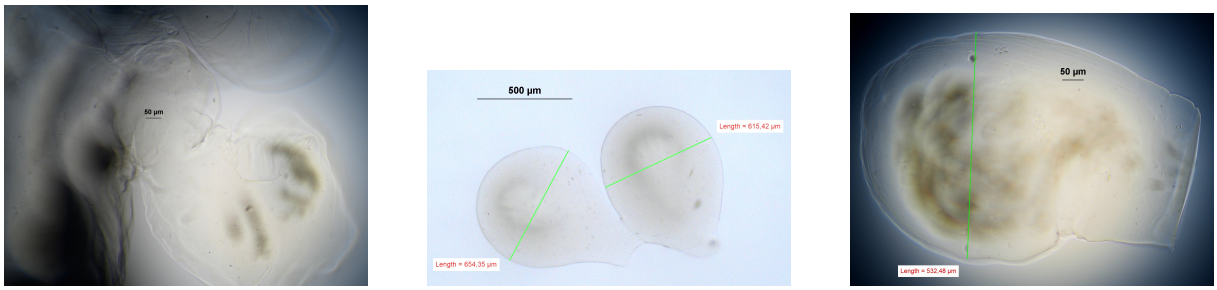


**(a)** pH 4, showing gel formation.

**(b)** pH 7, showing individual Ca-alginate particles.

**(c)** pH 9, showing a Ca-alginate particle.

**Figure 4.1:** Ca-alginate particle formation using extrusion dripping method at flowrate 4 mL/min, with solutions at pH 4, 7 and 9. The darker spot in the middle of a particle indicates the flattening of the particle's underside against the microscope glass.

The syringe pump flow rate might have been too high for singular droplets to form, resulting in a bulk of alginate hitting the crosslinking bath to crosslink into gel formation. The shape of the separate Ca-alginate particles followed a trend where flat tails could be seen. This shape could be assigned to the force with which the droplet hits the surface of the crosslinking bath. The gel formation and particle tail shape led to the decision of lowering the syringe pump flowrate to ensure separate particle formation. A test with Na-alginate solution onto a glass surface showed that a flowrate <3 mL/min would result in an unreliable stream of solution instead of droplets from the needle. The flowrate was therefore set at 3 mL/min for future experiments.

The lowered flowrate resulted in less significant flat edges of the particles, but the shapes were considered more tear-shaped than spherical. The particles now showed pointed tails that can be assigned to the way a droplet releases from the needle and hits the surface of the crosslinking bath. A schematic overview of the stages an alginate solution droplet goes through is provided in Figure 4.2.

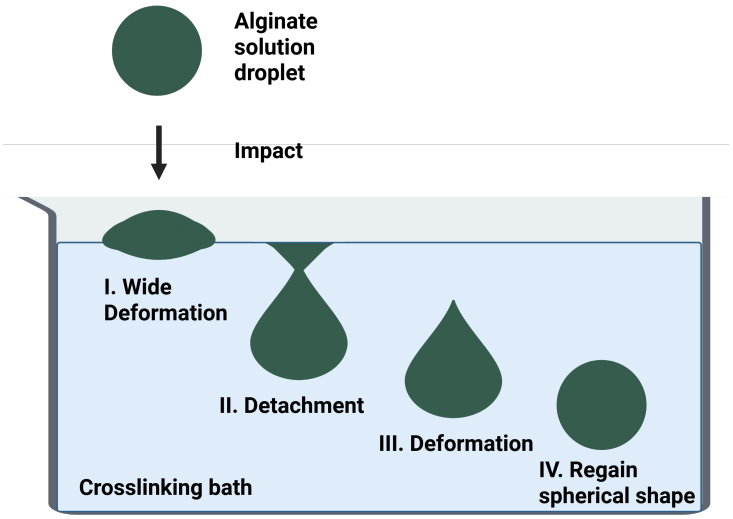


**Figure 4.2:** Stages of deformation of an alginate solution droplet hitting the crosslinking bath in the extrusion dripping method [77]. Created in BioRender [59].

A study by Davarci et al. investigated alginate droplet formation at the nozzle tip, the evolution of the droplet shape during falling and the penetration of the droplet in a $CaCl_2$ crosslinking bath [82]. In this study, the deformation of alginate droplets (2% w/v) increased when the viscosity of the crosslinking bath increased. It was also reported that the length of the droplet tail increased with increasing flow rate as well as with increasing needle diameter. This affected the time it took for an alginate droplet to become spherical while falling. Davarci et al. reported a minimum falling distance of 20 mm for the droplets to become spherical when a flowrate of 3 mL/min and a internal nozzle diameter of 0.6 mm was used. In this research, the department had a readily available setup for a collection distance of 6 cm. The needle size was the smallest available, with an internal diameter of 0.16 mm. However, the needle type was slanted, whereas Davarci et al. used a flat edged nozzle. It could be hypothesized that flat edged needles assist in creating spherical alginate droplets by reducing tail formation at the needle tip. Nevertheless, a flowrate of 3 mL/min allowed for adequate individual particle analysis to continue with pH experiments.

### 4.1.4. The effect of pH on particle formation

With the flowrate now set at 3 mL/min, the extrusion dripping method was performed using the three pH solutions and the reference solution without pH buffer in demiwater. The reference $CaCl_2$ solution had a pH of 7.40, and the reference alginate solution a pH of 6.85. The reference solution was used to indicate whether the pH buffer ions would have influence on the crosslinking besides affecting functional groups through protonation or deprotonation . After collecting and washing, the pH 7 Ca-alginate sample was visually more viscous in the tube than its pH 4 and pH 9 counterparts. The Ca-alginate was analysed under the optical microscope at 4x and 10x zoom. A picture for every pH at 10x zoom is presented in Figure 4.3, where a is pH 4, b is pH 7, c is pH 9 and d is the reference sample. The full collection of pictures can be found in Appendix A.1.

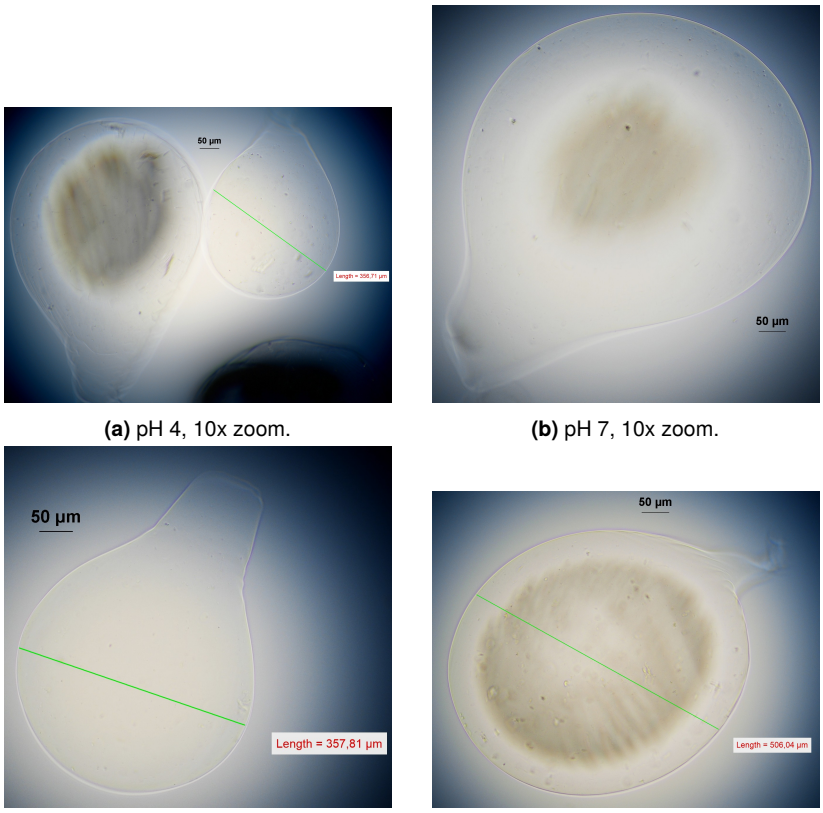


**(a)** pH 4, 10x zoom.

**(b)** pH 7, 10x zoom.

**(c)** pH 9, 10x zoom.

**(d)** Reference, 10x zoom.

**Figure 4.3:** Side-by-side comparison of Ca-alginate particles using extrusion dripping method at flowrate 3 mL/min. With solutions at pH 4, 7 and 9, and the reference solution without pH buffer. Singular particles at 10x zoom with scale bar 50 µm.

The particle size was analysed using the microscope pictures and the imaging software sizing tool. It needs to be noted that only clear spherical or nearly spherical particles, such as tear-shaped or flat-edged particles, were included, while gel formation or particle clustering was unaccounted for. This bias in the analysis influences the distribution. Especially pH 7 Ca-alginate was already more viscous due to gel formation, resulting in less opportunities for (near-)spherical particles. A definite conclusion on the size of particles from the microscope pictures alone should be approached carefully. If the extrusion dripping method is favoured for further research, the size of particles should be studied in a particle sizer or the collection of pictures should be increased and made with the intent of finding as many spherical particles as possible per sample. The particle size analysis is shown as histograms in Figure 4.4, showing the counts of particles in a size range for pH 4, 7, 9 and the reference sample. The dataset used to create the histograms can be found in Appendix A.2. pH 4 in this dataset provided the smallest particles around 400-500 µm. Between pH 7, 9 and the reference sample, there is no indication that a higher pH would lead to smaller particles. Considering the reference pH to be around 7, comparison of pH 7 to the reference sample in particle morphology and size indicated that the buffer ions did not have a significant effect on the crosslinking. Both samples contained crosslinked gel and particles formed were non-spherical with rough surfaces.

It can be noted from the microscope pictures that pH 4 gave the most opportunity for spherical particles with a smoother surface morphology, whereas particles at pH 9 obtained a wrinkled surface and the particles were more see-through. This study did not succeed in creating a homogeneous particle solution using the extrusion dripping method. Instead, the alginate mostly crosslinked into viscous gel formation, especially at pH 7 and pH 9. A study by Ramdhan et al. used cuboid gels at 2% w/v alginate and 100 mM $CaCl_2$ to study the viscosity. Ramdhan

et al. reported an increase in viscosity from pH 4 to pH 7, and a decrease in viscosity from pH 7 to pH 9. This was in line with the visual increase of viscosity at pH 7 in this research. Furthermore, the gel strength of cuboid alginate gels was shown to increase with decreasing pH. Besides the visual comparison of pH 4 and pH 9 morphology, the stability or strength of the Ca-alginate particles per pH was not further explored in this research. As the extrusion dripping method did not produce the desired particle size below 100 µm, the experimental phase was continued using the emulsification method. This shifted the focus and time to expansion of the emulsification method rather than the extrusion dripping method. The extrusion dripping method can be continued as research when particle size between 200-900 µm is preferred, and recommendations can be found in Chapter 6.

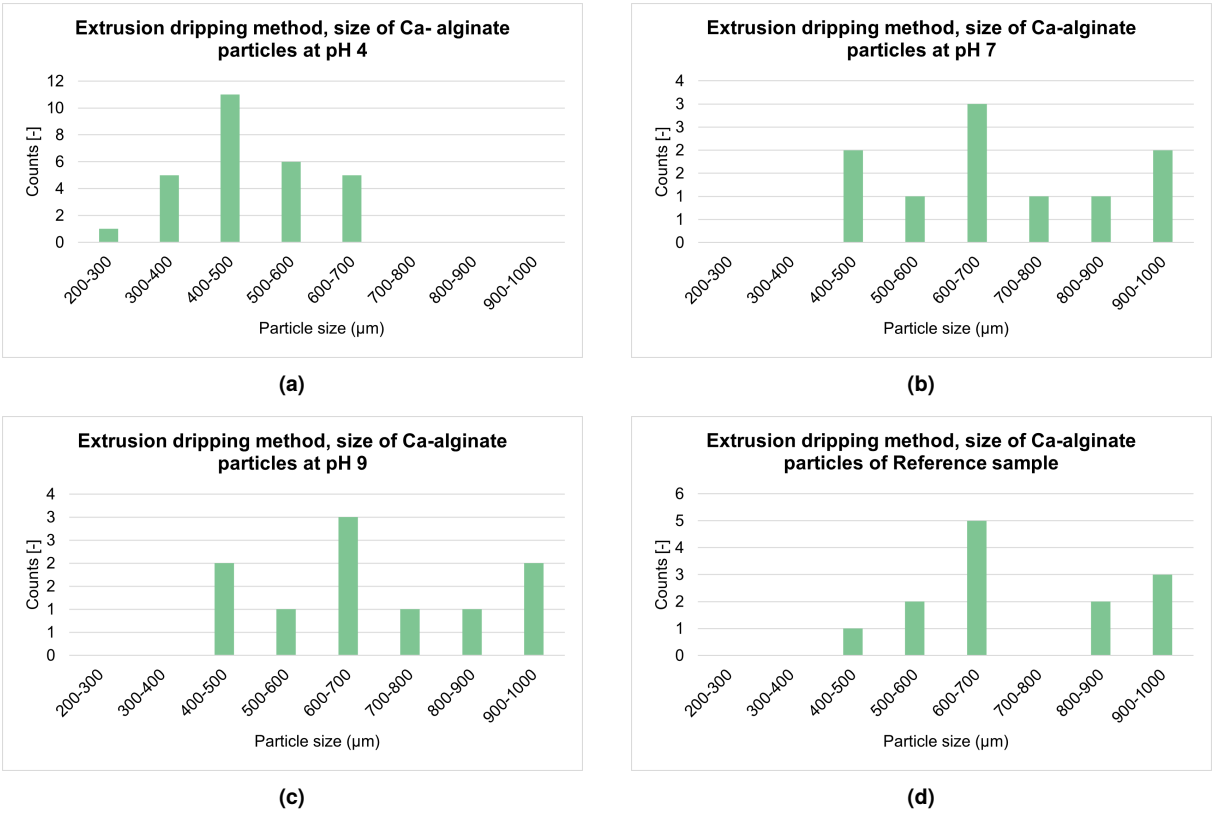


**Figure 4.4:** Size distribution of Ca-alginate particles at pH 4, 7, 9 and of the reference sample from the extrusion dripping method. The distributions were obtained by counting the alginate particles from the optical microscope analysis pictures. The dataset can be found in Appendix Section A.2.

## 4.2. Emulsification method

The emulsification experimental method was described in Section 3.2.2. Experiments were carried out using 26 or 52 mM $CaCO_3$ and 100 or 200 µL acetic acid. The choices of these experimental parameters are discussed in Section 4.2.1. The experimental results are presented and discussed in Section 4.2.2 to 4.2.4. At a later stage in the emulsification method experiments, the centrifuge settings were investigated for their efficiency during the washing steps, and results are presented in Section 4.2.5.

### 4.2.1. The choice of emulsification method parameters

Literature on alginate using emulsification as internal gelation used $CaCO_3$ molarities for calcium levels up to 144 mM [83]. This research was adapted from the research of Poncelet et al. and an initial molarity of 26 mM for the insoluble calcium salt was chosen [84]. This also included the choice of an initial acetic acid quantity of 100 µL. While Poncelet et al. dispersed the acetic acid in oil before adding it to the emulsion, this method did not produce alginate-microspheres in this research. The paraffin oil was too viscous in pipette tips, which made it difficult to add the paraffin-acetic acid mixture into the emulsion. The first experiments did not produce any Ca-alginate, and it was therefore decided to pipette the acetic acid directly from the stock.
During the emulsification, stirring speed creates the dispersion of the water-phase and oil-phase. A study by Alnaief et al. reported the change of mean diameter of alginate particles from 168 µm to 34 µm in an emulsion when the stirring speed was increased from 200 to 1400 rpm respectively [85]. The study by Poncelet et al. used a stirring rate of 200-500 rpm, resulting in only several small peaks below 150 µm in the particle size distribution. A study by Song et al. set the stirring speed at 200 rpm during emulsification while adding acetic acid, resulting in a mean diameter of 151.1 µm on the distribution [60]. To ensure smallest size possible to start with, the stirring rate in this research was decided at the maximum rate of the stirrer at 1500 rpm.
Three different combinations of $CaCO_3$ molarity and acetic acid quantity were investigated in this research: (1) 26 mM $CaCO_3$ with 100 µL acetic acid, (2) 52 mM $CaCO_3$ with 200 µL acetic acid, and (3) 26 mM $CaCO_3$ with 200 µL acetic acid. The alginate solution was kept at 2% w/v. The goal of these combinations was to find enough $CaCO_3$ to crosslink the alginate into microspheres without gel aggregation, and to find the right amount of acetic acid to release $Ca^{2+}$ from the $CaCO_3$.

### 4.2.2. Results on the 26 mM $CaCO_3$ and 100 µL acetic acid emulsification

The emulsification method was performed using 26 mM $CaCO_3$ and 100 µL acetic acid. The samples were washed twice with demiwater, and the results under the optical microscope are presented in Figure 4.5. More optical microscope pictures of these samples can be found in Appendix B.1.

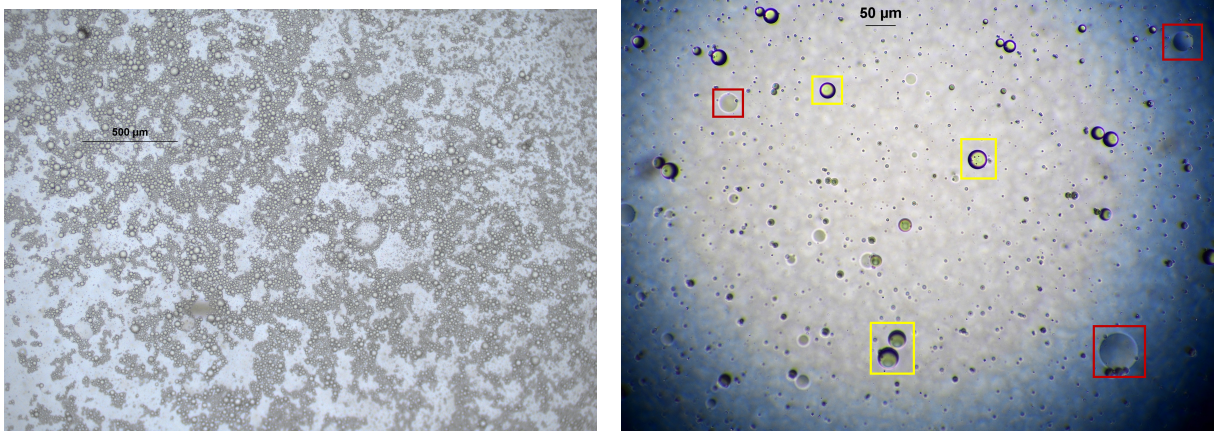


**(a)** 26 mM $CaCO_3$ and 100 µL acetic acid, 4x zoom.

**(b)** 26 mM $CaCO_3$ and 100 µL acetic acid, 10x zoom. Several oil droplets are indicated with red squares; Several alginate microspheres are indicated with yellow squares.

**Figure 4.5:** Optical microscope pictures of the 26 mM $CaCO_3$ and 100 µL acetic acid emulsification.

In recognizing alginate particles stabilized by surfactant, a study by Song et al. provides a picture of Ca-alginate particle morphology [60]. These particles were prepared using the emulsification method and rinsed with Tween 80. Another study by Lupo et al. rinsed the alginate microspheres with Tween 20 as surfactant [58]. An example of Span 80 as surfactant is provided by Leister et al., where demiwater droplets are characterised by a black border of surfactant [86]. These examples from literature are presented in Figure 4.6. The Ca-alginate particles from the emulsification experiment in this research, which was presented in Figure 4.5, correspond to the examples from literature. This indicates that the stabilisation of alginate was successful in the emulsification experiments.

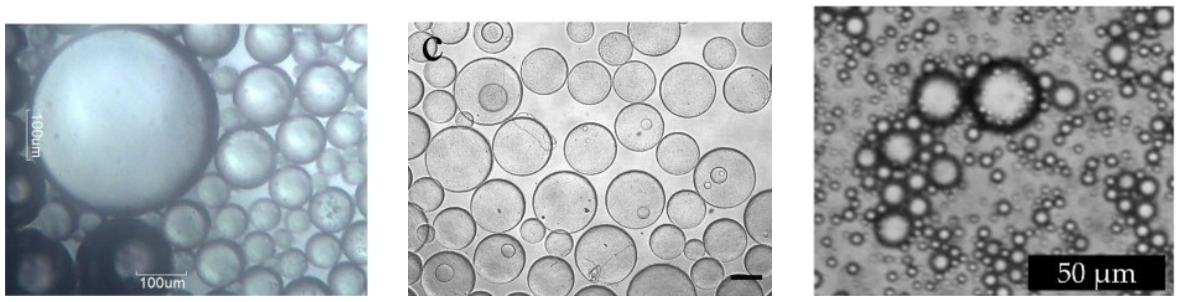


**(a)** **(b)** **(c)**

**Figure 4.6:** Literature comparison of (alginate) microparticles with surfactant; Ca-alginate particles with Tween 20 (a) [58], Ca-alginate particles with Tween 80 (b) [60], and demiwater droplets with Span 80 (c) [86].

As a size below 100 µm was not reached in previous unpublished research at the research department [76], the main goal of the emulsification method was to create alginate particles of the smallest size possible. From the optical microscope pictures, the 26 mM $CaCO_3$ and 100 µL acetic acid emulsification was successful in producing Ca-alginate microspheres between 5 to 100 µm. However, in future liver radioembolisation application, the goal size of alginate particles lies between 20 to 60 µm, as microspheres <10 µm would travel through the sinusoid network towards healthy tissue [22]. Further research could investigate parameters to bring the particle size between 20 to 60 µm, such as stirring speed. An indication of the particle size distribution

from the 26 mM $CaCO_3$ and 100 µL acetic acid emulsification was obtained using the particle sizer. These results are included at the end of this section. First, the washing with EtOH is presented and discussed.

### Washing with 60% EtOH

As shown in Figure 4.5b, numerous oil droplets still remained after washing twice with demiwater. In an attempt to remove the oil, a sample was washed twice with 60% EtOH. The optical microscope pictures are presented in Figure 4.7, accompanied by Appendix B.1.

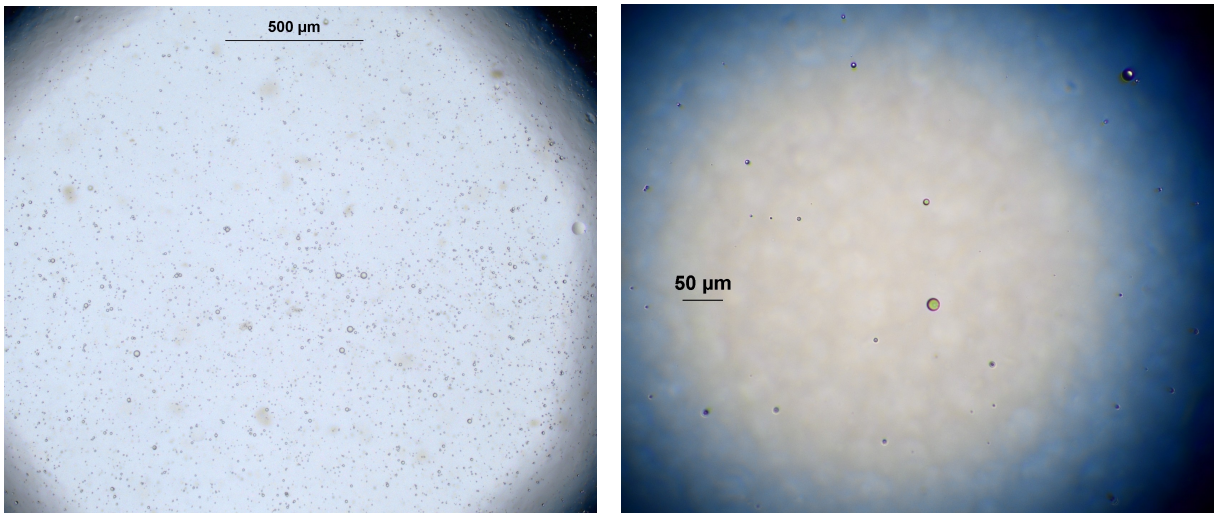


**(a)** 26 mM $CaCO_3$ and 100 µL acetic acid washed with 60% EtOH, 4x zoom.

**(b)** 26 mM $CaCO_3$ and 100 µL acetic acid washed with 60% EtOH, 10x zoom.

**Figure 4.7:** Optical microscope pictures of the 26 mM $CaCO_3$ and 100 µL acetic acid emulsification after washing with 60% EtOH.

From the optical microscope pictures, it can be concluded that EtOH washing was successful in removing the oil-droplets from the sample. However, Span 80 is soluble in organic solvents such as EtOH, and the alginate microspheres lose their black Span 80 border [87]. To analyse the remaining Ca-alginate microspheres under the optical microscope, the focus of the microscope is adjusted. The resulting picture of Ca-alginate microspheres is presented in Figure 4.8.

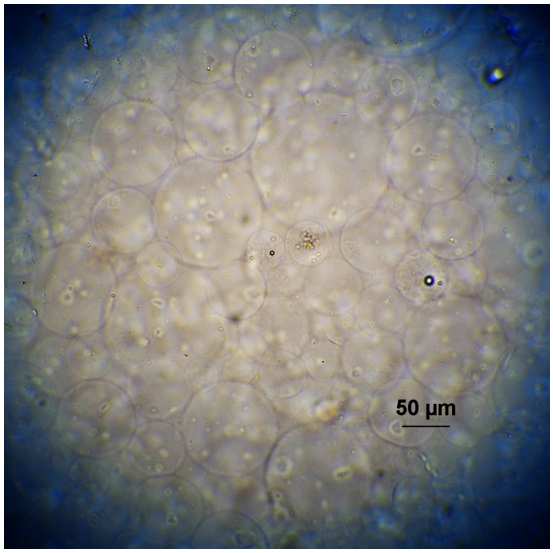


**Figure 4.8:** Optical microscope picture of the Ca-alginate microspheres from the 26 mM $CaCO_3$ and 100 µL acetic acid emulsification after washing with 60% EtOH, 10x zoom.

Even though the Span 80 was removed, the particles are individual and spherical. This indicates that the Ca-alginate microspheres were sufficiently crosslinked and remain stable even when the surfactant is removed. The EtOH-washed alginate particles did show an increase in diameter up to 100 µm, which could be assigned to swelling during washing. It must be said however that the increased transparency of the washed alginate microspheres made it difficult to find individual, perhaps smaller, particles between the mass of alginate microspheres. If these experiments were repeated, perhaps adding a surfactant which is less soluble in EtOH could assist in keeping the Ca-alginate microspheres within 20 to 60 µm particle size.

### Particle sizer

The particle sizer was used to measure 26 mM $CaCO_3$ and 100 µL acetic acid emulsification samples with three different washing steps: (1) washed twice with demiwater, (2) washed four times with demiwater, and (3) washed twice with 60% EtOH. The particle size was only measured when the concentration of sample in the isotone reached $\approx$ 5%. A lower concentration of sample was not recommended by the manufacturer. This resulted in three measurements for (1) and two measurements for (2) and (3), as there was no remaining sample for a third measurement. The graphs are presented in Figure 4.9(a-c) for the washing steps, respectively.

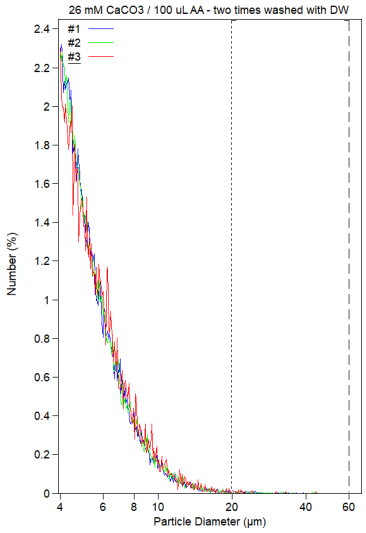


**(a)** Particle sizer results of 26 mM $CaCO_3$ and 100 µL acetic acid, two times washed with demiwater.

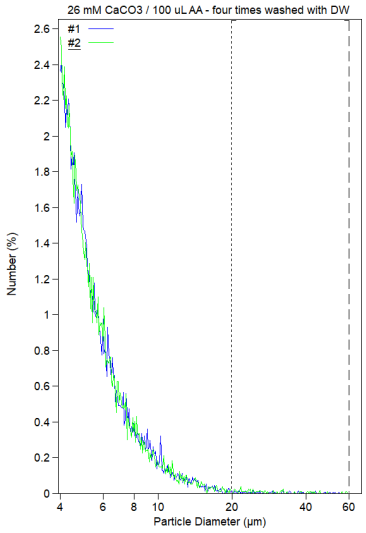


**(b)** Particle sizer results of 26 mM $CaCO_3$ and 100 µL acetic acid, four times washed with demiwater.

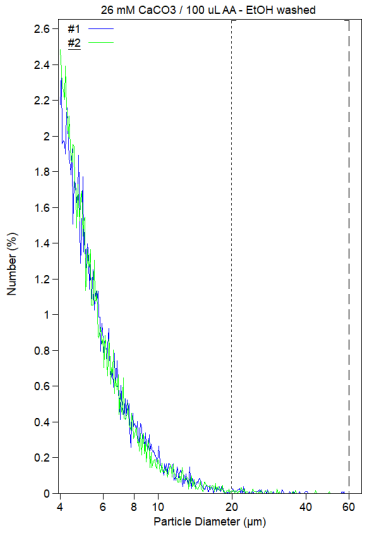


**(c)** Particle sizer results of 26 mM $CaCO_3$ and 100 µL acetic acid, two times washed with 60% EtOH.

**Figure 4.9:** Particle sizer results of the 26 mM $CaCO_3$ and 100 µL acetic acid emulsification with different washing steps: two times washed with demiwater (a), four times washed with demiwater (b), and two times washed with 60% EtOH (c).

The graphs were analysed with a lower bound of 20 µm and an upper bound of 60 µm to determine the amount of particles (in %) in this region. The results are given in Table 4.1.

**Table 4.1:** Overview of the particle sizer results for the amount of particles measured between 20 to 60 µm for the 26 mM $CaCO_3$ and 100 µL acetic acid emulsification. Samples were prepared by washing with demiwater (DW) or 60% EtOH.

| Amount of particles measured between 20 to 60 µm (%) | | | |
|---|---|---|---|
| **Sample:** | **2x DW washed** | **4x DW washed** | **EtOH washed** |
| Average | 0.17 $\pm$ 0.02 | 0.49 $\pm$ 0.08 | 0.44 $\pm$ 0.04 |
| #1 | 0.19 | 0.43 | 0.47 |
| #2 | 0.18 | 0.55 | 0.41 |
| #3 | 0.15 | | |

The measured percentage of particles between 20-60 µm is lower than 1% in the results from the particle sizer. These measured results do not compare to the imaging results of the Ca-alginate under the optical microscope. The optical microscope pictures of the sample two times washed with demiwater did show very small Span80 microparticles, which could be an explanation for the particle sizer results in Figure 4.9a. However, the optical microscope pictures of the sample washed four times with demiwater and the sample washed with 60% EtOH showed the majority of particles between 20-60 µm in size, whereas the measurements from Figure 4.9b-c do not agree with these imaging results. A possibility is the degradation of Ca-alginate particles in the isotone solution, which could degrade the microspheres and/or cause the microspheres to cluster into gel formations. Any particle size or gel formation >60 µm in size would not be measured with the aperture tube of 100 µm used in this research [66]. If further research aims to use the particle sizer again for Ca-alginate microsphere measurements, stability tests could be performed to explain the difference between the measurements and imaging results.

### 4.2.3. Results on the 52 mM $CaCO_3$ and 200 µL acetic acid emulsification

The 26 mM $CaCO_3$ and 100 µL acetic acid experiments showed promising results on particle formation, which resulted in the question whether doubling both the molarity and acetic acid quantity would have an effect on particle formation.

During crosslinking, the 52 mM $CaCO_3$ and 200 µL acetic acid emulsion created a thin film on top of the emulsion compared to the 26 mM $CaCO_3$ and 100 µL acetic acid emulsion. Even at the highest rpm, this film would remain on top and was not included in the vortex, indicating an unwanted gelation. Not surprisingly, this experiment showed visual gel-like structures after the emulsion was collected and washed in the tubes. The optical microscope pictures are presented in Figure 4.10, accompanied by Appendix B.2.

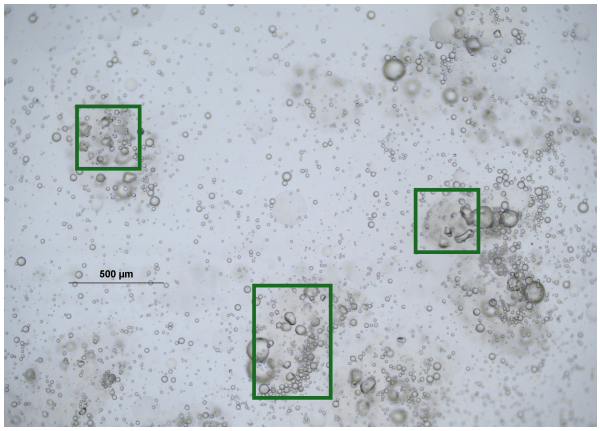


**(a)** 52 mM $CaCO_3$ and 200 µL acetic acid, 4x zoom. Several alginate gel formations are indicated with green squares.

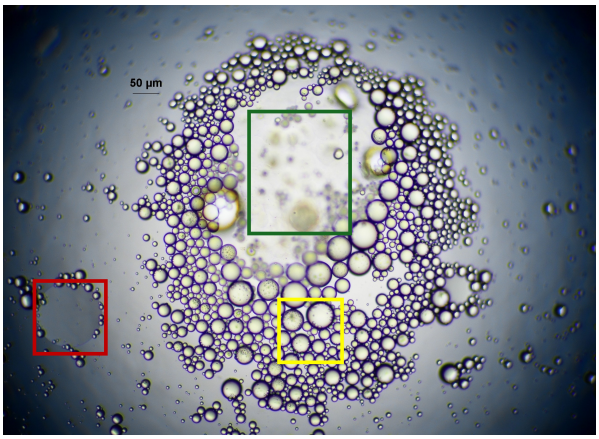


**(b)** 52 mM $CaCO_3$ and 200 µL acetic acid, 10x zoom. Several individual Ca-alginate particles are indicated with a yellow square. An alginate gel formation is indicated with a green square. An oil-droplet is indicated with a red square.

**Figure 4.10:** Optical microscope pictures of the 52 mM $CaCO_3$ and 200 µL acetic acid emulsification.

Several individual Ca-alginate microspheres are indicated with a yellow square in Figure 4.10b. These particles are characterized by their black-grey edges, caused by Span 80, and resembled the reference literature from Figure 4.6. Their colour is a sheen green at 10x zoom and the surface of the Ca-alginate microspheres present moon-crater like morphology, as shown at 40x zoom in Figure 4.11, indicated with yellow arrows. The microsphere diameters ranged between 5 and 50 µm.

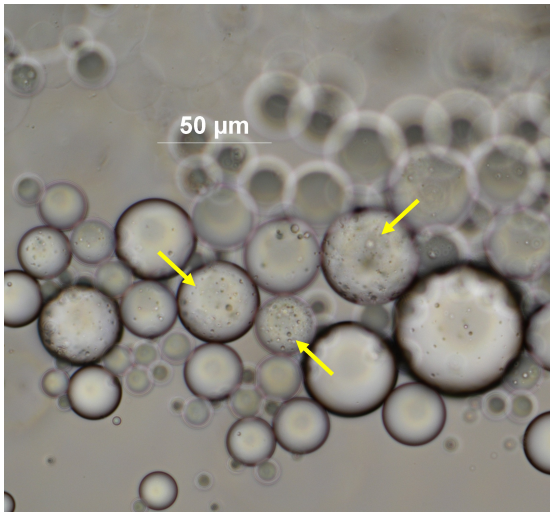


**Figure 4.11:** Optical microscope picture at 40x zoom of the 52 mM $CaCO_3$ and 200 µL acetic acid emulsification. The moon-crater surface structure of alginate microspheres is indicated with yellow arrows.

The optical microscope pictures also show major crosslinking of alginate into gel formations, indicated with green squares in Figure 4.10a-b. Figure 4.12a shows one of these alginate gel formations indicated with a green square, which is surrounded by individual alginate particles. Figure 4.12b has been edited post-production to show the typical iridescent sheen of oil on water, and the oil droplet surface is indicated with a red circle. Alginate microspheres are clustered around the surface of the oil-droplet. This clustering can be explained by the surfactant properties, as Span 80 has a hydrophilic-lipophilic balance (HLB) of 4.3 [87]. On the HLB scale, a

value of zero means the surfactant is completely lipophilic, while a value of twenty means the surfactant is completely hydrophilic. Span 80 shows lipophilic properties, where it is highly soluble in oil and organic solvent, but dispersible in water. An oil droplet will therefore attract the Span 80 alginate microspheres, resulting in the picture of Figure 4.12b.

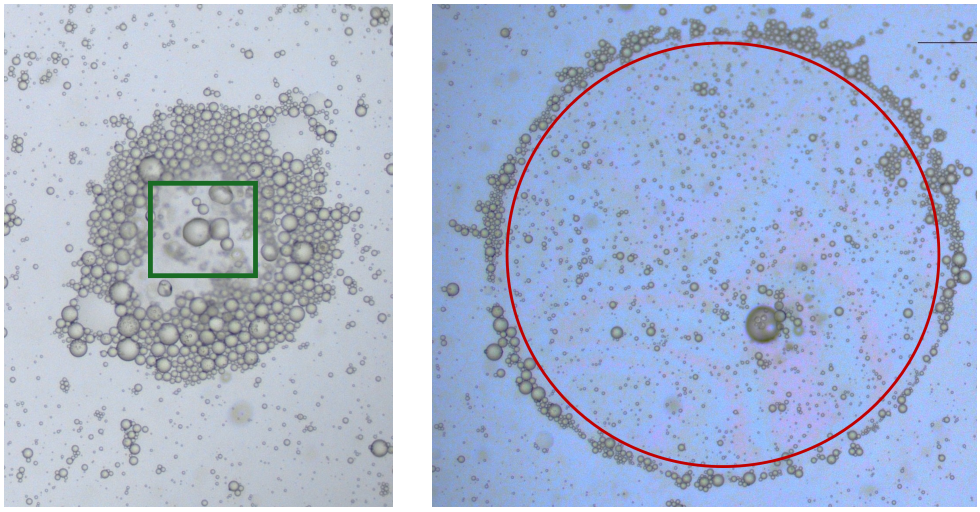

**(a)** Gel formation, indicated with a green square, can be seen surrounded by individual alginate microspheres.

**(b)** Individual alginate microspheres collect on the surface of an iridescent oil droplet, indicated with a red line.

**Figure 4.12:** Optical microscope pictures of a gel formation (a) and an oil-droplet (b) in the 52 mM $CaCO_3$ and 200 µL acetic acid emulsification.

It can be concluded that the emulsification of 52 mM $CaCO_3$ and 200 µL acetic acid resulted in individual alginate microspheres with promising particle size, but the alginate mostly crosslinked into gel formations.

### 4.2.4. Results on the 26 mM $CaCO_3$ and 200 µL acetic acid emulsification

The emulsification method was performed using 26 mM $CaCO_3$ with 200 µL acetic acid to investigate the influence of acetic acid on particle formation. After washing with demiwater, the solution visually contained less gel formation than its 52 mM $CaCO_3$ counterpart, and the colour was milky throughout the tube. The result under the optical microscope is presented in Figure 4.13.

In the 26 mM $CaCO_3$ with 200 µL acetic acid emulsification, the alginate microparticles were again characterised by a black Span 80 border. The alginate crosslinked into individual particles, without significant gel formation compared to the 52 mM $CaCO_3$ with 200 µL acetic acid emulsification. Figure 4.13c once more shows a collection of alginate microspheres around oil-droplets, indicated by red squares, due to the lipophilic properties of Span 80. The majority of measured particle size was in range of 10 to 60 µm, which comes close to the favoured range of 20 to 60 µm, but particles $<$10 µm were also present.

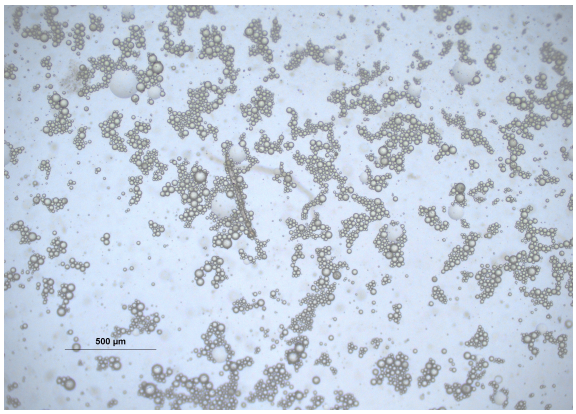


**(a)** 26 mM $CaCO_3$ and 200 µL acetic acid, 4x zoom.

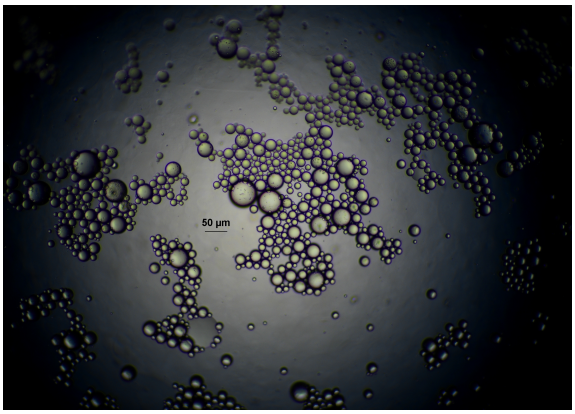


**(b)** 26 mM $CaCO_3$ and 200 µL acetic acid, 10x zoom.

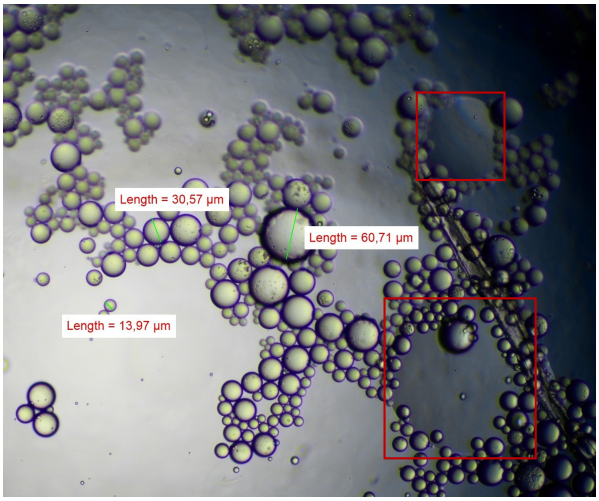


**(c)** 26 mM $CaCO_3$ and 200 µL acetic acid, 10x zoom. Oil droplets are indicated with red squares.

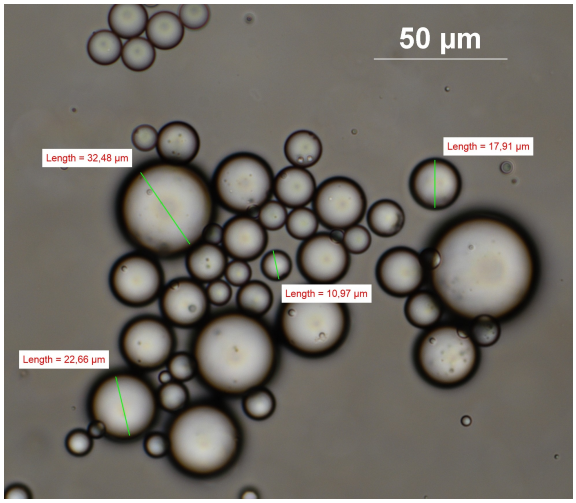


**(d)** 26 mM $CaCO_3$ and 200 µL acetic acid, 40x zoom.

**Figure 4.13:** Optical microscope pictures of the 26 mM $CaCO_3$ and 200 µL acetic acid emulsification.

Compared to the 26 mM $CaCO_3$ and 100 µL acetic acid experiments from Section 4.2.2, the doubled acetic acid quantity concluded in no direct remarks on the morphology or size of the Ca-alginate microspheres. As the desired size range of 20 to 60 µm could already be reached using 26 mM $CaCO_3$ with 100 µL acetic acid, these parameters were concluded to be optimal. It could be however interesting for further research to compare 100 µL to 200 µL acetic acid amount in terms of stability and hardness of the Ca-alginate microspheres. As already discussed in the extrusion dripping method, Section 4.1.2, a higher $Ca^{2+}$ concentration during crosslinking presents increased gel strength. A study by Pathak et al. investigated the effect of calcium-ion concentration on Ca-alginate characteristics. This study concluded that alginate crosslinked with higher concentration of calcium was more thermally more stable. The optimal acetic acid quantity for releasing $Ca^{2+}$ could be investigated by keeping the $CaCO_3$ concentration the same and adjusting the acetic acid volume. In the application of Ca-alginate towards radioembolisation, an optimal value of calcium crosslinked in the alginate structure could maximize the loading efficiency of holmium in the alginate. The comparison of acetic acid quantity versus the release of calcium for crosslinking was not of further interest, due to time restriction and the priority to moving on to holmium-calcium exchange experiments.

### 4.2.5. Evaluation of centrifuge settings

In the final stages of the emulsification method experiments, samples tubes had been left to settle for a couple days. These settled tubes showed a better separation of alginate than when the tubes were centrifuged during the emulsification experiments washing steps. The alginate had now formed a distinct white-coloured layer at the bottom of the tube, with a clear layer of demiwater on top. This discovery led to the revisiting of the 26 mM and 100 µL acetic acid emulsification samples from Figure 4.5 under the optical microscope to investigate the centrifuge settings. For this, one of the settled tubes was shaken and centrifuged. Optical microscope pictures were taken of the top layer of the centrifuged tube and of the top layer of a settled tube. The results are presented in Figure 4.14.

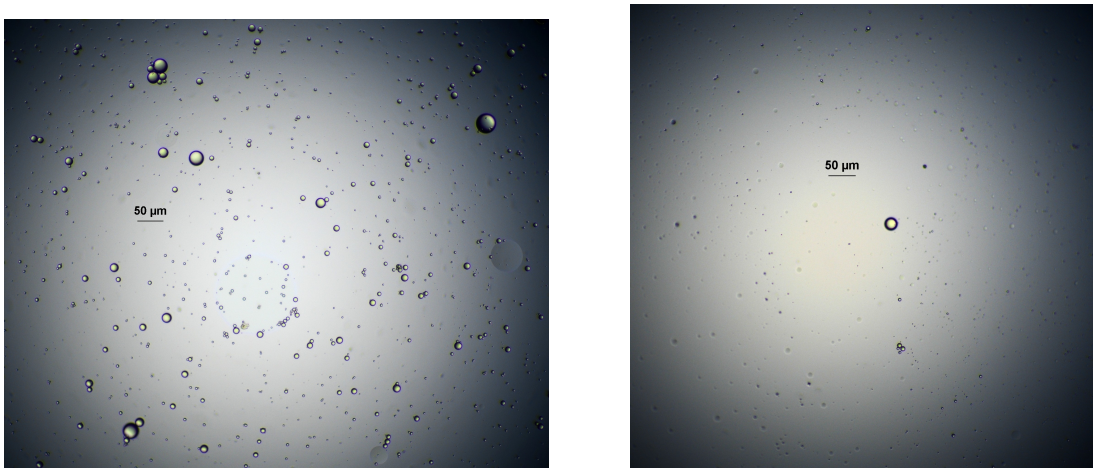


**(a)** Top layer of the centrifuged tube, 10x zoom.

**(b)** Top layer of the settled tube, 10x zoom.

**Figure 4.14:** Optical microscope pictures of the top layer of two sample tubes from the 26 mM $CaCO_3$ and 100 µL acetic acid emulsification; shaken and centrifuged (a); settled for a couple days (b).

It can be said that settlement was more successful in collecting alginate microspheres at the bottom of the tube. The settled top layer barely showed any alginate compared to the centrifuged top layer. The inefficiency of the centrifuge was further confirmed when the supernatant of the demiwater washing steps was analysed under the optical microscope. A picture of this supernatant is presented in Figure 4.15, showing a significant presence of Ca-alginate microspheres. This research was neither focused on the efficiency of washing nor the efficiency of microparticle collection, but it can be concluded that the centrifuge settings need to be revisited for future research. Especially towards production of alginate microspheres for radioembolisation, it is important to maximize the collection of particles from the emulsification method.

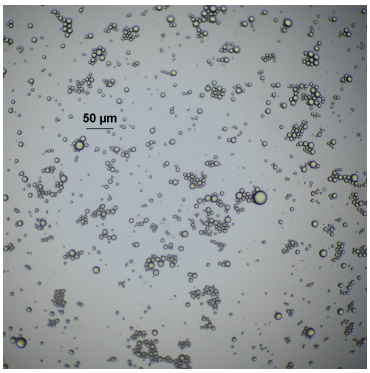


**Figure 4.15:** Optical microscope picture of the supernatant from the demiwater washing step in the 26 mM $CaCO_3$ and 100 µL acetic acid emulsification, 10x zoom.

## 4.3. Calcium-holmium exchange experiments

Crosslinking alginate with $Ho^{3+}$ was first attempted using stable $HoCl_3$. Without radioactivity, the Ho-alginate microspheres could be analysed under the optical microscope as well as under the SEM. Adding stable holmium directly to the emulsion was investigated for whether the trivalent cations had an influence on particle formation during internal crosslinking, and the results are discussed in Section 4.3.1.

However, alginate microspheres have to be crosslinked with radioactive holmium if they are destined for radioembolisation. If radioactive holmium was directly added to the emulsion, the 2.5 hour crosslinking time with washing steps would decrease the therapeutic activity significantly. In terms of radiation exposure, a radioactive emulsification with washing steps increases the exposure risk for radiation personnel involved. Instead, the alginate particles can be synthesized first by crosslinking with calcium. Then, the readily synthesized Ca-alginate microspheres are added to a bath of dissolved radioactive holmium solution. Here, calcium ions in the microsphere structure are exchanged with holmium ions, resulting in radioactive Ho-loaded alginate microspheres.

The experiments on exchange of Ca-alginate microspheres in a holmium bath were first carried out using stable holmium, discussed in Section 4.3.1. When the right concentration of the exchange bath was found, $Ho(NO_3)_3$ was irradiated to continue with radioactive exchange experiments. Here, the loading efficiency of alginate microspheres was determined in Section 4.3.2.

### 4.3.1. Crosslinking experiments using stable holmium

Two types of experiments were performed for the crosslinking of alginate with stable holmium: (1) Adding $HoCl_3$ stock solution into the emulsion, and (2) using synthesized Ca-alginate microspheres from previous emulsification experiments into a bath of $HoCl_3$ of different molarities.

#### Adding $HoCl_3$ to the emulsion

In this method, $HoCl_3$ was added during emulsification into the crosslinking bath to create a molar ratio of Ca:Ho of 50:1. The emulsification was done using 26 mM $CaCO_3$ and 100 µL acetic acid. The optical microscope pictures are presented in Figure 4.16. Alginate particles with a black Span80 border are seen in Figure 4.16a, indicated with yellow squares, with oil droplets present in the solution indicated with red squares. In Figure 4.16b, indicated with yellow squares, the alginate microspheres have lost their black Span 80 border and are more see-through. Both types of particles were spherical, with particle sizes in the same range as previously discussed Ca-alginate microspheres.

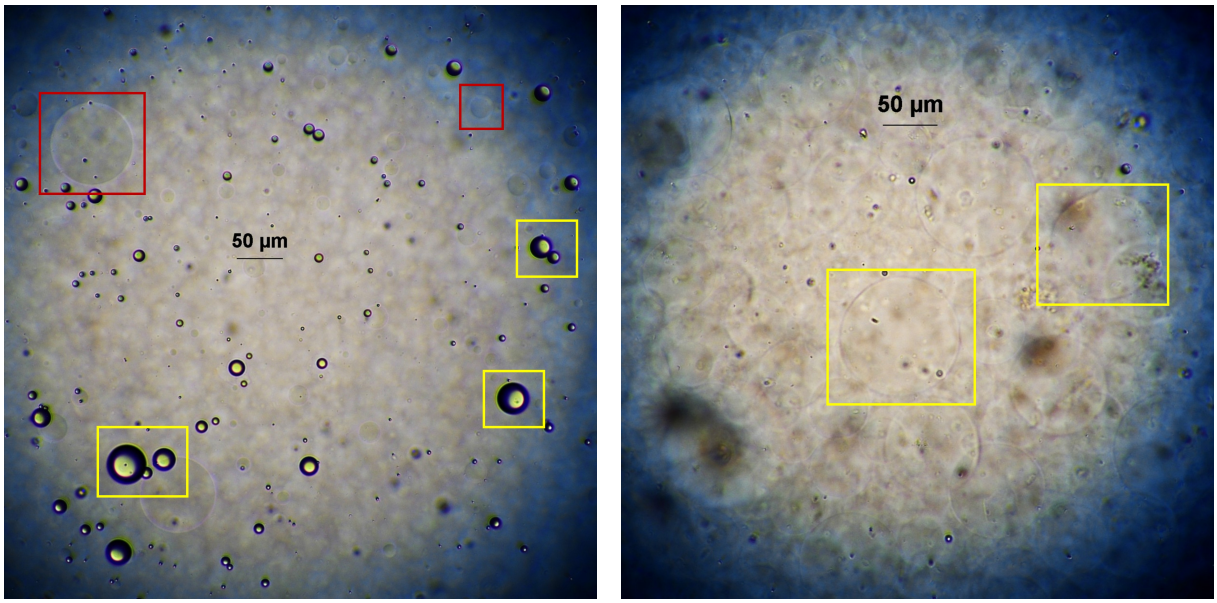


**Figure 4.16:** Optical microscope pictures at 10x zoom of the crosslinking experiments where $HoCl_3$ is directly added to the emulsion. Alginate microspheres are indicated with yellow squares. Oil-droplets are indicated with red squares.

For SEM analysis, a scoop of the sample was placed on the stub. As the alginate microparticles can not be seen with the naked eye, it was deemed unfeasible in terms of time to try to obtain individual particles on a SEM stub. As the alginate sample fused during air drying, this research does not include analysis on the size or surface of individual microspheres, nor the distribution of holmium within a single alginate microsphere. The SEM with EDS was only used to draw conclusions about the presence of holmium, and therefore whether the designed holmium crosslinking or exchange method was successful.

Several spots on the samples were checked for their elemental composition in EDS. A SEM image and its elemental analysis of one of these spots can be found in Figure 4.17. The elemental mapping on calcium shows that the particles seen on the SEM image are not linked to individual Ca-alginate microspheres, but rather impurities that collected during air-drying. The scoop of sample dried into a plaque of alginate on the carbon tape, which confirms the difficulty of trying to analyse individual alginate microspheres under the SEM. A calcium peak around 3.7 keV together with a sodium peak around 1 keV showed up on the elemental spectrum, but a holmium peak was missing. From here, it can be concluded that this method of crosslinking with holmium was unsuccessful, and the holmium was likely washed away in the process. Crosslinking could be improved with higher Ca:Ho ratios in the emulsion. However, in this research process parameters were not further investigated due to time restriction in favour of holmium exchange using synthesized Ca-alginate microspheres.

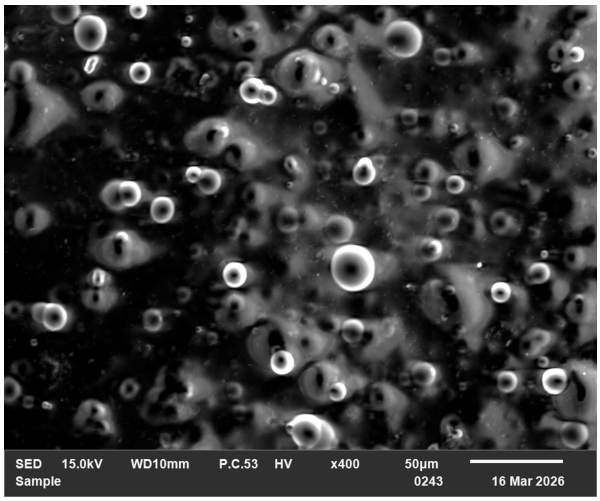


**(a)** SEM image at 400x zoom.

**(b)** EDS mapping of calcium from the SEM image.

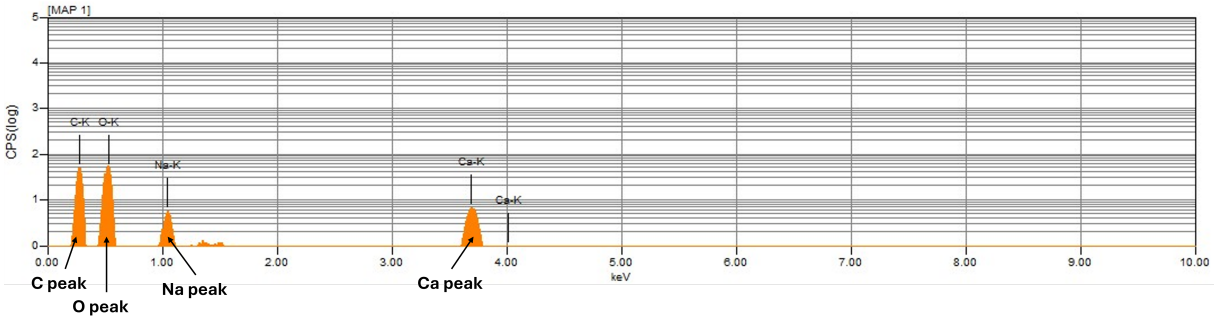


**(c)** EDS spectrum of the SEM image.

**Figure 4.17:** SEM image (a), its EDS mapping on calcium (b), and its EDS spectrum (c) of the 26 mM $CaCO_3$ and 100 µL acetic acid emulsification with $HoCl_3$ added to the crosslinking bath.

### Exchange of calcium with holmium using synthesized Ca-microspheres

For the exchange of calcium with stable holmium in synthesized Ca-alginate, the microspheres from the 26 mM $CaCO_3$ with 100 µL acetic acid emulsion experiments were used. This exchange method was done using a $HoCl_3$ bath at four different molarities: 26 mM, 2.6 mM, 260 µM and 26 µM. There is no data reported in literature related to using holmium to exchange with calcium in internal gelation experiments. There is, however, reported data related to external gelation with a $HoCl_3$ crosslinking bath of 5.0 mM, 25 mM and 100 mM [12, 13, 88]. Also, previous unpublished research at the research department had experimented with external gelation crosslinking baths at 6, 8, 10 and 20 mM holmium [76]. These baths were prepared by combining irradiated $Ho(NO_3)_3$ and stable $HoCl_3$. The reported molarities and previously used 26 mM $CaCO_3$ crosslinking bath provided a starting point for these experiments. In this research, 26 mM $HoCl_3$ was the highest concentration used. Lower concentrations were further explored to determine the optimal Ho-loading without affecting the morphology of the microspheres.

*Unwashed Ho-exchange experiments*

For every $HoCl_3$ concentration, the exchange bath was separated into two tubes. One tube was washed with demiwater to remove ions that were not crosslinked with alginate. The other tube was left unwashed, where the process of ion-exchange in the alginate microspheres continued in the tube. The unwashed tube was analysed to determine the impact of longer ion-exchange on the alginate microspheres. At the time of optical microscope analysis, the ion-exchange in the unwashed tubes had continued for at least 4 hours. Their pictures are provided in Appendix C.1, where a yellow colour at higher concentrations is caused by dissolved $HoCl_3$.

Unwashed sample of 26 mM and 2.6 mM $HoCl_3$ showed deformed particles or alginate debris instead of well-defined alginate microspheres. The 260 µM and 26 µM concentrations still contained alginate particles, but these appeared less spherical. The 260 µM samples also showed clustering of alginate particles into gel formations. From these results it can be concluded that washing the samples from the exchange bath with demiwater is essential in preserving the alginate microspheres in the solution, especially at higher holmium concentrations. For future research plans on investigating the exchange time versus loading efficiency, it is recommended to set intervals at ≤30 minutes when using higher holmium concentrations.

*Ho-exchange experiments washed with demiwater*
For the tubes washed with demiwater, the samples were analysed under the optical microscope and the SEM. The optical microscope pictures for the $HoCl_3$ exchange baths of 26 mM, 2.6 mM, 260 µM and 26 µM are presented in Figure 4.18a-d, respectively. The full picture collection can be found in Appendix C.2.

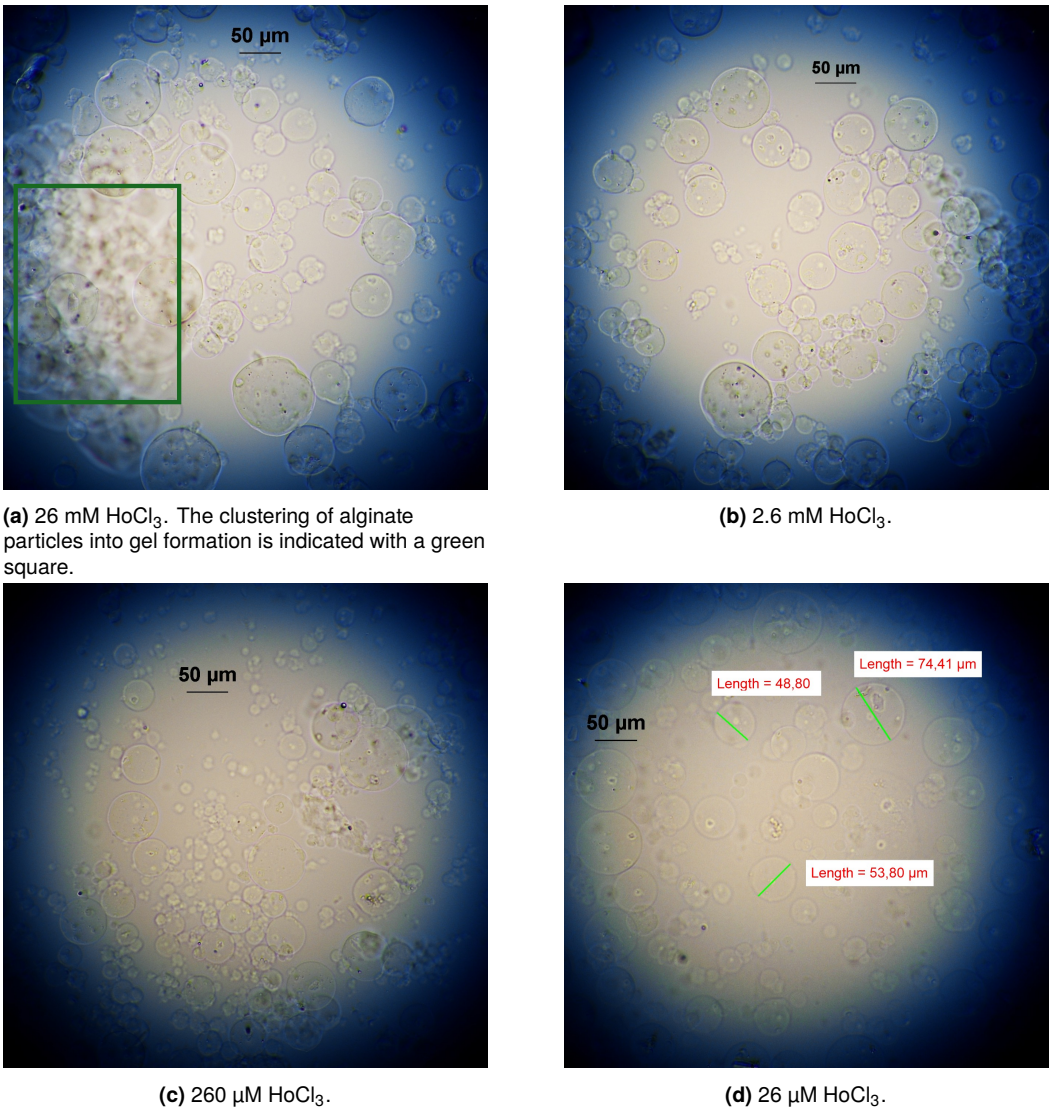


**(a)** 26 mM $HoCl_3$. The clustering of alginate particles into gel formation is indicated with a green square.

**(b)** 2.6 mM $HoCl_3$.

**(c)** 260 µM $HoCl_3$.

**(d)** 26 µM $HoCl_3$.

**Figure 4.18:** Optical microscope pictures of the exchange experiments washed with demiwater, using 26 mM, 2.6 mM, 260 µM and 26 µM $HoCl_3$ (a-d, respectively).

At 26 mM $HoCl_3$ the optical microscope images show clustering of alginate microspheres into large gel formations, indicated with a green square in Figure 4.18a. Most alginate microparticles in this sample have collapsed into irregular particle structures, and the surface of particles

became rough. When lowering the concentration to 2.6 mM $HoCl_3$, the clustering of alginate microspheres into gel formations is decreased significantly. The alginate particles are better defined, but their shape and surface remain mostly irregular. At 260 µM $HoCl_3$ the microspheres remain small and mostly well-defined, but irregular shaped particles below 50 µm are common here. Moving to 26 µM $HoCl_3$, the irregularity in shape and surface disappears. The alginate microspheres show minimal clustering, and non-clustered microparticles are spherical with smooth surface. The general particle size is between 20 to 60 µm, with outliers up to 100 µm.

The exchange experiments washed with demiwater were analysed using the SEM with EDS. The SEM images at 30x zoom in Figure 4.19 show how the scoops of alginate gel dried on the stubs. At 26 mM and 2.6 mM $HoCl_3$ concentration, the sample visibly cracks on the carbon tape. For 260 µM and 26 µM $HoCl_3$ concentration, the alginate sample is presented as a plaque on the carbon tape, still pulling on the carbon tape at the edges while it dries.

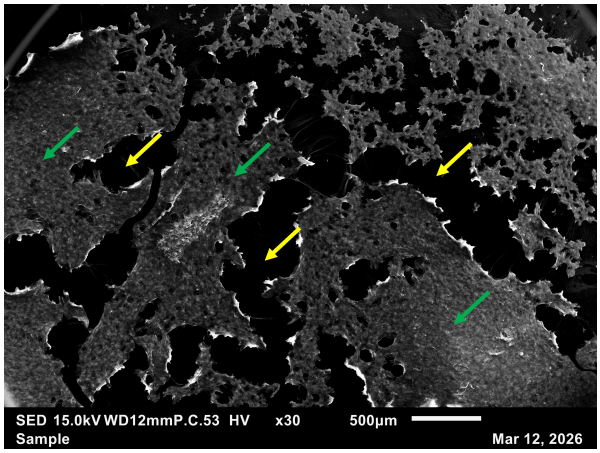


**(a)** 26 mM $HoCl_3$.

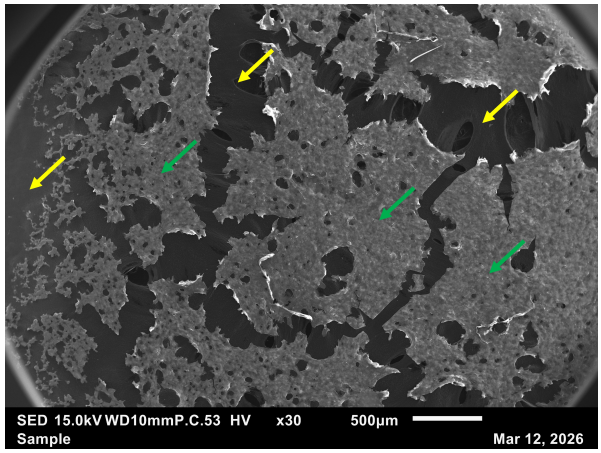


**(b)** 2.6 mM $HoCl_3$.

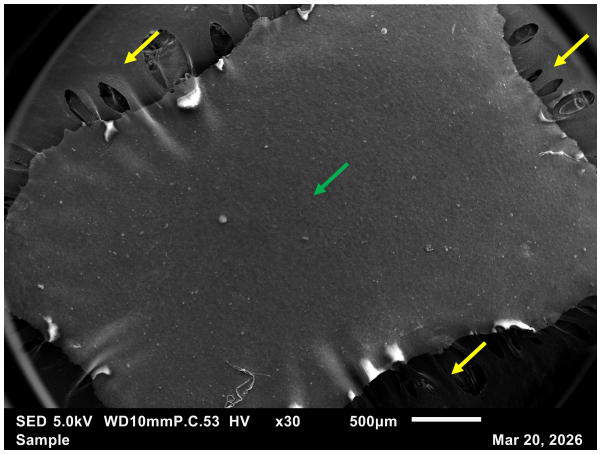


**(c)** 260 µM $HoCl_3$.

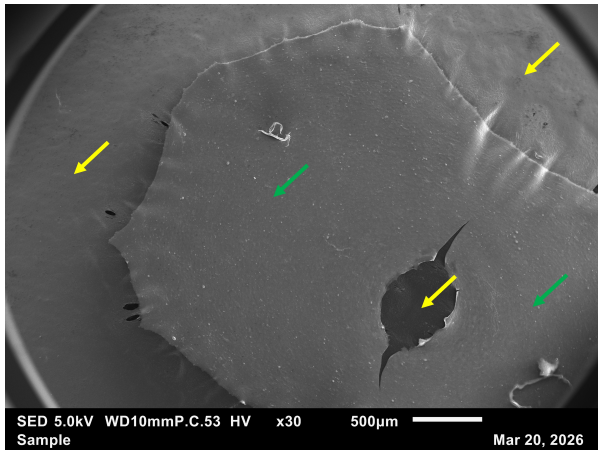


**(d)** 26 µM $HoCl_3$.

**Figure 4.19:** SEM images at 30x zoom of alginate sample from the exchange experiments for different $HoCl_3$ concentrations. Area of carbon tape is indicated with yellow arrows. Alginate sample areas are indicated with green arrows.

EDS was used to determine the presence of holmium in the samples. Pictures were taken at different spots on the sample, and element quantifications were obtained on carbon, oxygen, chloride, calcium and holmium. For every $HoCl_3$ concentration, the EDS average mass% of calcium, chloride and holmium is presented in Table 4.2. The average mass% is presented as n.a. when the EDS did not indicate atom presence in the sample, or if atom presence was not obtained for at least three images. The average mass% of holmium against different exchange bath concentrations are presented in Figure 4.20. The complete dataset can be found in Ap-

pendix C.3. The data in the appendix further proves why EDS quantifications should only be used as an indication of presence and not as a definite conclusion on the composition of the alginate. Namely, two separate measurements at the same location on the 26 mM $HoCl_3$ sample gave different EDS quantifications.

**Table 4.2:** Average mass% of calcium, chloride and holmium obtained from the EDS analysis of the exchange experiments using different $HoCl_3$ exchange bath concentrations.

| Average mass% | **26 mM** | **2.6 mM** | **260** µM | **26** µM | **HoCl3** |
|---|---|---|---|---|---|
| Ca | n.a. | n.a. | 4.24 | 5.74 | |
| Cl | 0.69 | 0.05 | n.a. | n.a. | |
| Ho | 15.73 | 8.42 | 6.32 | 1.76 | |

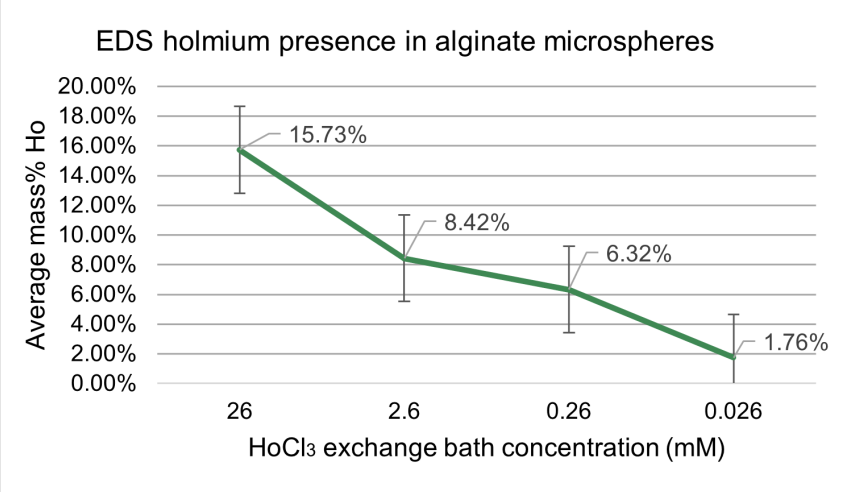


**Figure 4.20:** Graph of the holmium presence in EDS analysis of alginate microspheres, showing the average Ho mass% against the concentrations of the $HoCl_3$ exchange bath.

The elemental analysis shows no plateau of the average mass% of holmium in the alginate microspheres when the ion-exchange process is performed using different $HoCl_3$ concentrations. This indicated that the holmium content in the alginate microspheres is directly related to the $HoCl_3$ concentration. It was also found that chloride quantity increases with increasing $HoCl_3$ concentration, indicating that chloride ions can be ionically bound to the holmium ions in the alginate structure.
On the other hand, the calcium quantity decreases with increasing $HoCl_3$ concentration, and disappears completely at ≥2.6 mM $HoCl_3$ in the EDS analysis. In the exchange bath, both calcium and holmium are in competition for the binding sites in the alginate structure. An excess of holmium therefore shifts the equilibrium towards holmium and decreases the amount of calcium in the alginate. The optical microscope pictures at ≥2.6 mM $HoCl_3$, Figure 4.18a-b, showed collapsed microspheres with gel formation, but when the $HoCl_3$ concentration was decreased, the sphericity of the particles increased. A study by Pathak et al. reported on the effect of calcium concentration on alginate beads in terms of surface morphology and thermal stability [89]. It was concluded that increasing calcium concentrations gave increasingly dense bead surface with less pores, and thermal stability increased with increasing calcium concentration. These results indicate calcium is a necessary component in the stability of alginate microspheres. The EDS analysis on calcium can also explain the change of morphology of the alginate gel SED images from Figure 4.19. Calcium alginate beads reportedly dry through the surface of the particles while moisture is trapped inside [90]. As calcium content increases, the surface becomes dense with crosslinker and the particles become less prone to dehydration, leading to

a gel plaque on the carbon tape. When calcium content decreases due to increasing holmium content, the alginate gel can dehydrate and crack on the carbon tape while air-drying. Further research towards Ho-alginate particles for liver embolisation should therefore investigate the balance between calcium content and holmium loading in the microspheres. An ideal $HoCl_3$ concentration exchange bath should provide a holmium loading content for maximum radiation dose, while the alginate microparticles contain enough calcium content to remain spherical with a smooth surface.

As the microspheres were spherical and more intact using a 26 µM $HoCl_3$ exchange bath compared to higher concentrations, it was decided that the radioactive loading efficiency experiments should be carried out using a 26 µM $^{166}Ho(NO_3)_3$ bath.

### 4.3.2. Exchange experiments using radioactive holmium and loading efficiency

The loading efficiency of holmium into the alginate microspheres was determined by performing the ion-exchange process of calcium with Ho-166. These experiments were performed with an exchange bath of 10 mL 26 µM irradiated $Ho(NO_3)_3$ and 2 mL of synthesized Ca-alginate microsphere solution from the 26 mM $CaCO_3$ and 100 uL acetic acid emulsification. Ion-exchange time in this research was set at 30 minutes. The loading experiments were done in triplo.

The average loading efficiency was found to be (86.5 $\pm$ 1.4)% from these experiments. This can be considered an excellent loading efficiency percentage. The loading efficiency of $^{166}$Ho-alginate microspheres in ion-exchange has only been investigated by Zielhuis et al. up until now. This study used a 3 mL exchange bath at 7 µM Ho-166, and exchanged 2.5 g of Ca-alginate microspheres for 3 hours. The loading efficiency using these parameters was reported at (96 $\pm$ 2)% [12]. It must be noted however, that Zielhuis et al. produced Ca-alginate microspheres using the extrusion method, with external gelation. Externally gelated microspheres have a higher concentration of $Ca^{2+}$ on the surface of the microspheres, which could positively affect loading efficiency in ion-exchange. Therefore, this research should not be directly compared with the results from Zielhuis et al.
An extended ion-exchange time could have a positive effect on the loading efficiency, but this research was prevented due to time restriction. Nevertheless, the obtained loading efficiency was considered high enough to continue with stability experiments.

When all Ho-166 had decayed, the Ho-alginate microspheres were analysed under the optical microscope. The full picture collection can be found in Appendix C.4, of which one picture is presented in Figure 4.21. The general particle size was between 20 to 60 µm with outliers up to 100 µm, and the morphology was spherical and see-through. These results correspond to the optical microscope analysis from the stable holmium exchange in Section 4.3.1, Figure 4.18d. In radioembolisation, the particles need to keep their structure until the maximum radiation dosage is given to a patient and all radioactivity has decayed. The results under the optical microscope indicate that the radioactivity did not affect the alginate particle morphology in the exchange experiments. However, this research used a maximum activity of 4.5 MBq, whereas diagnostic or therapeutic applications reach activity levels of GBq. Future research in exposure time at different activity levels of Ho-166 could give insight on the radiation stability of the Ho-alginate microspheres. This research further focused on the radiochemical stability of Ho-alginate microspheres.

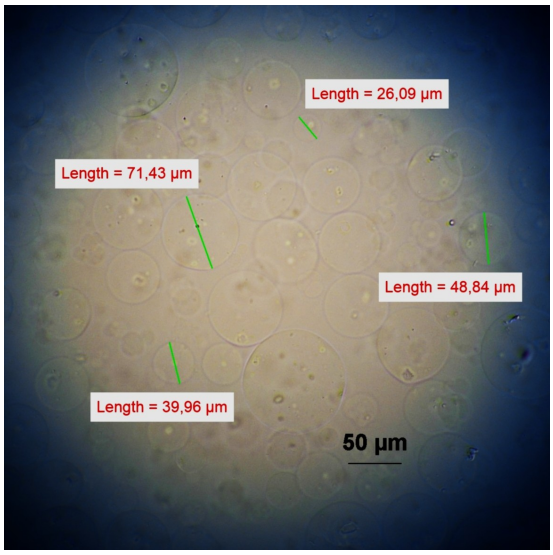


**Figure 4.21:** Optical microscope picture of the Ho-alginate microspheres from the radioactive holmium exchange experiments.

## 4.4. Stability experiments using radioactive holmium

$^{166}$Ho-microspheres destined for liver embolisation radiotherapy should have a high *in-vivo* stability to ensure no leakage of radioactive substance into the bloodstream of a patient. The stability of $^{166}$Ho-alginate microspheres was studied once before by Zielhuis et al. [12]. This study reported a radiochemical stability of (94 $\pm$ 2)% after incubation in human serum at 37°C for 48 hours. In the experiments of this research, a solution of 0.9% NaCl was used to study *in-vivo* stability of the $^{166}$Ho-alginate microspheres. This type of saline solution is often used in medicine, as a 0.9% NaCl solution represents a physiological environment [91].

The stability experiments were done using the $^{166}$Ho-alginate microspheres of the three samples from the loading efficiency experiment. In the first sample, 30 mL demiwater was added. In the second and the third sample, 30 mL 0.9% NaCl was added. After 5 minutes, 30 minutes, 1 hour, 3 hours and 24 hours, the solutions were centrifuged and supernatant was taken. The stability of the $^{166}$Ho-microspheres was determined through the retention of Ho-166, calculated using Equation 3.2. The calculated retention for every sample is presented against the time in Figure 4.22. It must be noted that the loading efficiency experiments and stability experiments are two separate methods with separate Wallac gamma counter measurements. Their standard deviation remains unknown and therefore their values should be compared carefully.

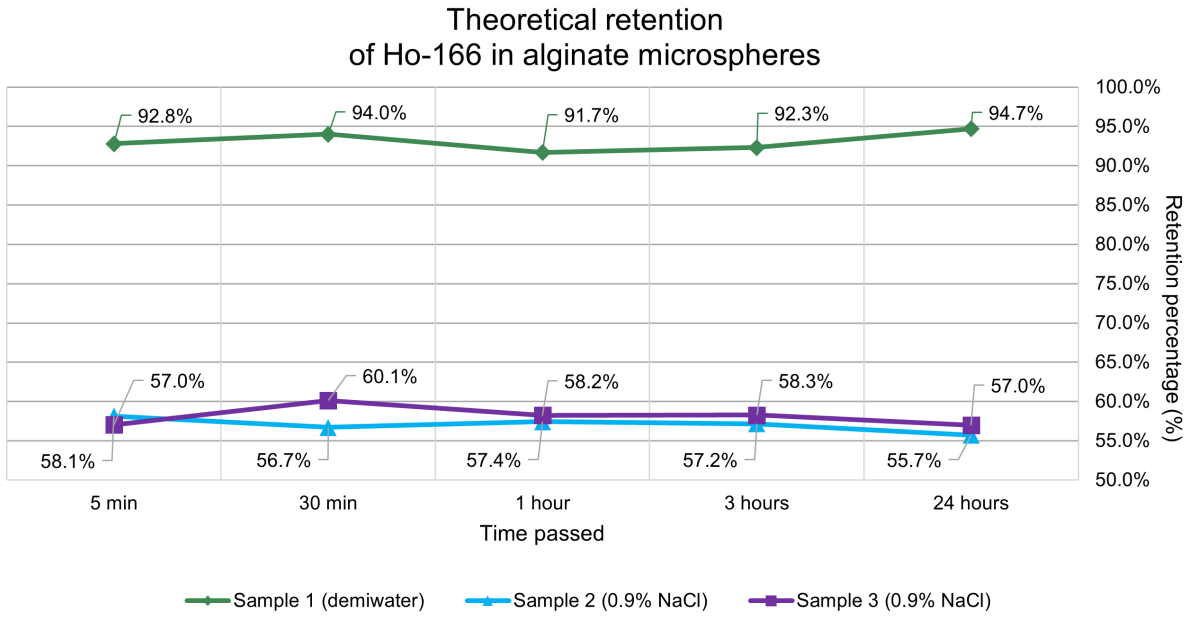


**Figure 4.22:** Graph of the retention percentage of Ho-166 in alginate microspheres from stability experiments with demiwater or 0.9% NaCl.

For the sample in demiwater, the retention percentage remains above 90% and stable even after 24 hours, showing excellent stability of the Ho-alginate microspheres. The graph shows a significant drop in retention after five minutes when 0.9% NaCl solution is added to the Ho-alginate. The retention percentage stabilizes between 50-60% for up to 24 hours afterwards. This indicated that the Ho-alginate microspheres were affected, but not completely disintegrated. As discussed previously in the extrusion method Section 4.1, the rate of degradation of alginate increases below pH 7, as reported by Haug et al. [72]. Human serum, as used in the stability tests by Zielhuis et al., will have a pH between 6.5 to 9.0 [12, 92]. The 0.9% NaCl solution had a pH of 5.45, which can influence the structure of alginate. This could lead to leakage of Ho-166 as the alginate structure degrades, but does not explain why only a part of the alginate microspheres is affected.

When all Ho-166 had decayed, the samples were analysed under the optical microscope. Imaging of the 0.9% NaCl samples proposed difficult, as the Ho-alginate was significantly more see-through than the microspheres in demiwater. Post-production editing was done in an attempt to visualize the microspheres in this report, and the results are presented in Figure 4.23. The full picture collection can be found in Appendix C.5. In accordance to the retention percentage results, the amount of Ho-alginate microspheres has decreased under the optical microscope. The alginate microspheres that remain are still spherical, and their morphology corresponds to the images from the stable holmium exchange in Figure 4.18d and the radioactive holmium exchange in Figure 4.21.

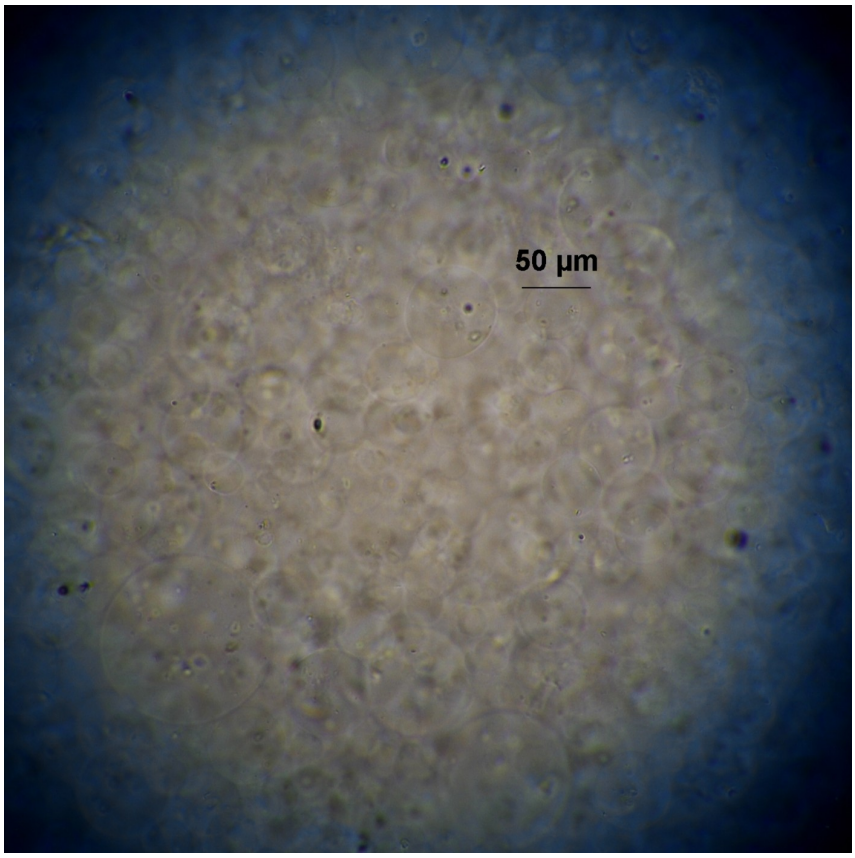


**(a)** Ho-alginate microspheres after demiwater stability experiments.

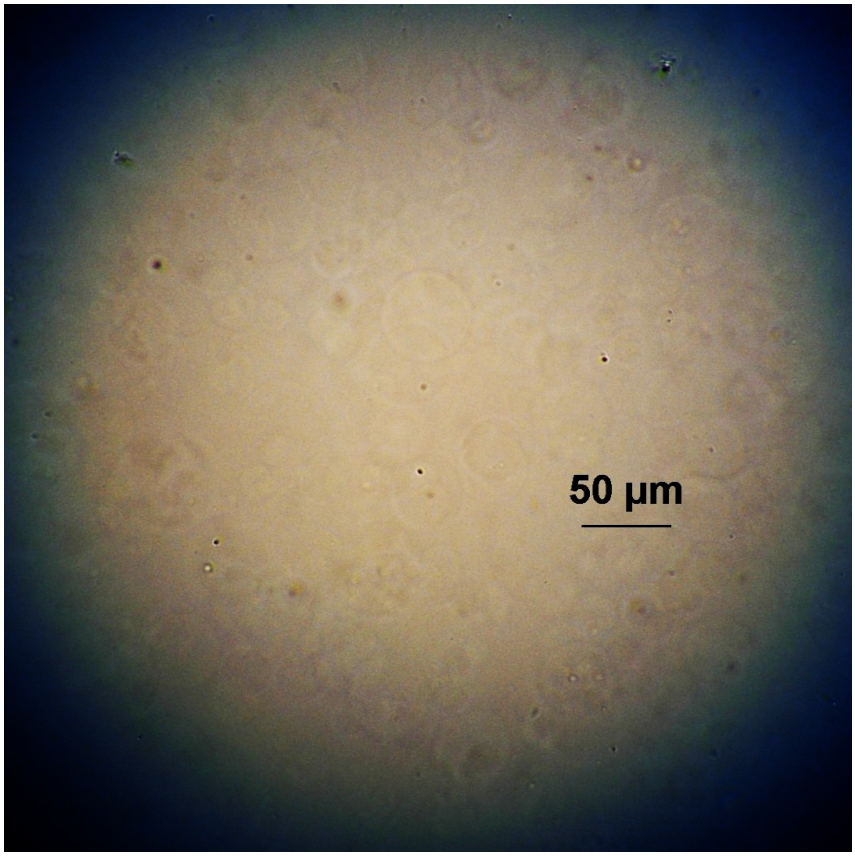


**(b)** Ho-alginate microspheres after 0.9% NaCl stability experiments.

**Figure 4.23:** Optical microscope pictures of the Ho-alginate microspheres after stability experiments with demiwater (a) and 0.9% NaCl (b).

# 5

# Conclusion

In search of a new type of radioembolic device for transarterial radioembolisation, the combination of alginate as carrier material with Ho-166 was proposed. The alginate microspheres can be loaded with Ho-166 in an ion-exchange process, and would provide a non-permanent embolisation solution. Ho-166 provides adequate radiation dose, has a favourable half-life, and can be imaged using Single Photon Emission Computed Tomography and Magnetic Resonance Imaging.

The aim of this research was first of all to investigate particle formation of alginate microspheres. Experiments were performed with two production methods, namely extrusion dripping method (1) and emulsification method (2). This research also investigated the ion-exchange process for replacing calcium in the alginate structure with holmium. The loading efficiency was investigated through ion exchange with Ho-166. Lastly, this research included experiments on the radiochemical stability of the produced $^{166}$Ho-alginate microspheres in demiwater and 0.9% NaCl solution.

### Production of alginate microspheres

In the extrusion dripping method, the effect of pH on alginate particle formation was studied. Analysis of particle size was difficult to obtain, as alginate mostly crosslinked into gel formation instead of individual particles. It was found that pH 4 offered the best conditions to produce spherical alginate particles with smoother surface morphology and smallest particle size. On the other hand, particles at pH 9 had a wrinkled surface. The majority of alginate at pH 7 crosslinked into viscous gel formations, and individual alginate particles were scarce here. Across all pH, the majority of particles had a diameter between 400 to 700 µm. Particle size below 100 µm was not obtained in the extrusion dripping method.

In the emulsification method, process parameters were investigated to obtain alginate particles having diameter of around 30 µm. This research succeeded in producing alginate microspheres with sizes $<$100 µm, and the majority of microspheres had a diameter between 10 to 60 µm. The optimal process parameters were found to be 26 mM $CaCO_3$ and 100 µL acetic acid when using 2% w/v sodium alginate. Washing with 60% EtOH was deemed successful in removing the oil-phase from the sample while keeping alginate microspheres intact. However, EtOH-washing also removed the Span 80, which resulted in increasing alginate microsphere diameters. Still, the particle size remained below 100 µm.

### Ion-exchange and loading efficiency

In the ion-exchange process, Ca-alginate microspheres from the emulsification method were added to a bath of holmium ions. In stable holmium exchange, the optimal holmium concentration was concluded to be 26 µM. Here, alginate microspheres remained individual and spherical, while holmium concentration >26 µM resulted in particle disintegration, irregular particle morphology or gel formation. The particle sizes of Ho-alginate microspheres resembled the particle sizes of Ca-alginate microspheres, with the majority being between 10 to 60 µm. When Ca-alginate particles were ion-exchanged using Ho-166, an average loading efficiency of (86.5 $\pm$ 1.4)% was found. The $^{166}$Ho-alginate microspheres remained individual and spherical, and particle size did not differ from the stable Ho-alginate microspheres.

### Stability of $^{166}$Ho-alginate microspheres

$^{166}$Ho-alginate microspheres were suspended in demiwater and 0.9% NaCl after loading efficiency experiments to investigate their radiochemical stability. The particles showed excellent stability in demiwater as retention percentage remained above 90% and constant for 24 hours. It was found that the retention percentage of $^{166}$Ho-alginate microspheres in 0.9% NaCl dropped to ~60% after five minutes. It was also discovered that the retention percentage did not further decrease, but instead remained stable for up to 24 hours. Remaining microspheres were spherical with particle size between 10 to 60 µm.

To conclude, this research demonstrates that alginate microspheres with a size between 20 and 60 µm can be produced using the emulsification method. The loading efficiency in this research demonstrated excellent ion-exchange of calcium with Ho-166 in the alginate structure. The theoretical retention of $^{166}$Ho-alginate microspheres in 0.9% NaCl solution dropped significantly after five minutes, but stabilized for up to 24 hours. Literature on Ho-alginate microspheres is very limited as of now, and this research takes a step towards $^{166}$Ho-alginate microspheres as radioembolic device for transarterial radioembolisation.

# 6

# Recommendations

The main focus of this research was obtaining alginate microspheres of 30 µm to develop a new type of radioembolic device. This chapter includes several points of interest for further research on the production of alginate microspheres using the extrusion dripping method and the emulsification method. Furthermore, several recommendations on the loading efficiency and stability of alginate microspheres are listed.

### Extrusion dripping method

In this research, the extrusion dripping method showed particle formation with a majority of particles between 400 to 700 µm. As a particle size between 20 to 60 µm is desired in radioembolic devices, this research advises the emulsification method above the extrusion dripping method. In terms of external gelation however, a lower pH could induce smaller particle size. Perhaps these findings could apply to other fields in medicine, such as production of alginate microspheres for drug delivery systems. If particle size between 200 and 900 µm is desired, the author proposes the following recommendations on the extrusion dripping method for alginate microspheres:

- Replacing the slanted needles with flat edged needles to promote spherical particle formation at the needle tip.
- Lowering the stirring speed to preserve the spherical shape of alginate microspheres in the crosslinking solution during gelation.
- Stability experiments to investigate the influence of the pH during crosslinking on the stability and strength of Ca-alginate microspheres. These could include suspending the alginate microspheres in 0.9% NaCl solution and investigate morphology change.

### Emulsification method

The emulsification method in this research was successful in reaching a size range of 20 to 60 µm, and therefore this production method can be further explored towards $^{166}$Ho-alginate microspheres as radioembolic device. The author proposes the following points of interest:

- Span 80 is necessary in this method to favour the formation of a water-in-oil emulsion. However, the surfactant is lipophilic, favours the paraffin oil, and is therefore washed away in the process of oil-removal. The alginate microsphere particle size was found to increase in this research when Span 80 was removed. Replacing the Span 80 with a different surfactant post-emulsification could investigate whether the alginate microspheres can be prevented from increasing in particle size. Here, surfactants with higher HLB values are preferred to keep the alginate microspheres dispersed in water, such as Tween 80 (HLB 15) or Tween 20 (HLB 16.7). For example, a study by Lupo et al. rinsed the alginate microspheres post-emulsification with a solution of $CaCl_2$ and Tween 20 [58]. A study by Song et al. rinsed Ca-alginate microspheres with Tween 80 [60].

- Instead of calcium carbonate ($CaCO_3$) as calcium source, calcium citrate ($Ca_3(C_6H_5O_7)$) has been investigated in literature. The calcium citrate was observed to crosslink the alginate into microspheres with a more uniform surface morphology [58]. This can be assigned to the formation of $CO_2$ during gelation with $CaCO_3$, which results in holes in the surface of alginate microspheres. The calcium citrate also produced smaller particle sizes. Further research could investigate whether the goal of 30 µm alginate microparticles with small size distribution can be reached with calcium citrate in the emulsification method.
- Acetic acid was necessary in the emulsification method to liberate $Ca^{2+}$ from $CaCO_3$. Increasing the acetic acid quantity in this research did not visually impact the alginate microspheres, however, literature reports that acetic acid can also induce gelation of alginate by lowering the pH and stabilising the alginate structure through intermolecular hydrogen bonds. Because of this phenomenon, the combination of acetic acid and alginate has been investigated before as medical application for anti-virus and anti-cancer properties [93–95]. If the relation between $Ca^{2+}$-release and acetic acid quantity is investigated in further research, this gelation phenomenon should be kept in mind.

### Loading efficiency and stability

Within the loading efficiency and stability experiments, this author proposes the following recommendations:

- The relation between ion-exchange time and resulting loading efficiency should be investigated. These experiments can assist in maximizing the loading efficiency of alginate microspheres with Ho-166.
- In the ion-exchange experiments, this research found a correlation between the degradation of alginate microspheres versus the holmium loading content. As radioembolic device, the alginate microspheres should be spherical, stable, with maximum $^{166}$Ho-content. Further research could investigate the balance between calcium content for stability and sphericity compared to maximum holmium loading within alginate microsphere.
- As radioembolic device, the microspheres should not display leakage of radioisotope. As of now, the stability of $^{166}$Ho-alginate microspheres has not been published extensively in literature. This research found stable $^{166}$Ho-alginate microspheres in 0.9% NaCl for up to 24 hours, but only after a significant leakage was found during the first five minutes of stability tests. Further research should investigate the stability of $^{166}$Ho-alginate microspheres in other physiological media, and explore ways of preventing degradation of microspheres. This could include the previously mentioned recommendation of adding surfactant post-emulsification.

# References


[1] Rebecca L. Siegel et al. “Cancer statistics, 2026”. In: *CA: A Cancer Journal for Clinicians* 76.1 (Jan. 2026). DOI: 10.3322/caac.70043.

[2] Nisar Amin et al. “Hepatocellular carcinoma: A comprehensive review”. In: *Diseases* 13.7 (2025). ISSN: 2079-9721. DOI: 10.3390/diseases13070207. URL: https://www.mdpi.com/2079-9721/13/7/207.

[3] Ezequiel Mauro et al. “Hepatocellular carcinoma: Epidemiology, diagnosis and treatment”. In: *JHEP Reports* 7.12 (Dec. 2025), p. 101571. DOI: 10.1016/j.jhepr.2025.101571.

[4] C. Bouvry et al. “Transarterial radioembolization (TARE) agents beyond 90Y-microspheres”. In: *BioMed Research International* 2018 (Dec. 2018), pp. 1–14. DOI: 10.1155/2018/1435302.

[5] Muhamad Serhal et al. “Transarterial radioembolization: Overview of radioembolic devices”. In: *Seminars in Interventional Radiology* 40.05 (Oct. 2023), pp. 461–466. DOI: 10.1055/s-0043-1772814.

[6] Martin Kropáček et al. “Preparation of holmium-166 labelled macroaggregates for radionuclide synovectomy”. In: *Nuclear Medicine Review* 6.1 (2003), pp. 1–4. ISSN: 1644-4345. URL: https://journals.viamedica.pl/nuclear_medicine_review/article/view/15394.

[7] Nienke J. M. Klaassen et al. “The various therapeutic applications of the medical isotope holmium-166: a narrative review”. In: *EJNMMI Radiopharmacy and Chemistry* 4.1 (Aug. 2019). DOI: 10.1186/s41181-019-0066-3.

[8] D. Nayak and S. Lahiri. “Application of radioisotopes in the field of nuclear medicine”. In: *Journal of Radioanalytical and Nuclear Chemistry* 242.2 (Nov. 1999), pp. 423–432. DOI: 10.1007/bf02345573.

[9] International Atomic Energy Agency. *IAEA - Live chart of nuclides*. Mar. 2025. URL: https://nds.iaea.org/relnsd/vcharthtml/VChartHTML.html (visited on 01/12/2026).

[10] Chris Oerlemans et al. “Alginate–lanthanide microspheres for MRI-guided embolotherapy”. In: *Acta Biomaterialia* 9.1 (Jan. 2013), pp. 4681–4687. DOI: 10.1016/j.actbio.2012.08.038.

[11] Gerrit H. van de Maat et al. “MRI-based biodistribution assessment of holmium-166 poly(L-lactic acid) microspheres after radioembolisation”. In: *European Radiology* 23.3 (Sept. 2012), pp. 827–835. DOI: 10.1007/s00330-012-2648-2.

[12] S.W. Zielhuis et al. “Characterization of holmium loaded alginate microspheres for multimodality imaging and therapeutic applications”. In: *Journal of Biomedical Materials Research Part A* 82.4 (Mar. 2007), pp. 892–898. DOI: 10.1002/jbm.a.31183.

[13] Chris Oerlemans et al. “Holmium–lipiodol–alginate microspheres for fluoroscopy-guided embolotherapy and multimodality imaging”. In: *International Journal of Pharmaceutics* 482.1-2 (Mar. 2015), pp. 47–53. DOI: 10.1016/j.ijpharm.2014.11.010.

[14] Maarten L. J. Smits et al. “The superior predictive value of 166Ho-scout compared with 99mTc-macroaggregated albumin prior to 166Ho-microspheres radioembolization in patients with liver metastases”. In: *European Journal of Nuclear Medicine and Molecular Imaging* 47.4 (Aug. 2019), pp. 798–806. DOI: 10.1007/s00259-019-04460-y.

[15] Dana da Silva et al. “Biocompatibility, biodegradation and excretion of polylactic acid (PLA) in medical implants and theranostic systems”. In: *Chemical Engineering Journal* 340 (May 2018), pp. 9–14. DOI: 10.1016/j.cej.2018.01.010.

[16] Shimon Ben-Shabat, Neeraj Kumar, and Abraham J. Domb. “PEG-PLA block copolymer as potential drug carrier: Preparation and characterization”. In: *Macromolecular Bioscience* 6.12 (Nov. 2006), pp. 1019–1025. DOI: 10.1002/mabi.200600165.

[17] Terumo Europe BV. *Important Communication; Subject: Holmium plaform products - produt discontinuation*. Statement of Terumo towards its customers. Apr. 2025. URL: https://cdn.ymaws.com/www.bnms.org.uk/resource/resmgr/website_documents/supply_updates_from_industry/30.04.2025_holmium_platform_.pdf.

[18] Su Hung Ching, Nidhi Bansal, and Bhesh Bhandari. “Alginate gel particles - A review of production techniques and physical properties”. In: *Critical Reviews in Food Science and Nutrition* 57.6 (May 2015), pp. 1133–1152. DOI: 10.1080/10408398.2014.965773.

[19] J. A. Goode. “Embolisation of cancer: what is the evidence?” In: *Cancer Imaging* 4.2 (Jan. 2004), pp. 133–141. DOI: 10.1102/1470-7330.2004.0021.

[20] Veronica M. Meade et al. “Distribution of different sized microspheres in experimental hepatic tumours”. In: *European Journal of Cancer and Clinical Oncology* 23.1 (Jan. 1987), pp. 37–41. DOI: 10.1016/0277-5379(87)90416-0.

[21] JH Anderson et al. “Regional delivery of microspheres to liver metastases: the effects of particle size and concentration on intrahepatic distribution”. In: *British Journal of Cancer* 64.6 (Dec. 1991), pp. 1031–1034. DOI: 10.1038/bjc.1991.459.

[22] Zuxing Kan and David Madoff. “Liver anatomy: microcirculation of the liver”. In: *Seminars in Interventional Radiology* 25.2 (June 2008), pp. 077–085. DOI: 10.1055/s-2008-1076685.

[23] James C. Andrews et al. “Hepatic radioembolization with Yttrium-90 containing glass microspheres: Preliminary results and clinical follow-Up”. In: *Journal of Nuclear Medicine* 35.10 (1994), pp. 1637–1644. ISSN: 0161-5505. eprint: https://jnm.snmjournals.org/content/35/10/1637.full.pdf. URL: https://jnm.snmjournals.org/content/35/10/1637.

[24] Janet E. Dancey et al. “Treatment of nonresectable hepatocellular carcinoma with intrahepatic 90Y-microspheres”. In: *Journal of Nuclear Medicine* 41.10 (2000), pp. 1673–1681. ISSN: 0161-5505. eprint: https://jnm.snmjournals.org/content/41/10/1673.full.pdf. URL: https://jnm.snmjournals.org/content/41/10/1673.

[25] National Institute for Health and Care Excellence. *Selective internal radiation therapies for treating hepatocellular carcinoma*. Last updated July 2025. Mar. 2021. URL: https://www.nice.org.uk/guidance/ta688/chapter/2-Information-about-QuiremSpheres-SIR-Spheres-and-TheraSphere (visited on 05/03/2026).

[26] Russell J. Mumper, U. Yun Ryo, and Michael Jay. “Neutron-activated holmium-166-poly (L-Lactic Acid) microspheres: A potential agent for the internal radiation therapy of hepatic tumors”. In: *Journal of Nuclear Medicine* 32.11 (1991), pp. 2139–2143. ISSN: 0161-5505. eprint: https://jnm.snmjournals.org/content/32/11/2139.full.pdf. URL: https://jnm.snmjournals.org/content/32/11/2139.

[27] Ekaterina. Dadachova et al. “Separation of carrier-free holmium-166 from neutron-irradiated dysprosium targets”. In: *Analytical Chemistry* 66.23 (Dec. 1994), pp. 4272–4277. DOI: 10.1021/ac00095a024.

[28] Susanta Lahiri, Kees J. Volkers, and Birgit Wierczinski. “Production of 166Ho through 164Dy(n,γ)165Dy(n, γ)166Dy(β−)166Ho and separation of 166Ho”. In: *Applied Radiation and Isotopes* 61.6 (Dec. 2004), pp. 1157–1161. DOI: 10.1016/j.apradiso.2004.03.117.

[29] B.E. Zimmerman. “A new evaluation of the decay data for 166Ho”. In: *Applied Radiation and Isotopes* 207 (May 2024), p. 111230. DOI: 10.1016/j.apradiso.2024.111230.

[30] Yi Shi, Amanda M. Johnsen, and Anthony J. Di Pasqua. “Holmium for use in cancer therapy”. In: *Comments on Inorganic Chemistry* 37.6 (May 2017), pp. 281–300. DOI: 10.1080/02603594.2017.1333498.

[31] Y. Danon et al. “Neutron total cross-section measurements and resonance parameter analysis of holmium, thulium, and erbium from 0.001 to 20 eV”. In: *Nuclear Science and Engineering* 128.1 (Jan. 1998), pp. 61–69. DOI: 10.13182/nse98-a1945.

[32] Balraj Singh. “Nuclear data sheets for A = 89”. In: *Nuclear Data Sheets* 114.1 (Jan. 2013), pp. 1–208. DOI: 10.1016/j.nds.2013.01.001.

[33] Ana M. Denis-Bacelar et al. “Bone lesion absorbed dose profiles in patients with metastatic prostate cancer treated with molecular radiotherapy”. In: *The British Journal of Radiology* 91.1084 (Feb. 2018). DOI: 10.1259/bjr.20170795.

[34] Joo Hyuk Sohn et al. “Phase II study of transarterial holmium-166-chitosan complex treatment in patients with a single, large hepatocellular carcinoma”. In: *Oncology* 76.1 (Nov. 2008), pp. 1–9. DOI: 10.1159/000173735.

[35] J. F. W. Nijsen et al. “Holmium-166 poly lactic acid microspheres applicable for intra-arterial radionuclide therapy of hepatic malignancies: effects of preparation and neutron activation techniques”. In: *European Journal of Nuclear Medicine and Molecular Imaging* 26.7 (June 1999), pp. 699–704. DOI: 10.1007/s002590050440.

[36] Johannes F. W. Nijsen et al. “Liver Tumors: MR imaging of radioactive holmium microspheres—phantom and rabbit study”. In: *Radiology* 231.2 (May 2004), pp. 491–499. DOI: 10.1148/radiol.2312030594.

[37] Piotr Rosiak et al. “Modification of alginates to modulate their physic-chemical properties and obtain biomaterials with different functional properties”. In: *Molecules* 26.23 (Nov. 2021), p. 7264. DOI: 10.3390/molecules26237264.

[38] Dinesh Dhamecha et al. “Applications of alginate microspheres in therapeutics delivery and cell culture: Past, present and future”. In: *International Journal of Pharmaceutics* 569 (Oct. 2019), p. 118627. DOI: 10.1016/j.ijpharm.2019.118627.

[39] Kuen Yong Lee and David J. Mooney. “Alginate: Properties and biomedical applications”. In: *Progress in Polymer Science* 37.1 (Jan. 2012), pp. 106–126. DOI: 10.1016/j.progpolymsci.2011.06.003.

[40] Amiruddin Amiruddin, Mahardian Rahmadi, and Dewı Harıyadı. “A review on calcium-alginate microspheres for drug delivery system: Characteristics, drug release, activity, stability and in-vivo studies”. In: *Fabad Journal of Pharmaceutical Sciences* 50.1 (Mar. 2025), pp. 169–186. DOI: 10.55262/fabadeczacilik.1511505.

[41] C.A. García-González et al. “Polysaccharide-based aerogel microspheres for oral drug delivery”. In: *Carbohydrate Polymers* 117 (Mar. 2015), pp. 797–806. DOI: 10.1016/j.carbpol.2014.10.045.

[42] Lissette Agüero et al. “Alginate microparticles as oral colon drug delivery device: A review”. In: *Carbohydrate Polymers* 168 (July 2017), pp. 32–43. DOI: 10.1016/j.carbpol.2017.03.033.

[43] Joanne Lai et al. “Alginate-based encapsulation fabrication technique for drug delivery: An updated review of particle type, formulation technique, pharmaceutical ingredient, and targeted delivery system”. In: *Pharmaceutics* 16.3 (Mar. 2024), p. 370. DOI: 10.3390/pharmaceutics16030370.

[44] Nguyen Thi Thanh Uyen et al. “Fabrication of alginate microspheres for drug delivery: A review”. In: *International Journal of Biological Macromolecules* 153 (June 2020), pp. 1035–1046. DOI: 10.1016/j.ijbiomac.2019.10.233.

[45] P. Saini, M. Arora, and M.N.V. Ravi Kumar. “Poly(lactic acid) blends in biomedical applications”. In: *Advanced Drug Delivery Reviews* 107 (Dec. 2016), pp. 47–59. DOI: 10.1016/j.addr.2016.06.014.

[46] Long Yu, Katherine Dean, and Lin Li. “Polymer blends and composites from renewable resources”. In: *Progress in Polymer Science* 31.6 (June 2006), pp. 576–602. DOI: 10.1016/j.progpolymsci.2006.03.002.

[47] Cecilia Mortalò et al. “Extruded composite films based on polylactic acid and sodium alginate”. In: *Polymer* 282 (Aug. 2023), p. 126162. DOI: 10.1016/j.polymer.2023.126162.

[48] Sijin Saji et al. “A brief review on the development of alginate extraction process and its sustainability”. In: *Sustainability* 14 (Apr. 2022), p. 5181. DOI: 10.3390/su14095181.

[49] Hylenne Bojorges et al. “Estimation of alginate purity and M/G ratio by methanolysis coupled with anion exchange chromatography”. In: *Carbohydrate Polymers* 321 (Dec. 2023), p. 121285. DOI: 10.1016/j.carbpol.2023.121285.

[50] Hans Grasdalen. “High-field, 1H-n.m.r. spectroscopy of alginate: sequential structure and linkage conformations”. In: *Carbohydrate Research* 118 (July 1983), pp. 255–260. DOI: 10.1016/0008-6215(83)88053-7.

[51] Hans Grasdalen, Bjørn Larsen, and Olav Smidsrød. “A p.m.r. study of the composition and sequence of uronate residues in alginates”. In: *Carbohydrate Research* 68.1 (Jan. 1979), pp. 23–31. DOI: 10.1016/s0008-6215(00)84051-3.

[52] Hengtong Zhang, Junqiu Cheng, and Qiang Ao. “Preparation of alginate-based biomaterials and their applications in biomedicine”. In: *Marine Drugs* 19.5 (May 2021), p. 264. DOI: 10.3390/md19050264.

[53] Isabelle Braccini and Serge Pérez. “Molecular basis of Ca2+-induced gelation in alginates and pectins: The Egg-Box Model revisited”. In: *Biomacromolecules* 2.4 (Sept. 2001), pp. 1089–1096. DOI: 10.1021/bm010008g.

[54] Isabelle Braccini, Robert P. Grasso, and Serge Pérez. “Conformational and configurational features of acidic polysaccharides and their interactions with calcium ions: a molecular modeling investigation”. In: *Carbohydrate Research* 317.1-4 (Apr. 1999), pp. 119–130. DOI: 10.1016/s0008-6215(99)00062-2.

[55] Yantao Wang et al. “Progress in research on metal ion crosslinking alginate-based gels”. In: *Gels* 11.1 (Dec. 2024), p. 16. DOI: 10.3390/gels11010016.

[56] Nicholas E. Simpson et al. “The role of the CaCl2–guluronic acid interaction on alginate encapsulated betaTC3 cells”. In: *Biomaterials* 25.13 (June 2004), pp. 2603–2610. DOI: 10.1016/j.biomaterials.2003.09.046.

[57] C.M. DeRamos et al. “13C NMR and molecular modeling studies of alginic acid binding with alkaline earth and lanthanide metal ions”. In: *Inorganica Chimica Acta* 256.1 (Mar. 1997), pp. 69–75. DOI: 10.1016/s0020-1693(96)05418-7.

[58] Bryshila Lupo et al. “Preparation of alginate microspheres by emulsification/internal gelation to encapsulate cocoa polyphenols”. In: *Food Hydrocolloids* 38 (July 2014), pp. 56–65. DOI: 10.1016/j.foodhyd.2013.11.003.

[59] BioRender. *Scientific image and illustration software*. Version 04-2026. URL: https://www.biorender.com/.

[60] Huiyi Song et al. “Microencapsulated probiotics using emulsification technique coupled with internal or external gelation process”. In: *Carbohydrate Polymers* 96.1 (July 2013), pp. 181–189. DOI: 10.1016/j.carbpol.2013.03.068.

[61] Joseph I. Goldstein et al. *Scanning Electron Microscopy and X-Ray microanalysis*. New York, NY: Springer New York, Jan. 2018. DOI: 10.1007/978-1-4939-6676-9.

[62] Nanoscience Instruments. *Scanning Electrom Microscopy*. URL: https://www.nanoscience.com/techniques/scanning-electron-microscopy/#interactions (visited on 05/02/2026).

[63] Weilie Zhou et al. “Fundamentals of Scanning Electron Microscopy (SEM)”. In: *Scanning Microscopy for Nanotechnology: Techniques and Applications*. Ed. by Weilie Zhou and Zhong Lin Wang. New York, NY: Springer New York, 2007, pp. 1–40. ISBN: 978-0-387-39620-0. DOI: 10.1007/978-0-387-39620-0_1. URL: https://doi.org/10.1007/978-0-387-39620-0_1.

[64] Juhani Aalto and Lauri Kaihola. *A guide to the state of art of gamma counting*. Perkin Elmer, June 1997. ISBN: 951-9489-33-9.

[65] Matthew Rhyner et al. *Application notes: Cellular analysis using the Coulter principle; Measurement with great accuracy and speed*. URL: https://www.mybeckman.nl/resources/reading-material/application-notes/cellular-analysis-using-the-coulter-principle (visited on 05/03/2026).

[66] Beckman Coulter. *Coulter Counter aperture tubes*. URL: https://www.mybeckman.nl/supplies/aperture-tube (visited on 05/03/2026).

[67] L. Peng, W. Wang, and L. Bai. “Performance evaluation of the Z2 coulter counter for WBC and RBC counting”. In: *International Journal of Laboratory Hematology* 29.5 (Aug. 2007), pp. 361–368. DOI: 10.1111/j.1751-553x.2007.00868.x.

[68] Seong Hoon Kim et al. “Arterial blood gas test to decide whether to reconstruct single or both the arteries in living donor liver transplantation”. In: *HepatoBiliary Surgery and Nutrition* 7.6 (Dec. 2018), pp. 440–442. DOI: 10.21037/hbsn.2018.10.04.

[69] Andrea Souza et al. “Role of pH and crosslinking ions on cell viability and metabolic activity in alginate–gelatin 3D prints”. In: *Gels* 9.11 (Oct. 2023), p. 853. DOI: 10.3390/gels9110853.

[70] Olav Smidsrød et al. “The influence of pH on the rate of hydrolysis of acidic polysaccharides”. In: *Acta Chemica Scandinavica* 20 (Jan. 1966), pp. 1026–1034. DOI: 10.3891/acta.chem.scand.20-1026.

[71] Nicola L. Francis et al. “An ice-templated, linearly aligned chitosan-alginate scaffold for neural tissue engineering”. In: *Journal of Biomedical Materials Research Part A* 101.12 (Apr. 2013), pp. 3493–3503. DOI: 10.1002/jbm.a.34668.

[72] Arne Haug et al. “The degradation of alginates at different pH values.” In: *Acta Chemica Scandinavica* 17 (Jan. 1963), pp. 1466–1468. DOI: 10.3891/acta.chem.scand.17-1466.

[73] Roya Abka-khajouei et al. “Structures, properties and applications of alginates”. In: *Marine Drugs* 20.6 (May 2022), p. 364. DOI: 10.3390/md20060364.

[74] Sigma-Aldrich. *Buffer Reference Center*. URL: https://www.sigmaaldrich.com/NL/en/technical-documents/protocol/protein-biology/protein-concentration-and-buffer-exchange/buffer-reference-center (visited on 11/2025).

[75] M.H. Al-Khaldi et al. “Reaction of citric acid with calcite”. In: *Chemical Engineering Science* 62.21 (Nov. 2007), pp. 5880–5896. DOI: 10.1016/j.ces.2007.06.021.

[76] Evora van Oost. “The synthesis of holmium-loaded alginate microspheres”. In: *Bachelor’s thesis (unpublished)* (June 2025).

[77] B.-B. Lee, P. Ravindra, and E.-S. Chan. “Size and shape of calcium alginate beads produced by extrusion dripping”. In: *Chemical Engineering & Technology* 36.10 (Sept. 2013), pp. 1627–1642. DOI: 10.1002/ceat.201300230.

[78] Jui-Jung Chuang et al. “Effects of pH on the shape of alginate particles and its release behavior”. In: *International Journal of Polymer Science* 2017 (Jan. 2017), pp. 1–9. DOI: 10.1155/2017/3902704.

[79] Tezar Ramdhan et al. “Time dependent gelling properties of cuboid alginate gels made by external gelation method: Effects of alginate-CaCl2 solution ratios and pH”. In: *Food Hydrocolloids* 90 (May 2019), pp. 232–240. DOI: 10.1016/j.foodhyd.2018.12.022.

[80] Bushra Almari et al. “Fabrication of amyloid-$\beta$-secreting alginate microbeads for use in modelling alzheimer’s disease”. In: *Journal of Visualized Experiments* 149 (July 2019). DOI: 10.3791/59597.

[81] Donghee Lee et al. “3D printed alginate bead generator for high-throughput cell culture”. In: *Biomedical Microdevices* 23.2 (Apr. 2021). DOI: 10.1007/s10544-021-00561-4.

[82] Fatma Davarcı et al. “The influence of solution viscosities and surface tension on calcium-alginate microbead formation using dripping technique”. In: *Food Hydrocolloids* 62 (Jan. 2017), pp. 119–127. DOI: 10.1016/j.foodhyd.2016.06.029.

[83] Jinah Jang et al. “Effects of alginate hydrogel cross-linking density on mechanical and biological behaviors for tissue engineering”. In: *Journal of the Mechanical Behavior of Biomedical Materials* 37 (Sept. 2014), pp. 69–77. DOI: 10.1016/j.jmbbm.2014.05.004.

[84] D. Poncelet et al. “Production of alginate beads by emulsification/internal gelation. II. Physicochemistry”. In: *Applied Microbiology and Biotechnology* 43.4 (Sept. 1995), pp. 644–650. DOI: 10.1007/bf00164768.

[85] M. Alnaief et al. “Preparation of biodegradable nanoporous microspherical aerogel based on alginate”. In: *Carbohydrate Polymers* 84.3 (Mar. 2011), pp. 1011–1018. DOI: 10.1016/j.carbpol.2010.12.060.

[86] Nico Leister, Chenhui Yan, and Heike Petra Karbstein. “Oil droplet coalescence in w/o/w double emulsions examined in models from micrometer- to millimeter-sized droplets”. In: *Colloids and Interfaces* 6.1 (Feb. 2022), p. 12. DOI: 10.3390/colloids6010012.

[87] Xue-li Wang et al. “Study on the solubilization capacity of bio-oil in diesel by microemulsion technology with Span80 as surfactant”. In: *Fuel Processing Technology* 118 (Feb. 2014), pp. 141–147. DOI: 10.1016/j.fuproc.2013.08.020.

[88] Merel van Elk et al. “Alginate microspheres containing temperature sensitive liposomes (TSL) for MR-guided embolization and triggered release of doxorubicin”. In: *PLOS ONE* 10.11 (Nov. 2015), e0141626. DOI: 10.1371/journal.pone.0141626.

[89] Tara Sankar Pathak et al. “Effect of calcium ion (cross-linker) concentration on porosity, surface morphology and thermal behavior of calcium alginates prepared from algae (Undaria pinnatifida)”. In: *Carbohydrate Polymers* 81.3 (July 2010), pp. 633–639. DOI: 10.1016/j.carbpol.2010.03.025.

[90] Margaret E. Lyn and DanYang Ying. “Drying model for calcium alginate beads”. In: *Industrial & Engineering Chemistry Research* 49.4 (Jan. 2010), pp. 1986–1990. DOI: 10.1021/ie901451m.

[91] World Health Organization. *The selection and use of essential medicines, 2025: WHO Model List of Essential Medicines, 24th list*. Sept. 2025. URL: https://www.who.int/publications/i/item/B09474.

[92] Sigma-Aldrich. *Certificate of Analysis; Human serum from human male AB plasma, USA origin, sterile-filtered human plasma*. Feb. 2026. URL: https://www.sigmaaldrich.com/NL/en/product/sigma/h4522 (visited on 04/27/2026).

[93] Kurt Ingar Draget, Gudmund Skjåk-Bræk, and Bjørn Torger Stokke. “Similarities and differences between alginic acid gels and ionically crosslinked alginate gels”. In: *Food Hydrocolloids* 20.2-3 (Mar. 2006), pp. 170–175. DOI: 10.1016/j.foodhyd.2004.03.009.

[94] Alba Cano-Vicent et al. “Biocompatible alginate hydrogel film containing acetic acid manifests broad-spectrum antiviral and anticancer activities”. In: *Biomedicines* 11.9 (Sept. 2023), p. 2549. DOI: 10.3390/biomedicines11092549.

[95] Thomas E. Robinson et al. “Simultaneous viscoelasticity and sprayability in antimicrobial acetic acid-alginate fluid gels”. In: *Biomaterials Advances* 166 (Jan. 2025), p. 214051. DOI: 10.1016/j.bioadv.2024.214051.

# A

# Extrusion dripping method

The extrusion dripping method results were presented and discussed in Section 4.1. This appendix includes the full picture collections of the optical microscope in Section A.1 and the dataset of the particle analysis in Section A.2.

## A.1. Optical microscope picture collection of 3 mL/min flow rate

Optical microscope pictures were taken of extrusion dripping method samples using 3 mL/min flowrate at pH 4, 7, 9 and the reference sample. The results and discussion are found in Section 4.1.4. The full picture collection is given here, and an overview is given in Table A.1.

**Table A.1:** Overview of the appendix picture collection.

| | Zoom 4x | Zoom 10x |
|---|---|---|
| Side-by-side comparison | Figure A.1 | |
| pH 4 | Figure A.2 | Figure A.3 |
| pH 7 | Figure A.4 | Figure A.5 |
| pH 9 | Figure A.6 | Figure A.7 |
| Reference | Figure A.8 | Figure A.9 |

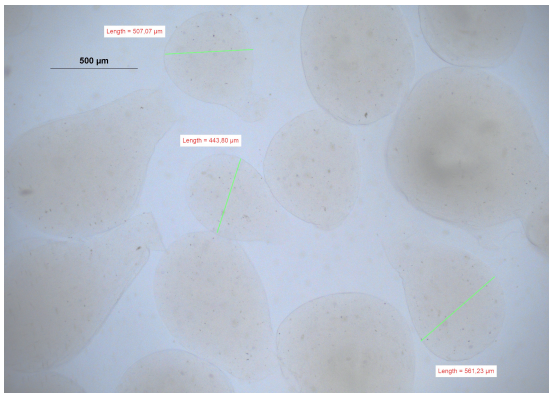


**(a)** pH 4, 4x zoom.

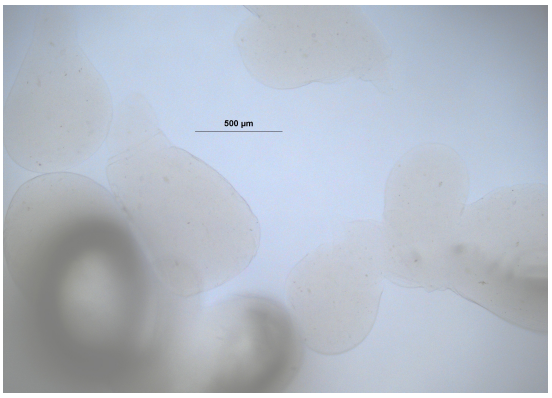


**(b)** pH 7, 4x zoom.

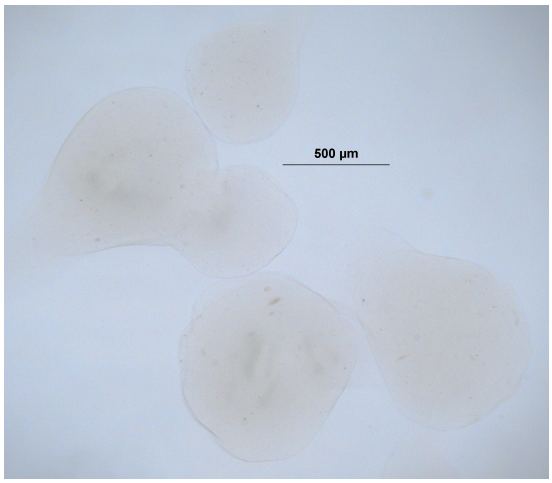


**(c)** pH 9, 4x zoom.

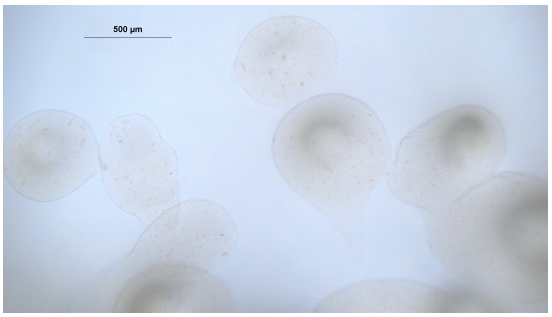


**(d)** Reference, 4x zoom

**Figure A.1:** Side-by-side comparison of the Ca-alginate particles from the extrusion dripping method at flowrate 3 mL/min. With solutions at pH 4, 7 and 9, and the reference solution without pH buffer. At 4x zoom with scale bar of 500 µm.

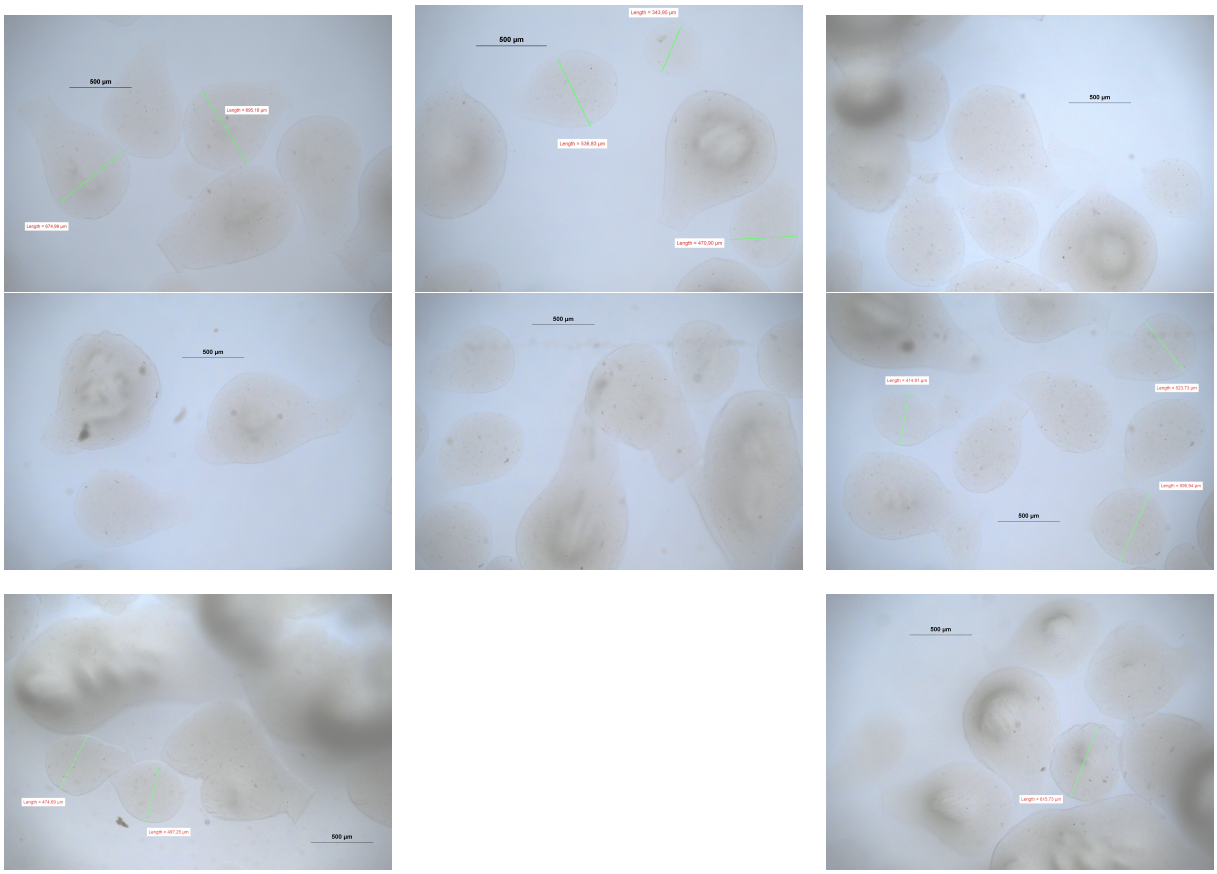

**Figure A.2:** Picture collection of the optical microscope at pH 4, flowrate 3 mL/min, 4x zoom with scale bar of 500 µm.

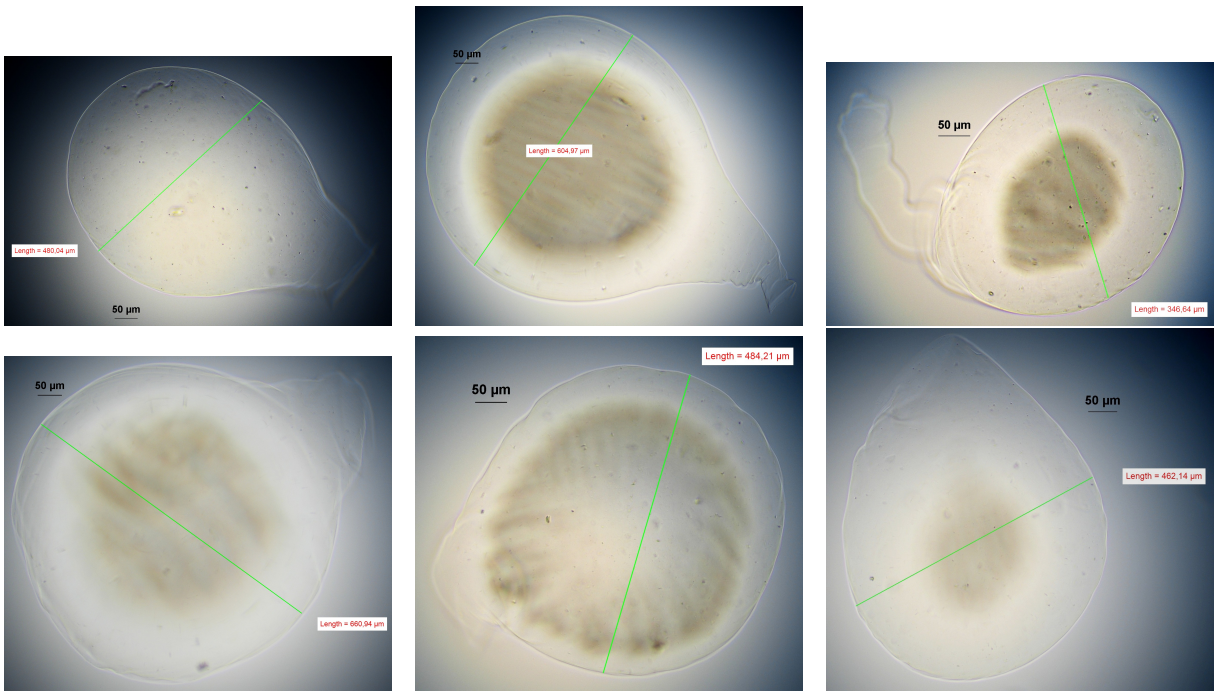


**Figure A.3:** Picture collection of the optical microscope at pH 4, flowrate 3 mL/min, 10x zoom with scale bar of 50 µm.

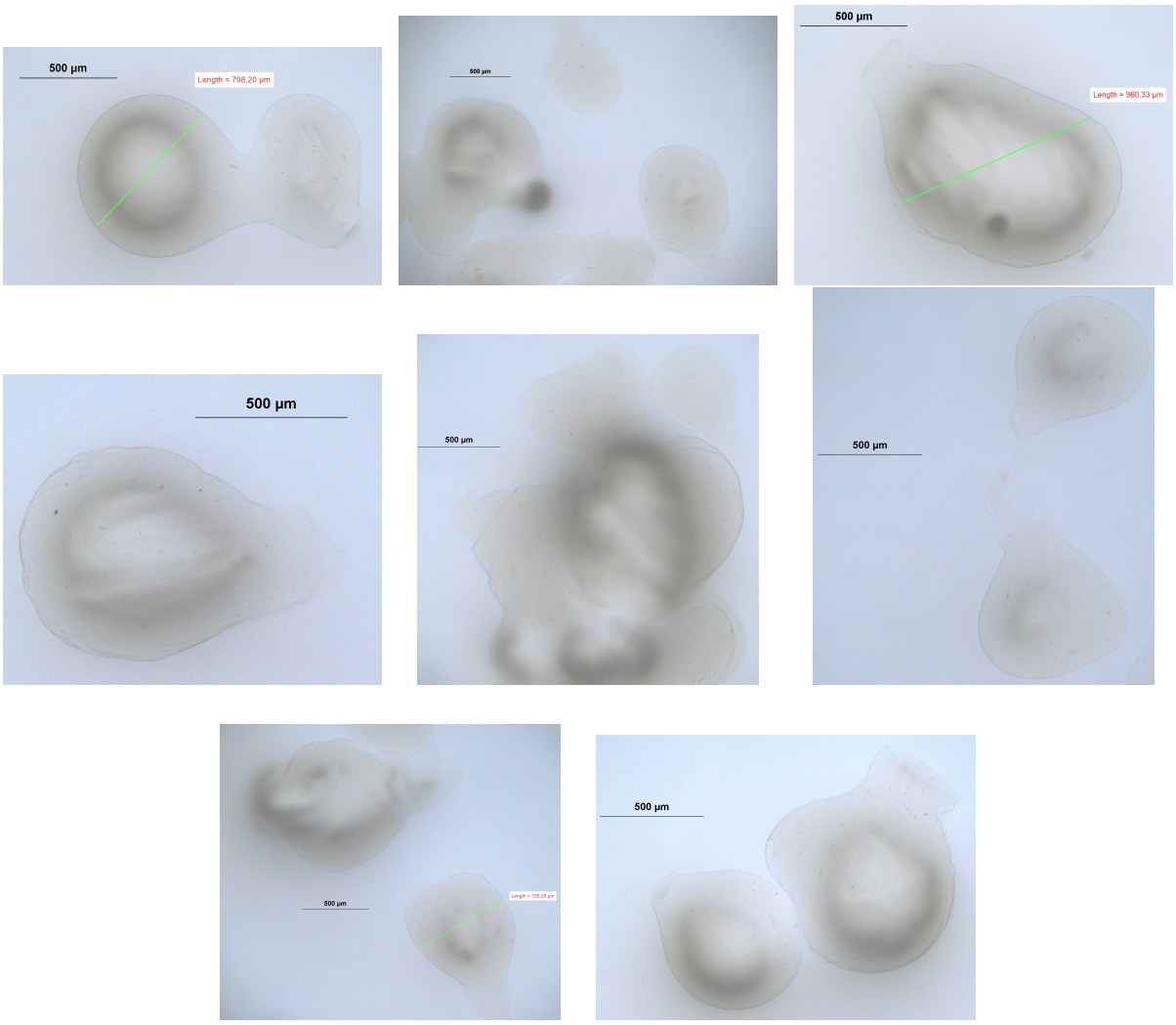


**Figure A.4:** Picture collection of the optical microscope at pH 7, flowrate 3 mL/min, 4x zoom with scale bar of 500 µm.

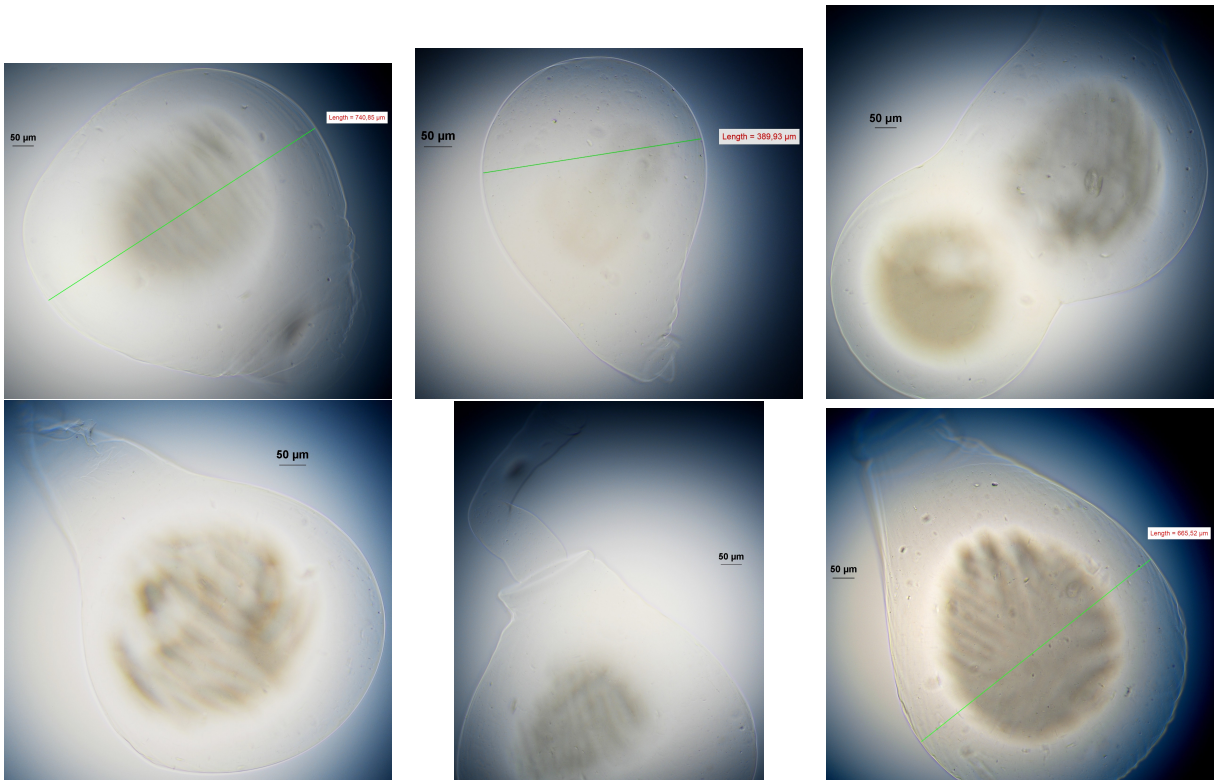


**Figure A.5:** Picture collection of the optical microscope at pH 7, flowrate 3 mL/min, 10x zoom with scale bar of 50 µm.

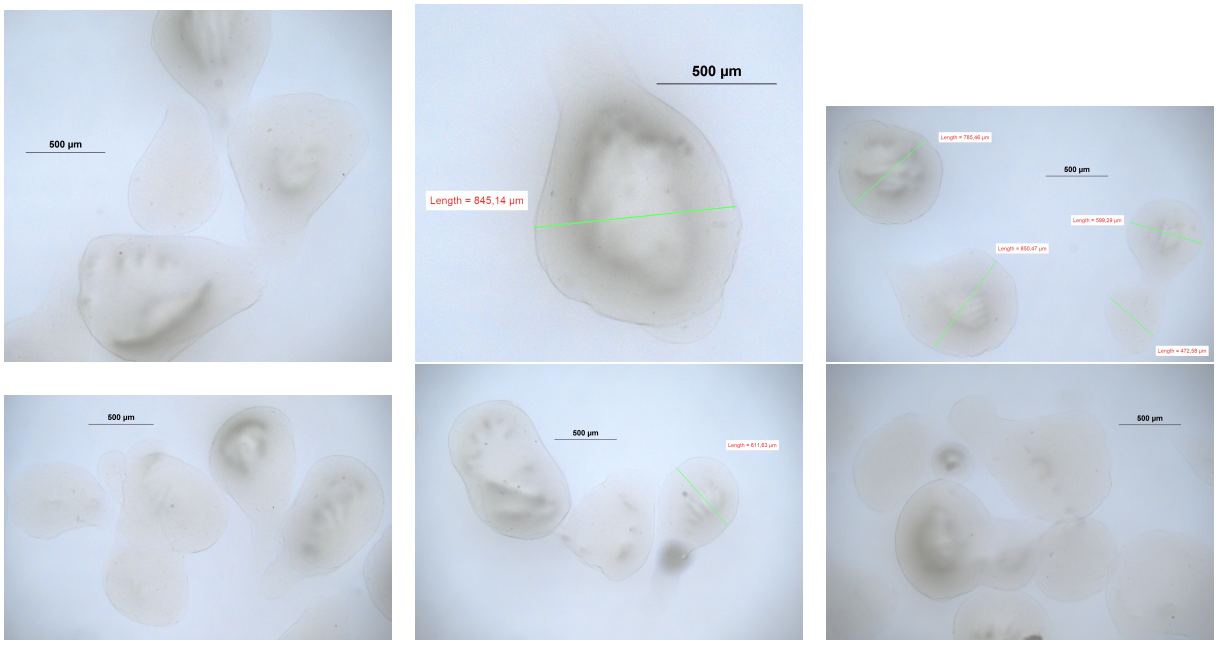


**Figure A.6:** Picture collection of the optical microscope at pH 9, flowrate 3 mL/min, 4x zoom with scale bar of 500 µm.

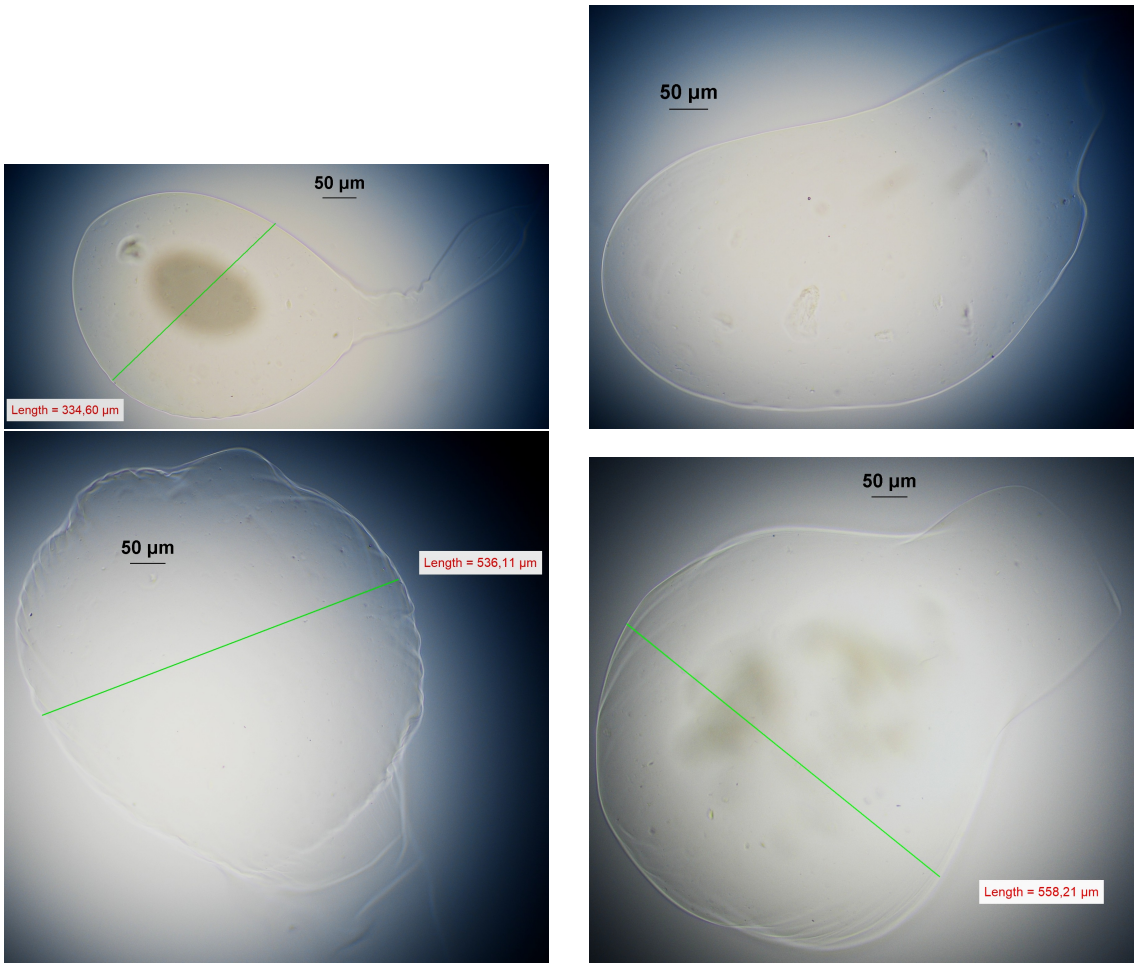


**Figure A.7:** Picture collection of the optical microscope at pH 9, flowrate 3 mL/min, 10x zoom with scale bar of 50 µm.

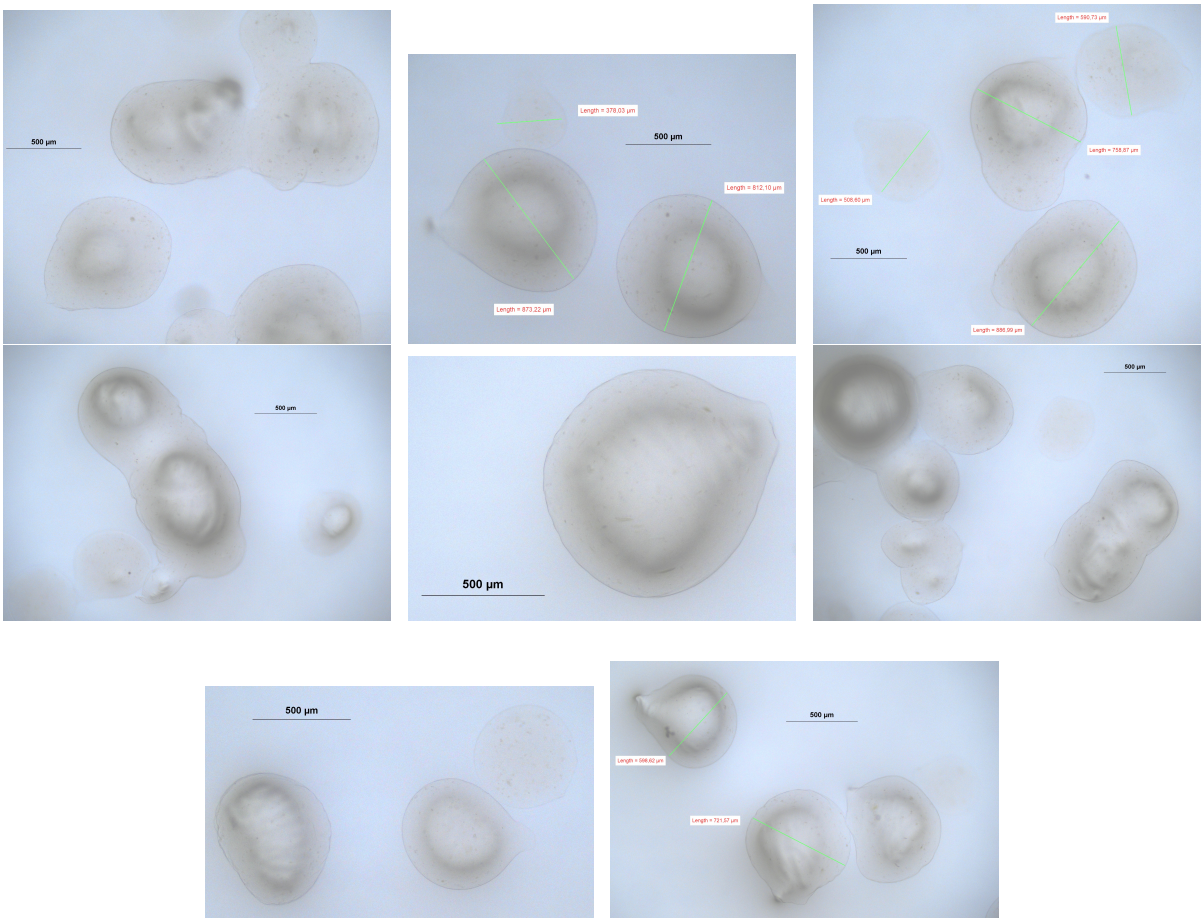


**Figure A.8:** Picture collection of the optical microscope of the reference sample, flowrate 3 mL/min, 4x zoom with scale bar of 500 µm.

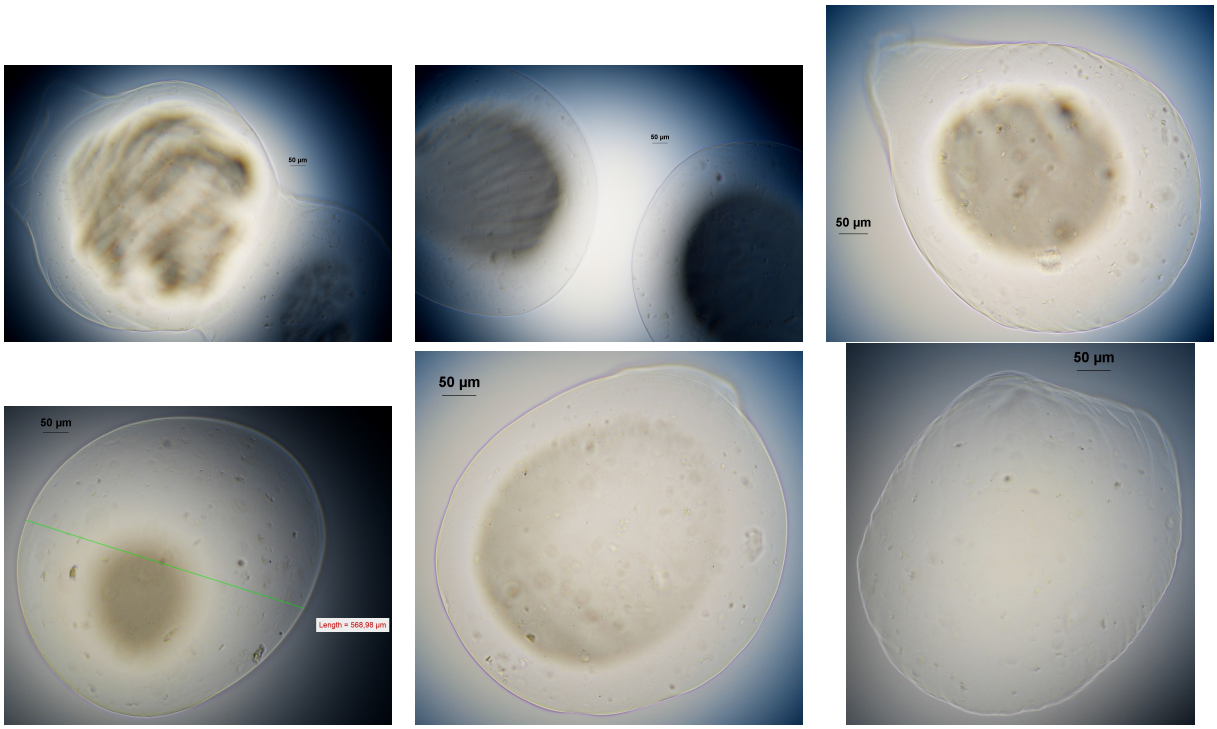


**Figure A.9:** Picture collection of the optical microscope of the reference sample, flowrate 3 mL/min, 10x zoom with scale bar of 50 µm.

## A.2. Data collection of the particle size analysis

The data collection used in the histograms from Section 4.1.4, Figure 4.4, is presented in Table A.2. Data was collected under the optical microscope using the analysis software.

**Table A.2:** Particle size analysis in the extrusion dripping method, for pH 4, 7, 9 and the reference sample.

| **pH** | **4** | **7** | **9** | **Ref** |
|---|---|---|---|---|
| **Particle size (μm)** | 674.99 | 740.85 | 611.63 | 378.03 |
| | 695.16 | 665.52 | 536.11 | 873.22 |
| | 536.83 | 798.20 | 845.14 | 812.10 |
| | 343.95 | 960.33 | 785.46 | 590.73 |
| | 470.90 | 719.52 | 850.47 | 758.87 |
| | 660.94 | 383.24 | 599.29 | 508.60 |
| | 369.88 | 389.93 | 472.58 | 886.99 |
| | 290.55 | 547.88 | 357.81 | 568.98 |
| | 575.82 | 653.48 | 558.21 | 486.84 |
| | 604.97 | 716.92 | 334.60 | 477.89 |
| | 346.64 | 726.28 | | 506.04 |
| | 356.71 | | | 598.62 |
| | 330.56 | | | 721.57 |
| | 472.33 | | | |
| | 482.92 | | | |
| | 481.21 | | | |
| | 462.14 | | | |
| | 480.04 | | | |
| | 414.91 | | | |
| | 523.73 | | | |
| | 595.94 | | | |
| | 507.07 | | | |
| | 443.80 | | | |
| | 561.23 | | | |
| | 474.69 | | | |
| | 497.25 | | | |
| | 615.73 | | | |
| | 493.87 | | | |

# B

# Emulsification method

The emulsification method experiments were carried out using 26 or 52 mM $CaCO_3$ and 100 or 200 µL acetic acid. The experimental results were presented and discussed in Section 4.2. This appendix includes additional optical microscope images.

## B.1. Optical microscope picture collection of 26 mM $CaCO_3$ and 100 µL acetic acid

The emulsification method using 26 mM $CaCO_3$ and 100 µL acetic acid was discussed in Section 4.2.2. Additional optical microscope images of samples washed with demiwater can be found in Figure B.1. Additional optical microscope images of samples washed with 60% EtOH can be found in Figure B.2.

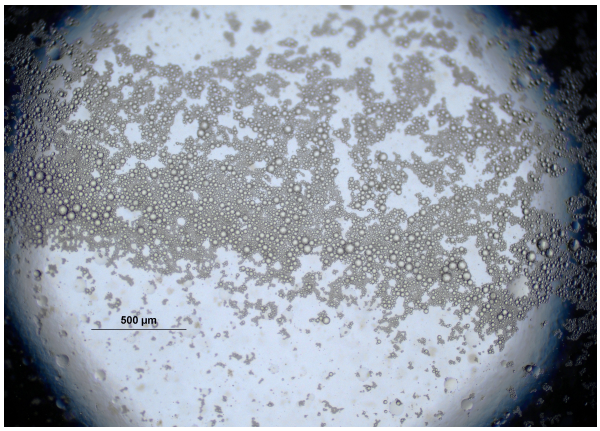


**(a)** 26 mM $CaCO_3$ and 100 µL acetic acid, 4x zoom.

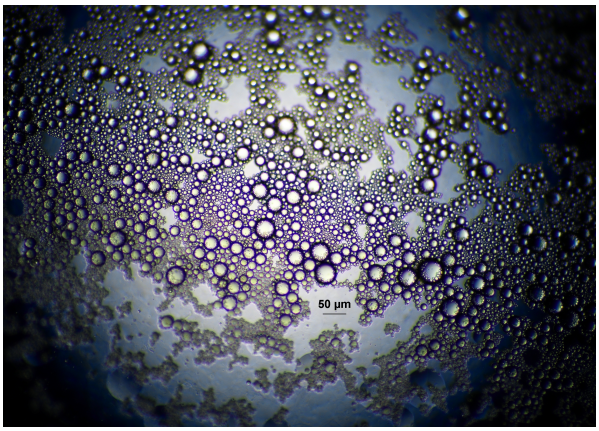


**(b)** 26 mM $CaCO_3$ and 100 µL acetic acid, 10x zoom.

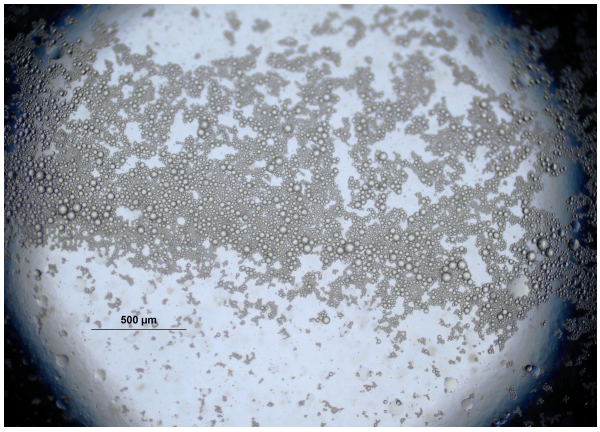


**(c)** 26 mM $CaCO_3$ and 100 µL acetic acid, 4x zoom.

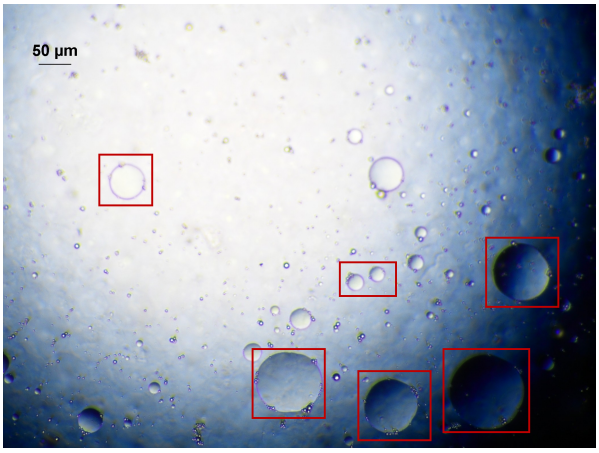


**(d)** 26 mM $CaCO_3$ and 100 µL acetic acid, 10x zoom. Several oil droplets are indicated with red squares.

**Figure B.1:** Optical microscope pictures of the 26 mM $CaCO_3$ and 100 µL acetic acid emulsification after washing with demiwater.

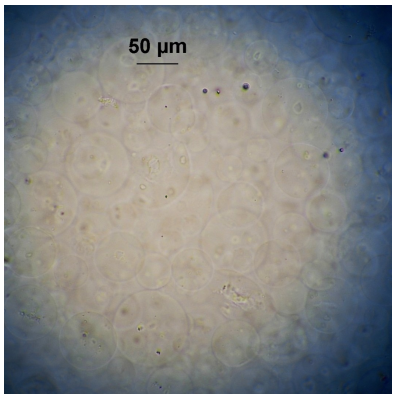


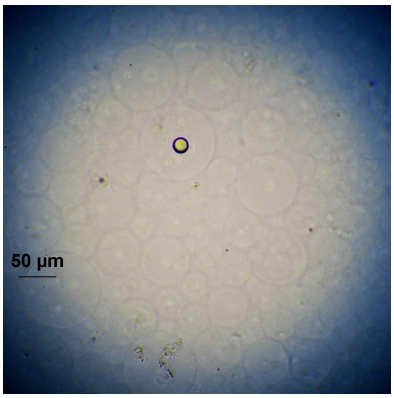


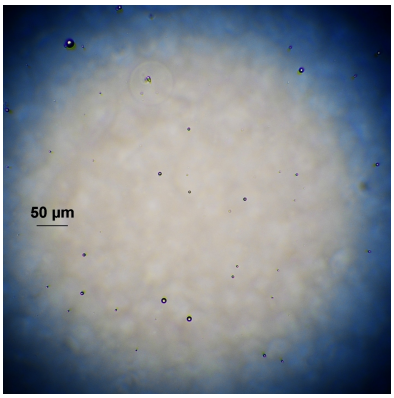


**Figure B.2:** Optical microscope pictures of the 26 mM $CaCO_3$ and 100 µL acetic acid emulsification after washing with 60% EtOH, 10x zoom.

## B.2. Optical microscope picture collection of 52 mM $CaCO_3$ and 200 µL acetic acid

The emulsification method using 52 mM $CaCO_3$ and 200 µL acetic acid was discussed in Section 4.2.3. Additional optical microscope images of samples can be found in Figure B.3.

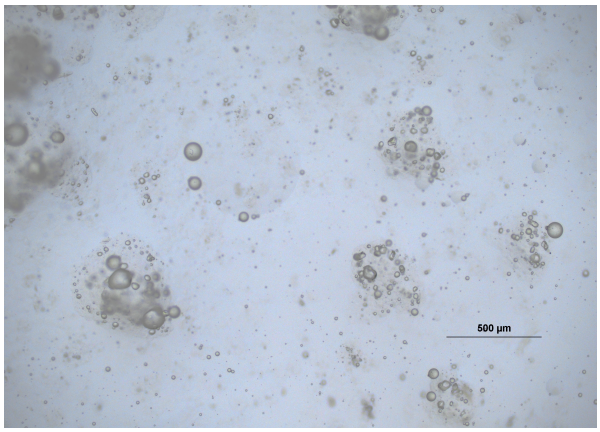


**(a)** 52 mM $CaCO_3$ and 200 µL acetic acid, 4x zoom.

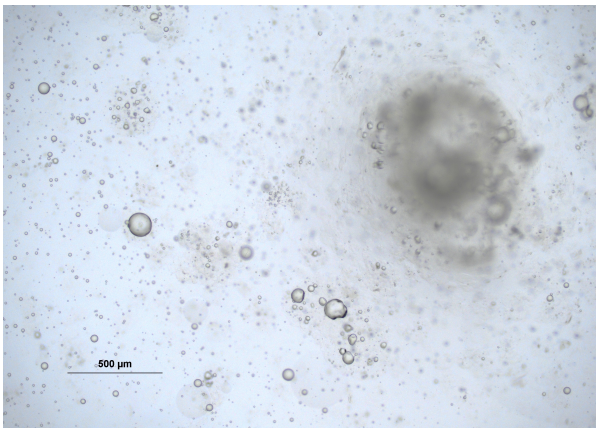


**(b)** 52 mM $CaCO_3$ and 200 µL acetic acid, 4x zoom

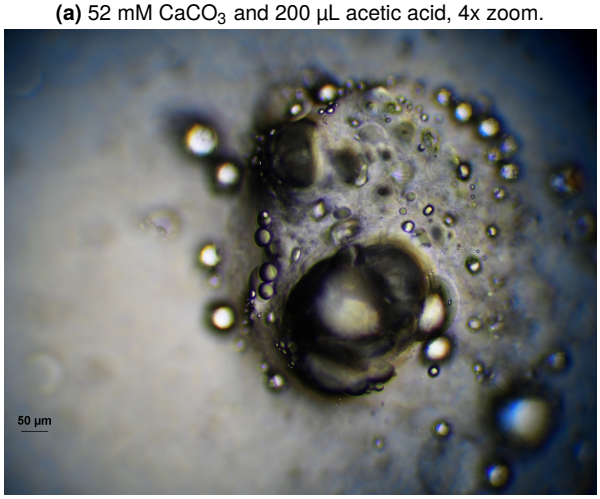


**(c)** 52 mM $CaCO_3$ and 200 µL acetic acid, 10x zoom.

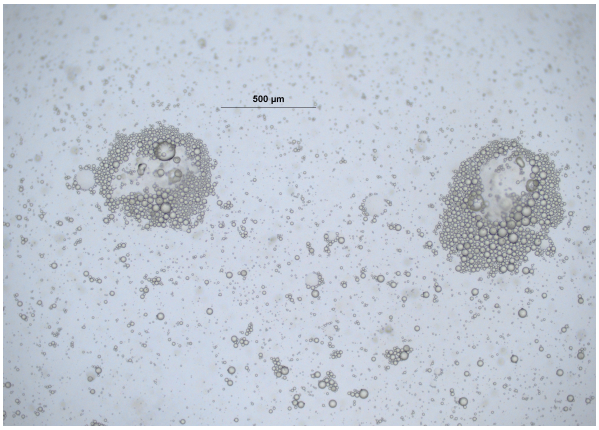


**(d)** 52 mM $CaCO_3$ and 200 µL acetic acid, 4x zoom.

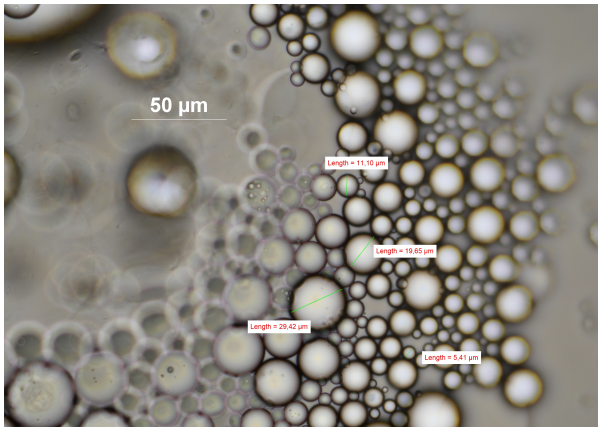


**(e)** 52 mM $CaCO_3$ and 200 µL acetic acid, 40x zoom.

**Figure B.3:** Optical microscope pictures of the 52 mM $CaCO_3$ and 200 µL emulsification.

# C

# Exchange experiments and stability experiments

The exchange experiments were first performed using stable holmium with synthesized Ca-alginate microspheres from the 26 µM $CaCO_3$ and 100 µL emulsification. The results were discussed in Section 4.3.1. For every exchange bath, one tube was washed with demiwater while the other tube was left unwashed. The optical microscope picture collections of the unwashed sample and the washed sample can be found in Section C.1 and C.2, respectively. The quantification dataset of the EDS analysis from the washed sample can be found in Section C.3.

The labelling efficiency was determined through $^{166}$Ho exchange experiments, discussed in Section 4.3.2. The alginate microspheres were analysed under the optical microscope when all $^{166}$Ho had decayed, and the picture collection is given in Section C.4.

The stability of radioactive Ho-alginate microspheres in demiwater and 0.9% NaCl solution was discussed in Section 4.4. The alginate microspheres were analysed under the optical microscope when all $^{166}$Ho had decayed, and the picture collection is given in Section C.5.

## C.1. Optical microscope picture collection of the unwashed stable holmium exchange experiments

The optical microscope pictures of unwashed stable holmium exchange experiments are presented in Figure C.1 for 26 mM and 2.6 mM, and Figure C.2 for 260 µM and 26 µM.

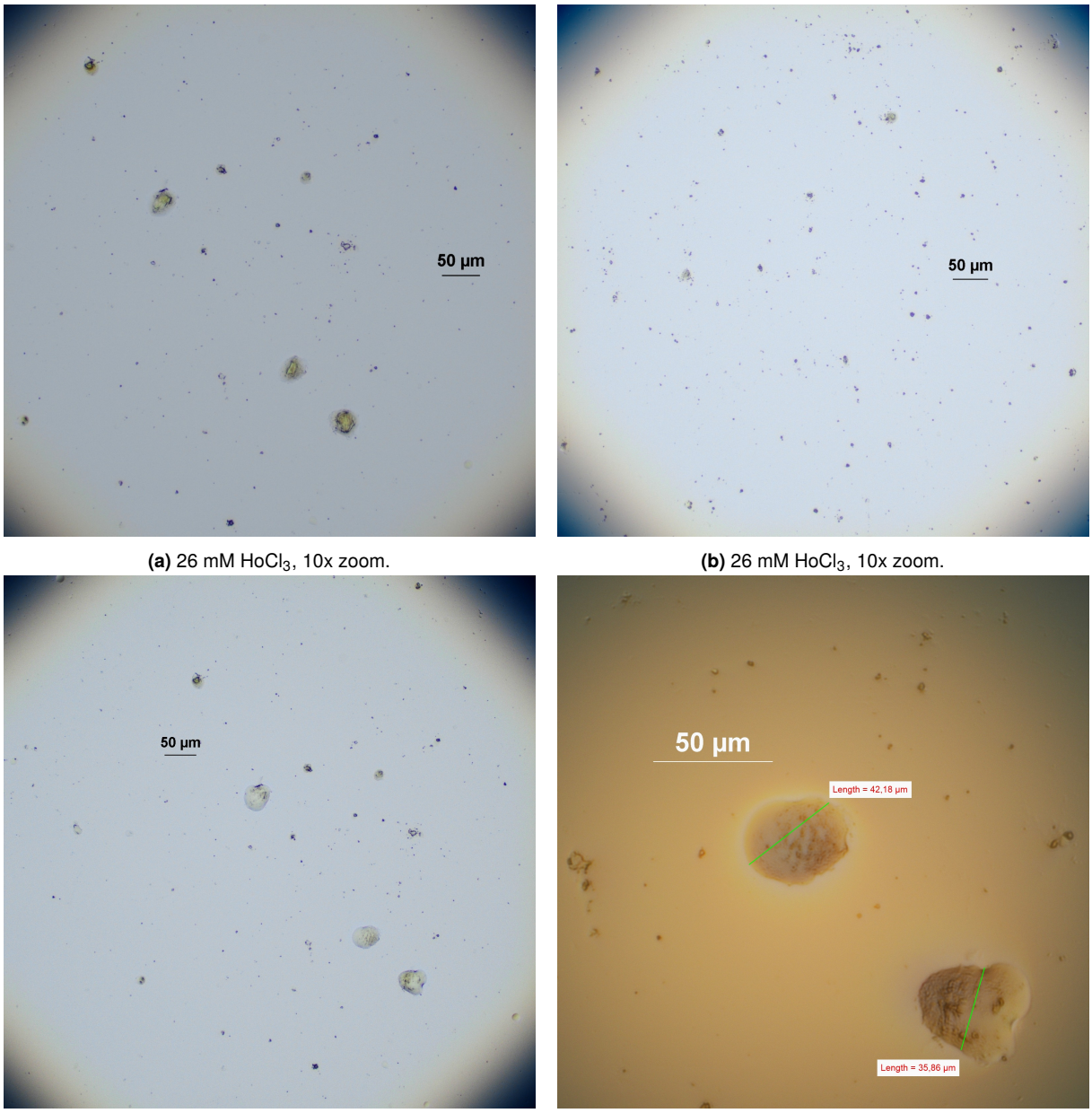


**(a)** 26 mM $HoCl_3$, 10x zoom.

**(b)** 26 mM $HoCl_3$, 10x zoom.

**(c)** 2.6 mM $HoCl_3$, 10x zoom.

**(d)** 2.6 mM $HoCl_3$, 40x zoom.

**Figure C.1:** Optical microscope pictures of the unwashed exchange experiments using $HoCl_3$ at 26 mM (a,b) and 2.6 mM (c,d).

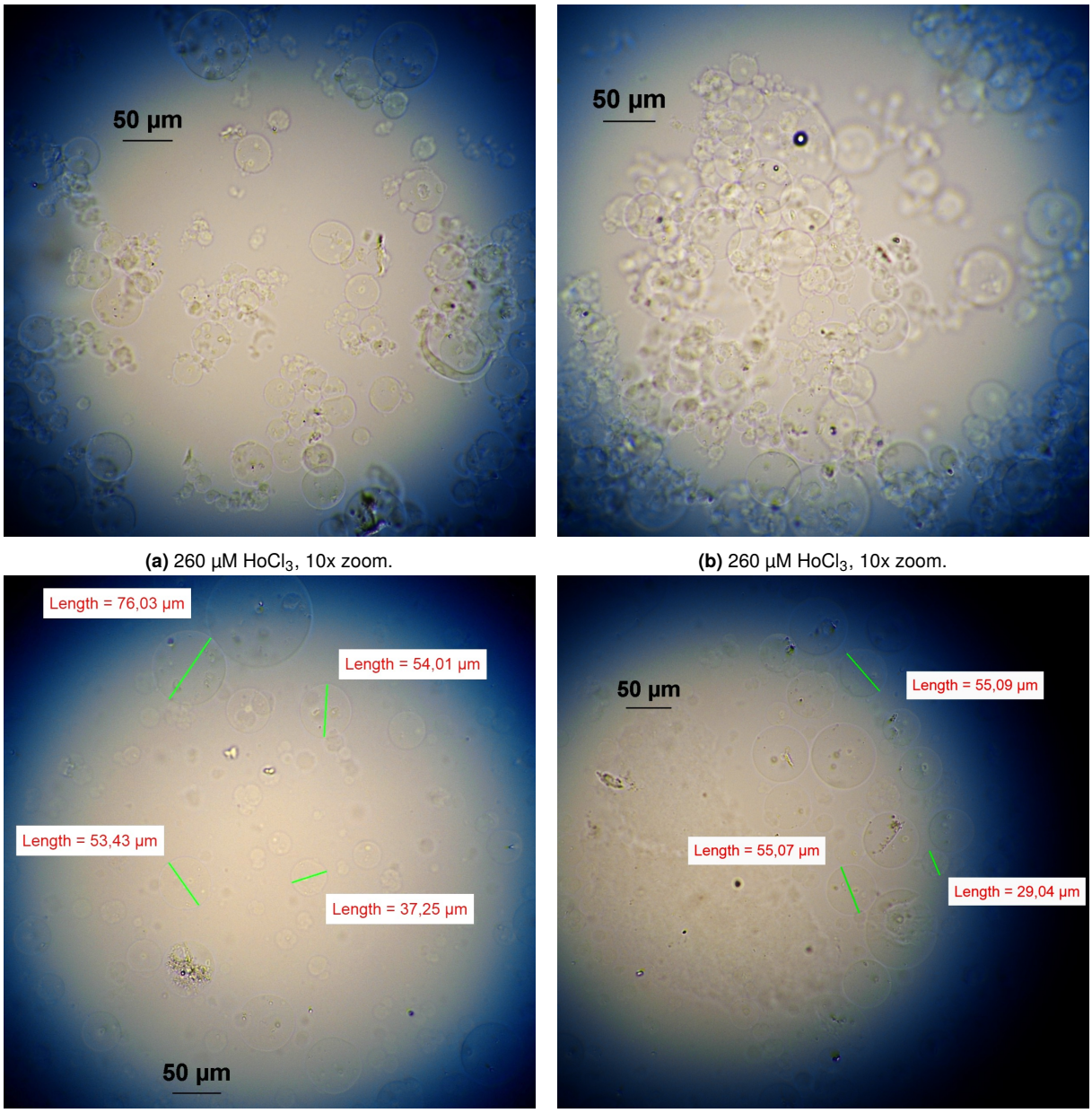


**(a)** 260 µM $HoCl_3$, 10x zoom.

**(b)** 260 µM $HoCl_3$, 10x zoom.

**(c)** 26 µM $HoCl_3$, 10x zoom.

**(d)** 26 µM $HoCl_3$, 10x zoom.

**Figure C.2:** Optical microscope pictures of the unwashed exchange experiments using $HoCl_3$ at 260 µM (a,b) and 26 µM (c,d).

## C.2. Optical microscope picture collection of the stable holmium exchange experiments washed with demiwater

The optical microscope picture collections of the stable holmium exchange experiments washed with demiwater are presented in Figure C.3-C.6 for 26 mM, 2.6 mM, 260 µM and 26 µM $HoCl_3$, respectively.

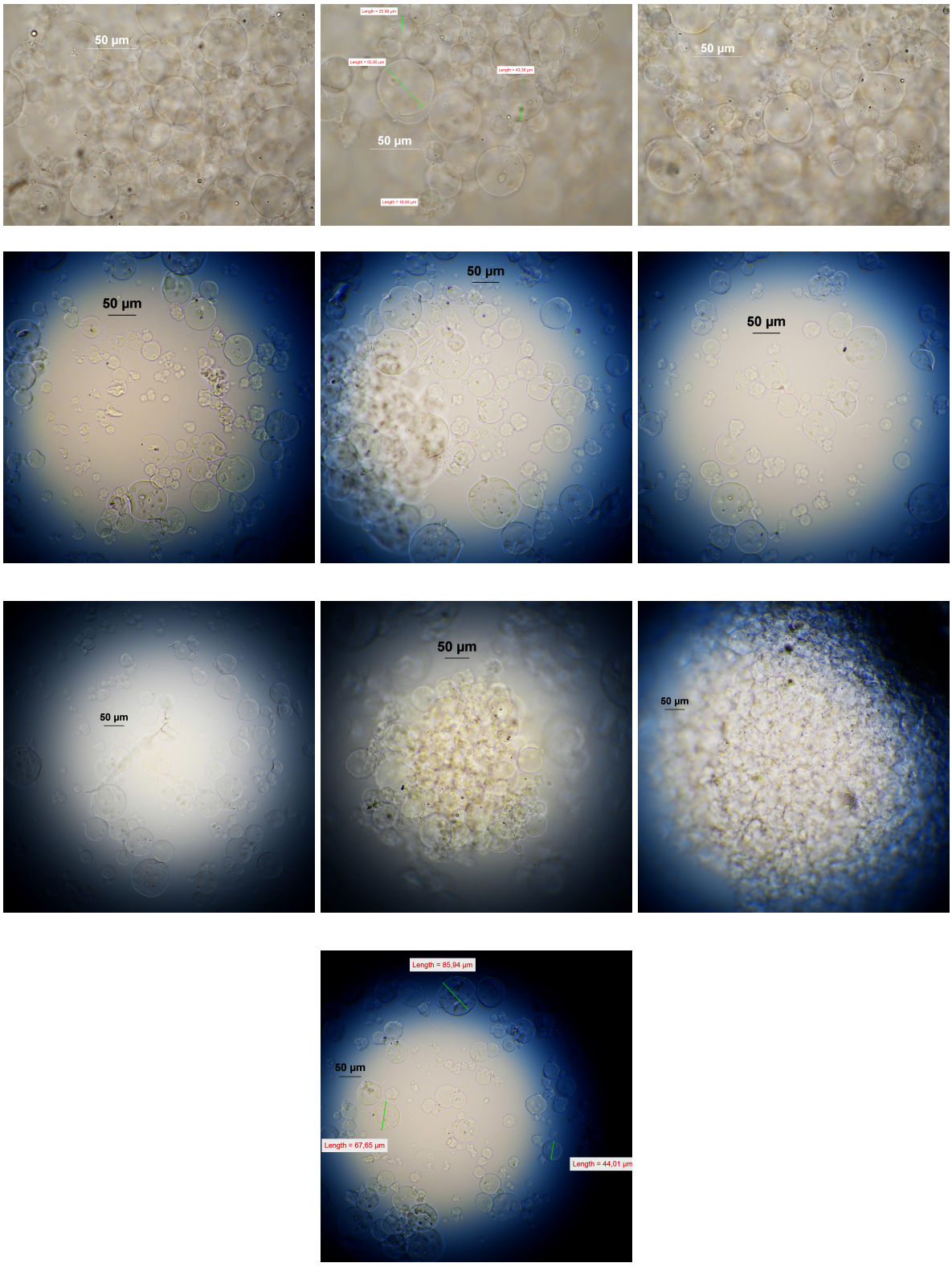


**Figure C.3:** Optical microscope pictures of the exchange experiment with 26 mM $HoCl_3$ after washing with demiwater.

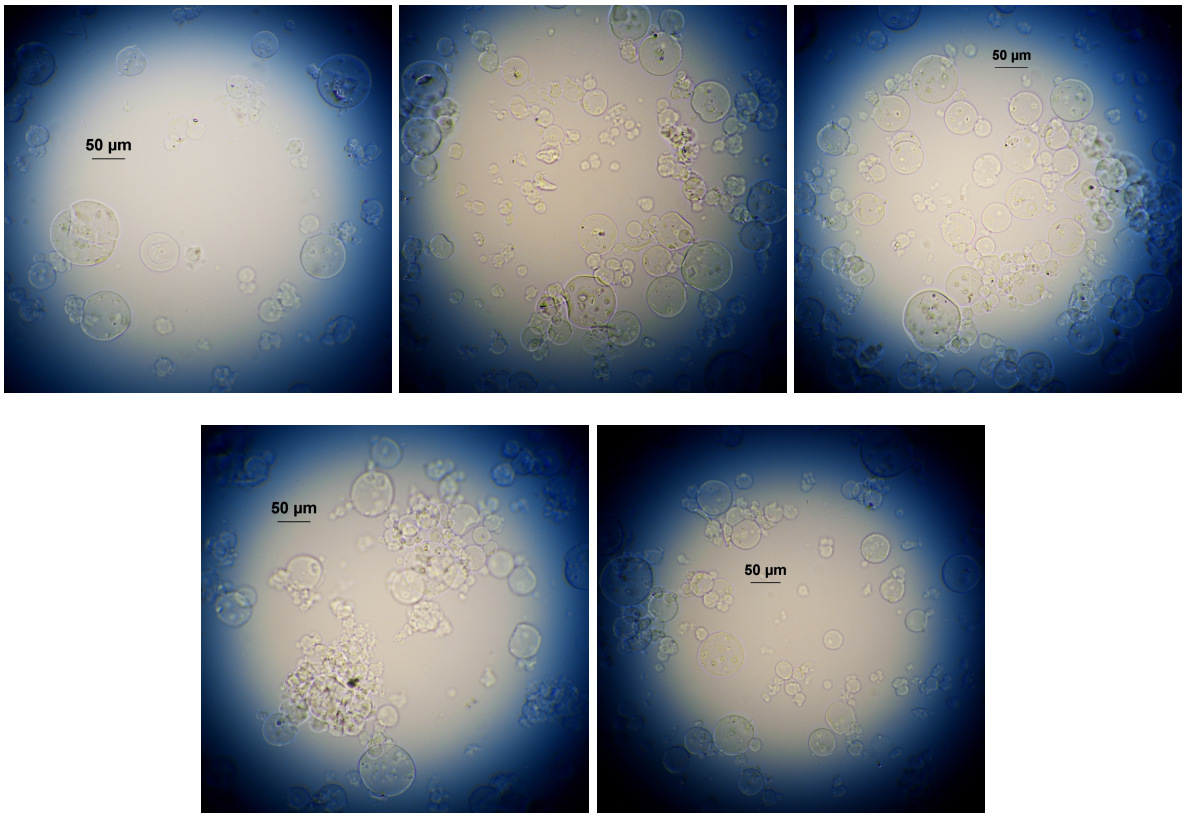


**Figure C.4:** Optical microscope pictures of the exchange experiment with 2.6 mM $HoCl_3$ after washing with demiwater.

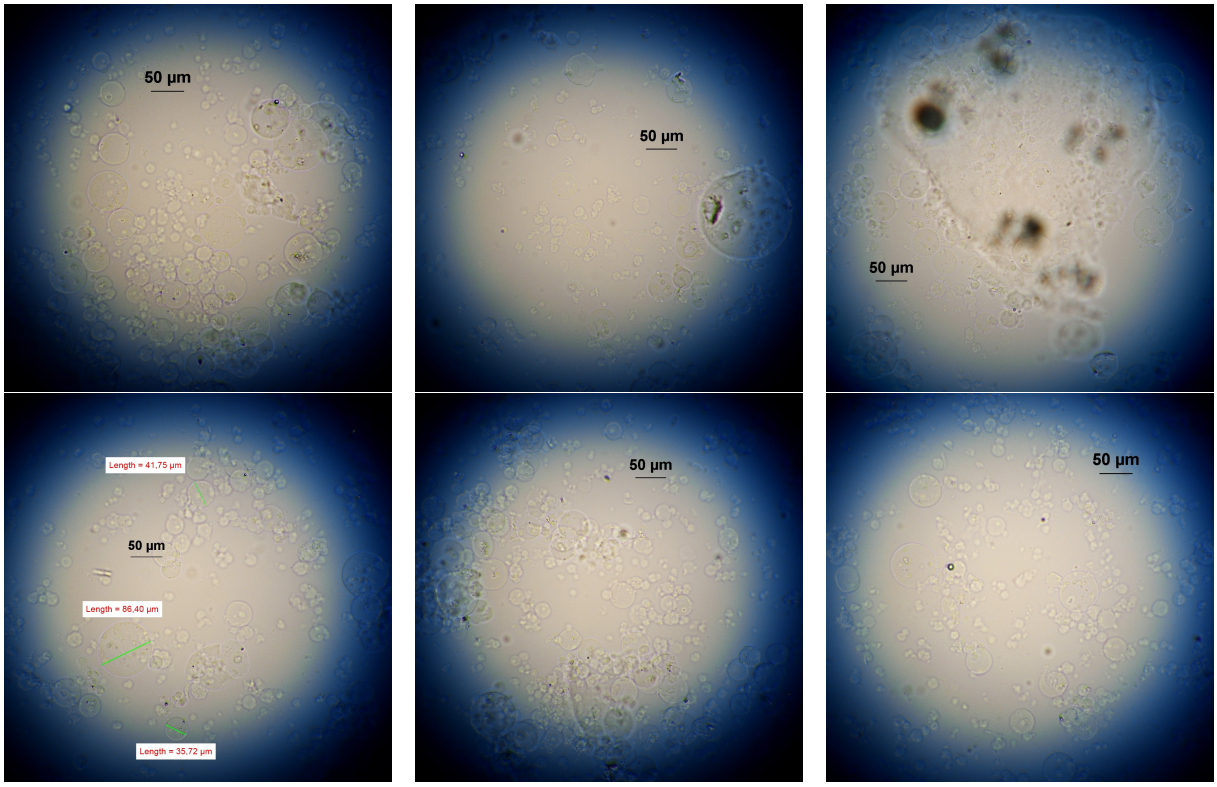


**Figure C.5:** Optical microscope pictures of the exchange experiment with 260 µM $HoCl_3$ after washing with demiwater.

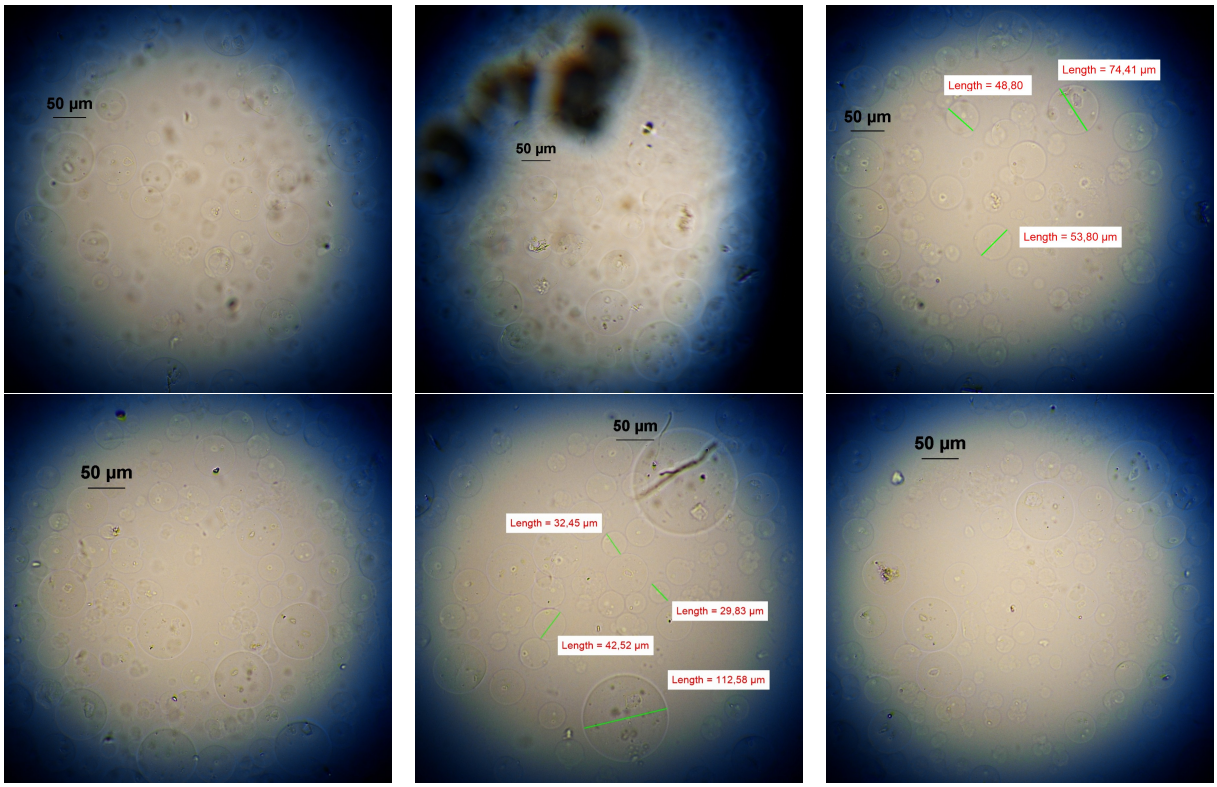


**Figure C.6:** Optical microscope pictures of the exchange experiment with 26 µM $HoCl_3$ after washing with demiwater.

## C.3. EDS analysis quantification dataset of stable holmium exchange

The EDS analysis of the exchange experiments washed with demiwater using stable $HoCl_3$ at different concentrations was discussed in Section 4.3.1. The average mass% of calcium, chloride and holmium was presented in Table 4.2. The complete dataset can be found here in Table C.1, C.2, C.3, and C.4 for $HoCl_3$ exchange bath concentrations of 26 mM, 2.6 mM, 260 µM, and 26 µM, respectively.

**Table C.1:** EDS analysis quantification of three images for the exchange experiment with 26 mM $HoCl_3$.

| Concentration $HoCl_3$: | **26** | **mM** | | | | |
|---|---|---|---|---|---|---|
| Formula | mass% | Atom% | Sigma | Net | K ratio | Line |
| C | 42.84 | 55.8 | 0.01 | 497715 | 0.011168 | K |
| O | 43.73 | 42.76 | 0.05 | 403061 | 0.031467 | K |
| Cl | 0.45 | 0.2 | 0.01 | 16561 | 0.000887 | K |
| Ho | 12.97 | 1.23 | 0.09 | 53386 | 0.018482 | L |
| Total | 100 | 100 | | | | |
| C | 35.37 | 50.36 | 0.03 | 81286 | 0.005977 | K |
| O | 44.15 | 47.19 | 0.12 | 98865 | 0.025291 | K |
| Cl | 0.88 | 0.43 | 0.02 | 6595 | 0.001158 | K |
| Ho | 19.59 | 2.03 | 0.25 | 17236 | 0.019553 | L |
| Total | 100 | 100 | | | | |
| C | 38.58 | 51.81 | 0.01 | 422537 | 0.009481 | K |
| O | 46.03 | 46.41 | 0.05 | 453950 | 0.03544 | K |
| Cl | 0.75 | 0.34 | 0.01 | 26570 | 0.001424 | K |
| Ho | 14.64 | 1.43 | 0.09 | 59495 | 0.020597 | L |
| Total | 100 | 100 | | | | |

**Table C.2:** EDS analysis quantification of three images for the exchange experiment with 2.6 mM $HoCl_3$.

| Concentration $HoCl_3$: | **2.6** | **mM** | | | | |
|---|---|---|---|---|---|---|
| Formula | mass% | Atom% | Sigma | Net | K ratio | Line |
| C | 54.73 | 64.86 | 0.01 | 831352 | 0.018655 | K |
| O | 38.88 | 34.59 | 0.04 | 336932 | 0.026304 | K |
| Ho | 6.39 | 0.55 | 0.06 | 30610 | 0.010597 | L |
| Total | 100 | 100 | | | | |
| Formula | mass% | Atom% | Sigma | Net | K ratio | Line |
| C | 51.7 | 62.8 | 0.01 | 713236 | 0.016004 | K |
| O | 39.92 | 36.41 | 0.05 | 342503 | 0.026739 | K |
| Cl | 0.14 | 0.06 | 0.01 | 5661 | 0.000303 | K |
| Ho | 8.24 | 0.73 | 0.07 | 37066 | 0.012832 | L |
| Total | 100 | 100 | | | | |
| Formula | mass% | Atom% | Sigma | Net | K ratio | Line |
| C | 45.37 | 57.3 | 0.01 | 596174 | 0.013377 | K |
| O | 43.99 | 41.72 | 0.04 | 418648 | 0.032684 | K |
| Ho | 10.64 | 0.98 | 0.08 | 46963 | 0.016259 | L |
| Total | 100 | 100 | | | | |

**Table C.3:** EDS analysis quantification of four images for the exchange experiment with 260 µM $HoCl_3$.

| Concentration $HoCl_3$: | **260** | µM | | | | |
|---|---|---|---|---|---|---|
| Formula | mass% | Atom% | Sigma | Net | K ratio | Line |
| C | 33.14 | 43.69 | 0.01 | 344056 | 0.00772 | K |
| O | 54.53 | 53.97 | 0.05 | 510867 | 0.039884 | K |
| Ca | 3.87 | 1.53 | 0.02 | 96627 | 0.007696 | K |
| Ho | 8.46 | 0.81 | 0.08 | 31096 | 0.010766 | L |
| Total | 100 | 100 | | | | |
| Formula | mass% | Atom% | Sigma | Net | K ratio | Line |
| C | 34.97 | 44.72 | 0.01 | 378644 | 0.008496 | K |
| O | 55.24 | 53.04 | 0.05 | 505676 | 0.039478 | K |
| Ca | 4.58 | 1.76 | 0.02 | 118424 | 0.009433 | K |
| Ho | 5.2 | 0.48 | 0.07 | 19611 | 0.006789 | L |
| Total | 100 | 100 | | | | |
| Formula | mass% | Atom% | Sigma | Net | K ratio | Line |
| C | 35.94 | 45.22 | 0.01 | 420582 | 0.009437 | K |
| O | 55.74 | 52.65 | 0.05 | 535450 | 0.041803 | K |
| Ca | 4.76 | 1.8 | 0.02 | 132355 | 0.010542 | K |
| Ho | 3.55 | 0.33 | 0.06 | 14329 | 0.004961 | L |
| Total | 100 | 100 | | | | |
| Formula | mass% | Atom% | Sigma | Net | K ratio | Line |
| C | 34.56 | 45.17 | 0.01 | 356549 | 0.008001 | K |
| O | 53.6 | 52.59 | 0.05 | 481805 | 0.037615 | K |
| Ca | 3.76 | 1.47 | 0.02 | 92785 | 0.007391 | K |
| Ho | 8.07 | 0.77 | 0.08 | 29254 | 0.010128 | L |
| Total | 100 | 100 | | | | |

**Table C.4:** EDS analysis quantification of three images for the exchange experiment with 26 µM $HoCl_3$.

| Concentration $HoCl_3$: | **26** | µM | | | | |
|---|---|---|---|---|---|---|
| Formula | mass% | Atom% | Sigma | Net | K ratio | Line |
| C | 36.91 | 45.84 | 0.01 | 408682 | 0.00917 | K |
| O | 55.64 | 51.89 | 0.05 | 480557 | 0.037517 | K |
| Ca | 5.65 | 2.1 | 0.02 | 147844 | 0.011776 | K |
| Ho | 1.8 | 0.16 | 0.05 | 6789 | 0.00235 | L |
| Total | 100 | 100 | | | | |
| Formula | mass% | Atom% | Sigma | Net | K ratio | Line |
| C | 36.98 | 46 | 0.01 | 410849 | 0.009219 | K |
| O | 55.36 | 51.69 | 0.05 | 477085 | 0.037246 | K |
| Ca | 5.75 | 2.14 | 0.02 | 150846 | 0.012015 | K |
| Ho | 1.9 | 0.17 | 0.05 | 7194 | 0.00249 | L |
| Total | 100 | 100 | | | | |
| Formula | mass% | Atom% | Sigma | Net | K ratio | Line |
| C | 37.05 | 45.96 | 0.01 | 409033 | 0.009178 | K |
| O | 55.55 | 51.73 | 0.05 | 473924 | 0.036999 | K |
| Ca | 5.82 | 2.17 | 0.02 | 151662 | 0.01208 | K |
| Ho | 1.57 | 0.14 | 0.05 | 5916 | 0.002048 | L |
| Total | 100 | 100 | | | | |

The corresponding images to the EDS quantification in the previous tables are presented in Figure C.7-C.10, respectively. The order of pictures from left to right is the order of quantifications top to bottom in the previous tables.

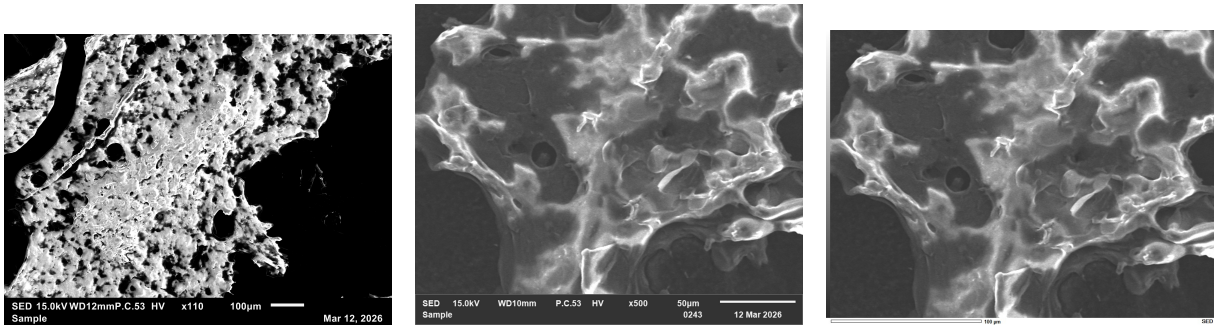


**Figure C.7:** SEM images corresponding to the dataset from Table C.1, using a 26 mM $HoCl_3$ exchange bath.

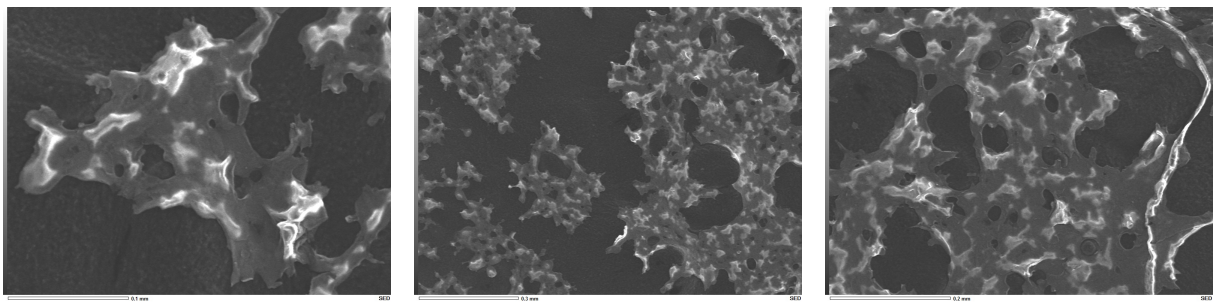

**Figure C.8:** SEM images corresponding to the dataset from Table C.2, using a 2.6 mM $HoCl_3$ exchange bath.

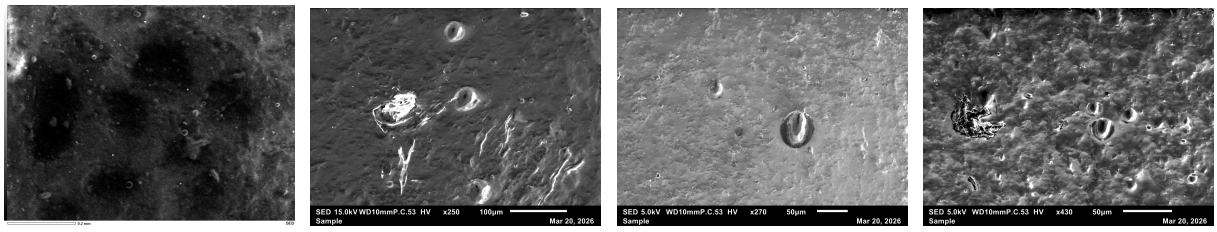


**Figure C.9:** SEM images corresponding to the dataset from Table C.3, using a 260 µM $HoCl_3$ exchange bath.

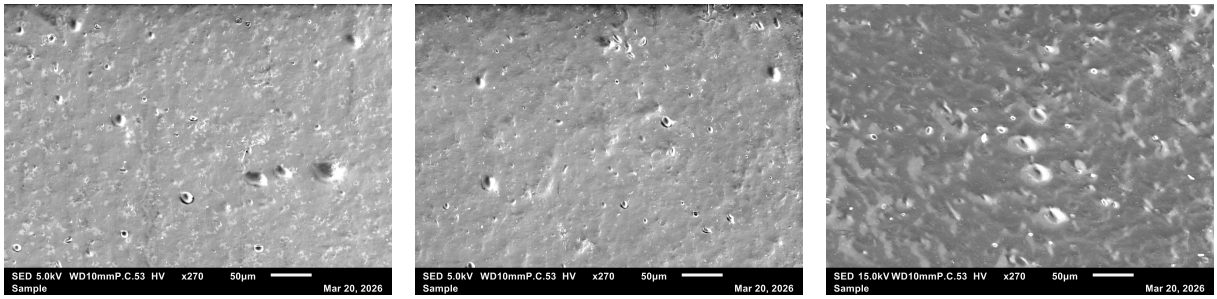


**Figure C.10:** SEM images corresponding to the dataset from Table C.4, using a 26 µM $HoCl_3$ exchange bath.

The average mass% of the dataset for all elements found in the EDS analysis is presented in Table C.5. If an element was not detected or not found in at least three images, the average is noted as n.a.

**Table C.5:** Average mass% of elements in the EDS analysis of exchange experiments using different $HoCl_3$ concentrations.

| Average mass% | **26 mM** | **2.6 mM** | **260** µM | **26** µM | **HoCl3** |
|---|---|---|---|---|---|
| C | 38.93 | 50.60 | 34.65 | 36.98 | |
| O | 44.64 | 40.93 | 54.78 | 55.52 | |
| Ca | n.a. | n.a. | 4.24 | 5.74 | |
| Cl | 0.69 | n.a. | n.a. | n.a. | |
| Ho | 15.73 | 8.42 | 6.32 | 1.76 | |

## C.4. Optical microscope picture collection of radioactive holmium exchange experiments

As discussed in Section 4.3.2, radioactive holmium exchange was used to determine the loading efficiency of alginate microspheres. When all Ho-166 had decayed, the microspheres were analysed under the optical microscope. The picture collection is given in Figure C.11.

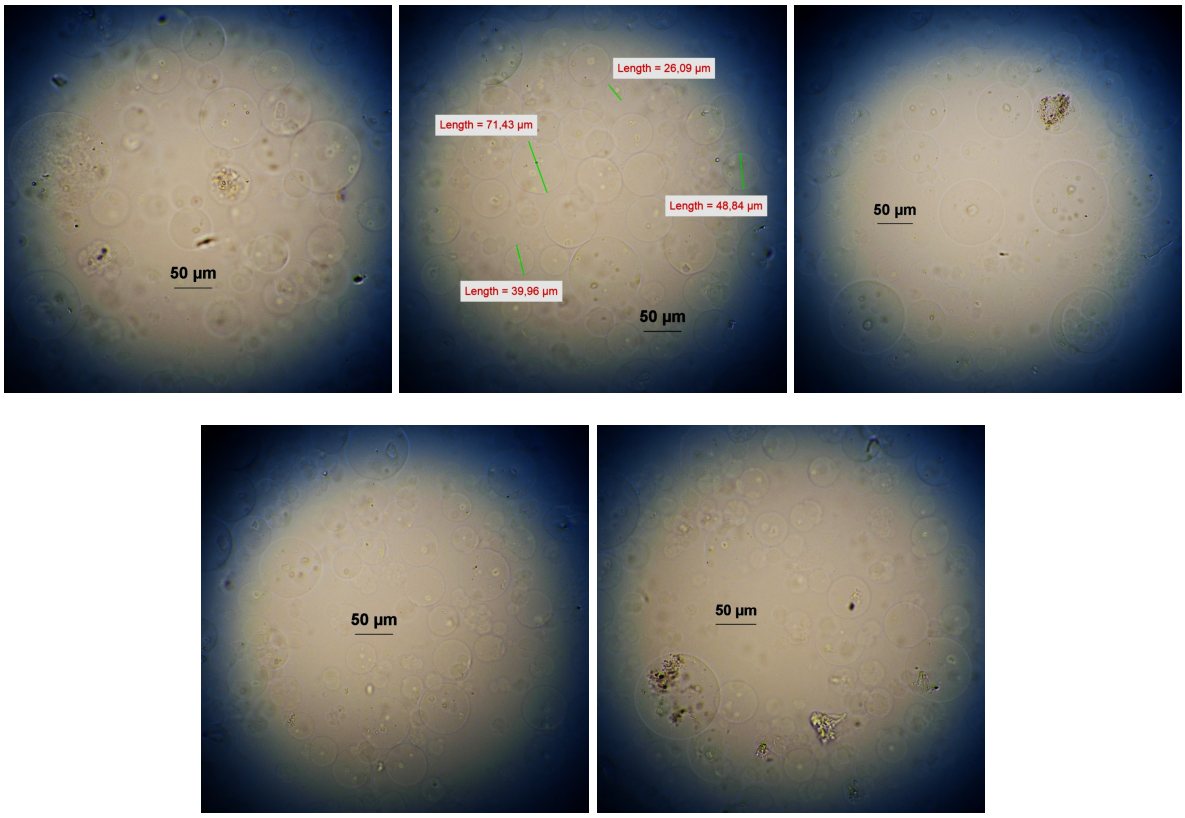


**Figure C.11:** Optical microscope pictures of the Ho-alginate microspheres from the radioactive holmium exchange experiments.

## C.5. Optical microscope picture collection of stability experiments

As discussed in Section 4.4, radioactive Ho-alginate microspheres were investigated on their stability in demiwater and 0.9% NaCl solution. When all $^{166}$Ho had decayed, the microspheres were analysed under the optical microscope. The picture collection is given in Figure C.12. Several alginate microspheres in the 0.9% NaCl samples are indicated by green squares.

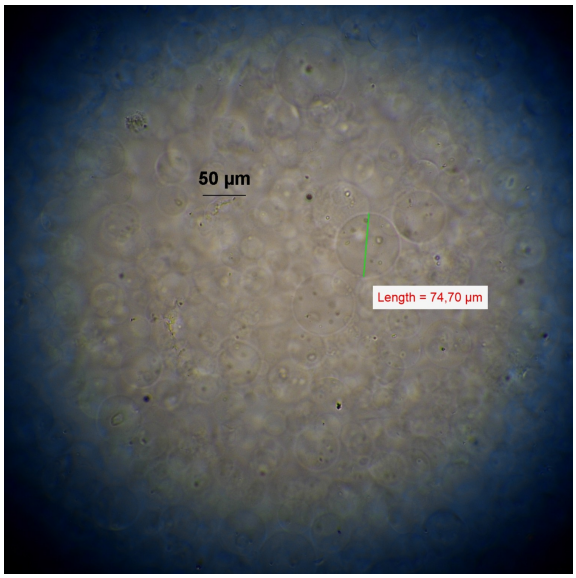


**(a)** Ho-alginate microspheres after demiwater stability.

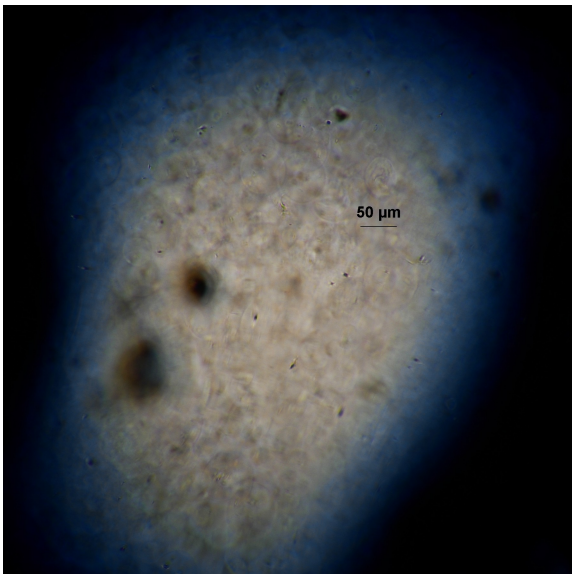


**(b)** Ho-alginate microspheres after demiwater stability.

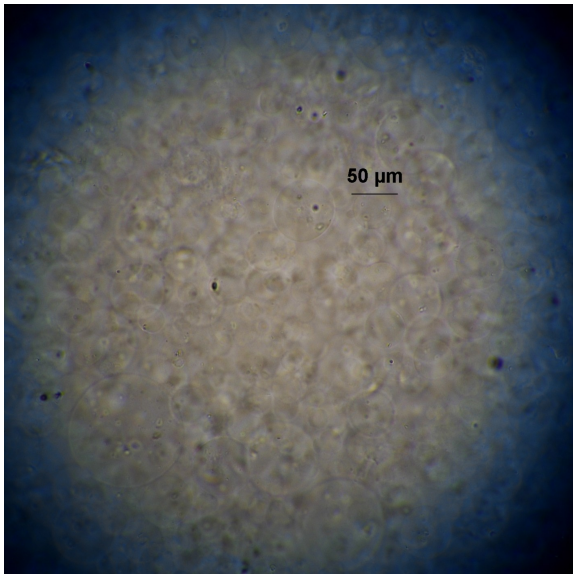


**(c)** Ho-alginate microspheres after demiwater stability.

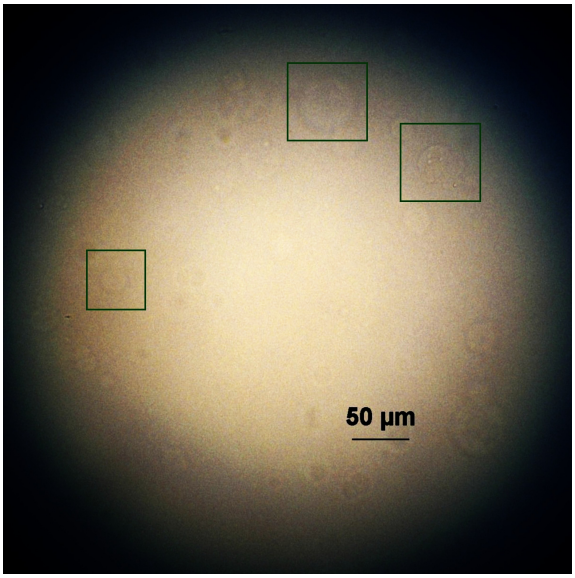


**(d)** Ho-alginate microspheres after 0.9% NaCl stability.

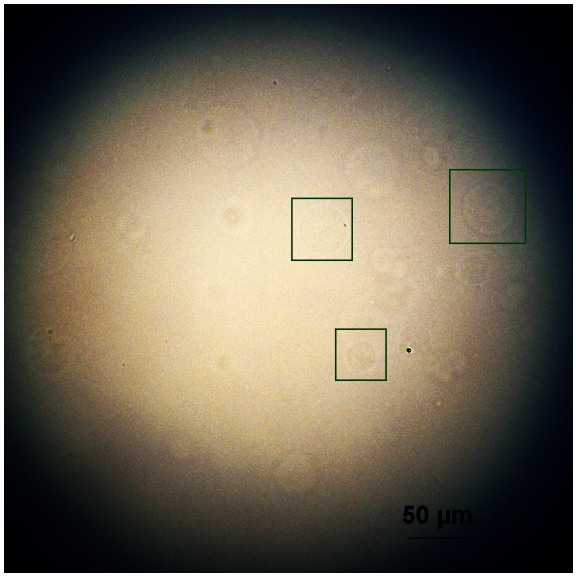


**(e)** Ho-alginate microspheres after 0.9% NaCl stability.

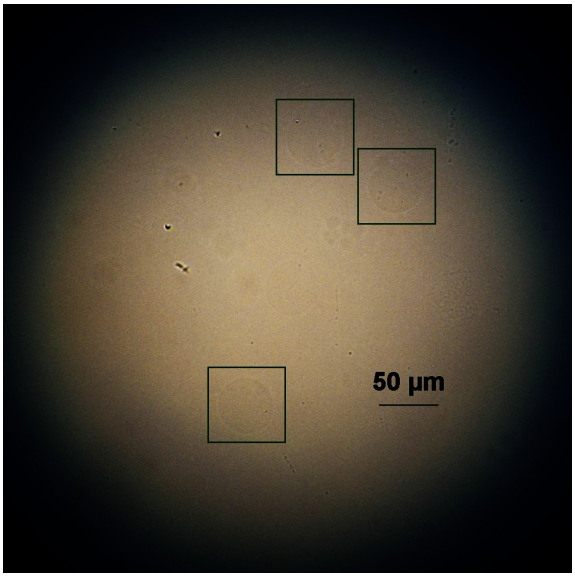


**(f)** Ho-alginate microspheres after 0.9% NaCl stability.

**Figure C.12:** Optical microscope pictures of the Ho-alginate microspheres after stability experiments with demiwater (a-c) and 0.9% NaCl solution (d-f). Several alginate microspheres in the 0.9% NaCl samples are indicated by green squares.

# D

# Supporting hand-needling experiments

The extrusion dripping method and the choice of parameters was discussed in Section 4.1. At the start of the experimental phase, different crosslinking concentrations and alginate concentrations were tested by hand-needling the alginate solution into a crosslinking bath. These supporting experiments are described here. It must be noted that these experiments were performed before precipitation issues with citric acid was addressed. Therefore, the hand-needling experiments use a lower bound of pH 3.

**Hand-needling experiments method**

Buffer solutions of 100 mM citric acid and HEPES were adjusted using NaOH to pH 3 and 7, respectively. Sodium alginate solutions were prepared at 2% or 3% w/v by dissolving sodium-alginate in demiwater. In a petridisk, 25 mL of buffer solution was stirred with 2 mL of 100 mM or 50 mM $CaCl_2$ solution, creating a 4 mM or 8 mM $CaCl_2$ crosslinking bath. A syringe with an internal diameter of 1.2 cm was loaded with 3 mL alginate solution. A 30G x 1/2" (0.3 x 13 mm) needle was used. The alginate was added to the crosslinking bath by hand-needling, catching the first and the last drops from the needle. The solution was left to crosslink for 30 minutes under gentle stirring.

**Hand-needling experiments results**

In search of the right alginate w/v and experimenting with $CaCl_2$ concentrations, different combinations were investigated. The conclusions of the hand-needling experiments are summarized in Table D.1, accompanied by Figure D.1. The results were further discussed in Section 4.1.2.

**Table D.1:** Conclusions of the hand-needling extrusion dripping experiments using different combinations of alginate and $CaCl_2$ concentrations.

| pH used | $CaCl_2$ (mM) | Alginate w/v | Conclusion |
|---|---|---|---|
| 3 and 7 | 4 | 2% | Alginate did not crosslink |
| 7 | 8 | 3% | Alginate crosslinked into gel formation |
| 3 and 7 | 8 | 2% | Alginate crosslinked into particles |

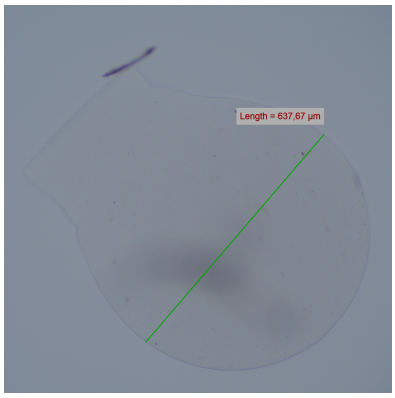


**(a)** Optical microscope picture of 2% w/v alginate, 8 mM $CaCl_2$ crosslinking bath, pH 3.

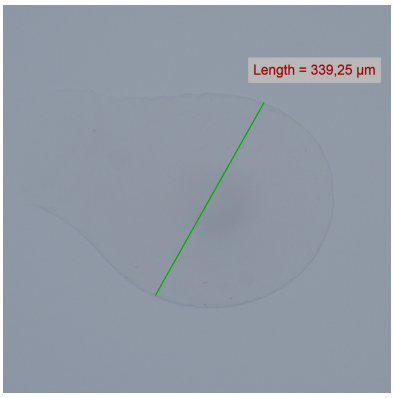


**(b)** Optical microscope picture of 2% w/v alginate, 8 mM $CaCl_2$ crosslinking bath, pH 7.

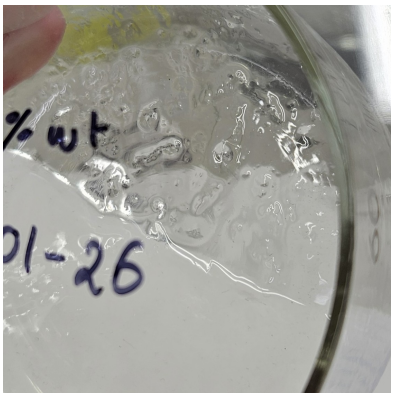


**(c)** Picture of 3% w/v alginate, 8 mM $CaCl_2$ crosslinking bath, pH 7.

**Figure D.1:** Supporting pictures of the hand-needling experiments, using alginate solution at 2% w/v (a,b) and 3% w/v (c) in a 8 mM $CaCl_2$ crosslinking bath at different pH. The alginate crosslinked into individual particles (a,b) or gel formation (c).

# E

# Acknowledgement of AI-use

For understanding basic concepts such as abbreviations and simple (medical) terms and techniques during literature research, I used Google AI-mode, automatically implemented in Google Search, to obtain basic explanations on the theory and methods behind (medical) treatment systems to familiarize myself with (medical) concepts that I was not yet educated in. I found the theory to be a method to further understand what I was looking into and I read the literature articles connected to the methods as soon as I understood the basic concepts. I found the short AI statements to be helpful in quick assessment, but they did not further explain limitations, did not compare medical treatment options, and did not include technical specifications such as isotope choice or radiation dosage.

For correct code writing or fixing errors in LaTeX code lines, I used ChatGPT to obtain the basic use of LaTeX coding. I found this helpful in setting up basic coding, however not all problems were easily solved and I used further online documenting to adjust my code lines accordingly.

For creating pictures and lay-out using LaTeX TikZ package, I used Google AI-mode and ChatGPT to obtain LaTeX code lines, I found this method to be time efficient and I used literature based values where necessary. I found using AI drastically decreased time spent on trying to figure out LaTeX, but I still had to correct the majority of AI code lines to have the pictures the way I wanted them to look.